Aalto University
School of Engineering

Aalto University of Technology

MEC-E2004 - Ship Dynamics

Saimaa Hybrid

2.6.2021

Ahmed Yosri

Jonas Korpela

Akseli Kjellberg

Oskar Vainionpää

Aaron Körkkö

Instructor: Prof. Spyros Hirdaris

Contents

Table of Figures

Project introduction

This project aims to introduce a novel, zero-emission and futuristic vessel to the marine world. The vessel can carry both cargo and passengers to meet the highly fluctuating market demand in the Saimaa canal throughout the year. The vessel can carry around 300 passengers in the summer season when the passenger demand is high. The cargo (bulk timber) is intended to be carried in the deep compartments far from the passenger's facilities. The Saimaa Hybrid iterative design began from the PNA course and culminated in the Ship Design Portfolio, Ship Dynamics and Ship Structures & Construction courses. Hence, the study here covers the hydrostatics, static stability, dynamic stability, structural finite element analysis, motions, responses, etc. This report focuses mainly on the dynamic aspects of the project.

As the ship has a requirement of zero-emission, the powering is executed with fuel cells. The ship main particulars are presented in table below. The General Arrangement of the ship is presented on Appenix 1.

Table 1 Ship's main particulars

Particular	**Value**
Overall length (LOA)	92.5 m
Length between perpendiculars (LPP)	89.2 m
Breadth (B)	12.6 m
Draft (T)	4.45 m
Displacement (∇)	3604 m^3
Gross tonnage	
Propulsion motor power	2 x 800 kW
Total power	1625 kW
Battery capacity	1920 kWh
Ice class	Finnish-Swedish 1C

1 Introduction

Saimaa Hybrid vessel is intended to operate in lake Saimaa, Saimaa Canal and the Gulf of Finland. The vessel is designed to carry passengers and cargo at the same time. Regular route of the vessel is Lappeenranta – St. Petersburg passing through Vyborg in Russia. Length of the route from Lappeenranta to Vyborg is roughly 60km and from Vyborg to St. Petersburg roughly 170 kilometers, making the total length of the route 230 kilometers. We have realized that the extension of the route to St. Petersburg comparing with our previous design (last station was Vyborg) will have a great impact on the expected income from passengers. The cargo trading is much profitable between Lappeenranta and Vyborg, while the passenger demand is higher from Vyborg to St Petersburg. Based on this information we have selected our loading conditions as follows:

- From Lappeenranta to Vyborg (or Vyborg to Lappeenranta) the cargo load is expected to be up to 70% of the dead weight, depending on the season.
- Vyborg/ St. Petersburg the vessel will carry more passengers comparing with the first route in both summer and winter seasons.

Our design also aims to have a sustainable vessel that has zero emissions and meets eight sustainable goals (SDGs) of the United Nations; decent work and economic growth, industry innovation and infrastructure, sustainable cities and communities, responsible consumption and production, climate action, life below water, life on land and finally the partnerships for the goals, which can be achieved by the collaboration between Russia and Finland towards cleaner environment. To achieve the zero-emission target, the vessel will operate by using batteries and hydrogen fuel.

The design of the vessel is aimed to be futuristic compared to all previous vessels in similar use in the area. Expansion of the Saimaa Canal offers a chance to create a larger ship than before, but the passenger demand must be kept in mind. One large exception compared to existing Saimaa area passenger vessels that operate during the summertime, is that our project ship will need ice classification to operate partly in winter.

2 Operational profile and conditions

2.1 Operational profile

Details on the operational route are presented in this chapter. Overview of the route is shown in *Figure 2-1* The operational profile is shown in *Figure 2-2*.

Online data was used to create the operating profile. Google Earth was used to approximate the length of the route, the distances between locks and the connected lakes. Time spent in the locks was approximated by using a time-lapse video of a vessel passing through the canal.

Figure 2-1 Ship's route on Google Earth.

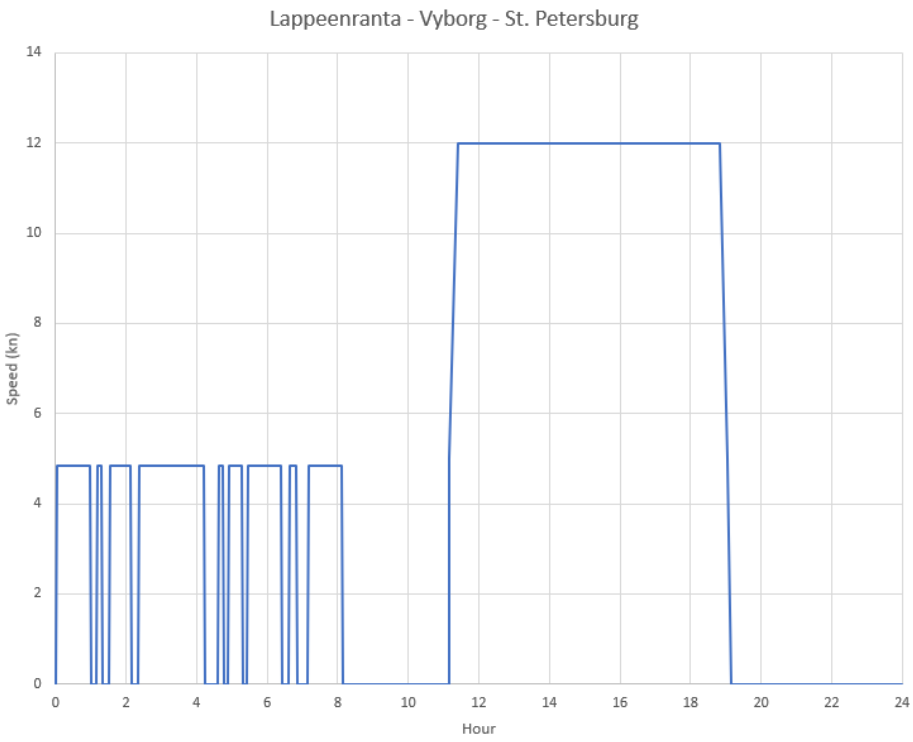

Figure 2-2 Ship's operational profile.

Trip	**Distance**
Lappeenranta – Vyborg	60 km
Vyborg – St. Petersburg	170 km
Total	230 km

Explanation for operational profile:
Departure from Lappeenranta
Arrival to Vyborg 8 hours after departure from Lappeenranta
Departure from Vyborg 11 hours after departure from Lappeenranta
Arrival to St. Petersburg 19 hours after departure from Lappeenranta

The operational profile is based on open water conditions. It can be noticed that trip from Lappeenranta to Vyborg takes a bit over 8 hours as the speed is highly limited by the Saimaa canal locks and speed limit of 4.85 knots. The ship has a 3-hour stop at Vyborg, after which it continues to St. Petersburg. On this stage, the design speed of 12 knots can be used. Trip from Vyborg to St. Petersburg takes roughly 8 hours as well. With this schedule, the ship would arrive to St. Petersburg a bit over 19 hours after the departure from Lappeenranta.

With these, we created a schedule for our operation. Note that this schedule does not take into account the different time zones on Finnish and Russian sides of the border. The schedule is also based on open water conditions and thus it is unachievable during winter, when ice is present. Due to the rough ice conditions at certain years and months, year-round operation is not possible for the ship. Ice conditions are further discussed in the next chapter.

Table 2 Ship's operational schedule.

Port	departure/arrival	Time
Lappeenranta	departure	07:00
Vyborg	arrival	15:00
Vyborg	departure	18:00
St. Petersburg	arrival	02:00
St. Petersburg	departure	07:00
Vyborg	arrival	15:00
Vyborg	departure	18:00
Lappeenranta	arrival	02:00

With this schedule, it is possible to depart from Lappeenranta and St. Petersburg every 48 hours. We believe that the port-times (3 hours in Vyborg and 5 hours in Lappeenranta & St. Petersburg) are enough to refuel and load/unload the cargo.

2.2 Water depths on route

Water depths on route were studied by using navigational chart by Navionics.

Generally, the Saimaa Lake and canal area can be considered very shallow. Water depths at the shipping lanes of Saimaa Lake and canal are varying between 5-6 meters. Good navigation is important as often water depths just outside of the lane are less than 3 meters. The lakes that connect different parts of the canal are somewhat deeper. Depths in the four connecting lakes vary between 5-22 meters. Still, the average water depth in the connecting lakes is less than 10 meters. Between the canal and Vyborg harbor, water depth on the shipping lane varies between 5-7 meters. After departing Vyborg and heading towards Gulf of Finland at the Bay of Vyborg, the shipping lane depth varies between 7-13 meters, while seemingly getting deeper closer to Gulf of Finland. On Gulf of Finland, close to the Russian shoreline, the water depth on the shipping lane is generally more than 20 meters with some minor exceptions where depths are around 10 meters. Same applies when moving further away from the coast where depths are varying between 20-35 meters. Water is shallower in the eastern Gulf of Finland, close to St. Petersburg. Depth of shipping lane varies between 7-15 meters.

Numbers regarding water depths are presented in the table below. Also, rough estimates of the average depths in different parts of the route were made. Note, that these values represent the water depths of the shipping lanes along the route, not the entire region. For explanation of h/T -ratio, see chapter 10.

Table 3 Water depths on route.

Area	Depth variation (m)	Average depth (m)	h/T -ratio
Saimaa lake	5 - 6	5.2	Very shallow
Saimaa canal	5 - 6	5.2	Very shallow
Connecting lakes	5 - 22	9	Medium deep
Between canal & Vyborg	5 - 7	6	Shallow
Bay of Vyborg	7 - 13	10	Medium deep
Gulf of Finland, close to shore	20 - 30	23	Deep
Gulf of Finland	20 - 35	27	Deep
Gulf of Finland, close to St. Petersburg	7 - 15	10	Medium deep

2.3 Operational conditions

Saimaa lake, canal and Gulf of Finland are usually frozen roughly three months annually. On average, this leaves us a 9-month period where it is possible to operate in open water conditions according to the schedule presented earlier. It is still noteworthy that ice conditions vary between years. Most of Gulf of Finland may be ice-free in some winters, but usually the eastern part (close to St. Petersburg) is frozen between 4 and 5 months every year. Ice thickness may reach more than 0.5 meters at eastern part of Gulf of Finland near the Russian shore.

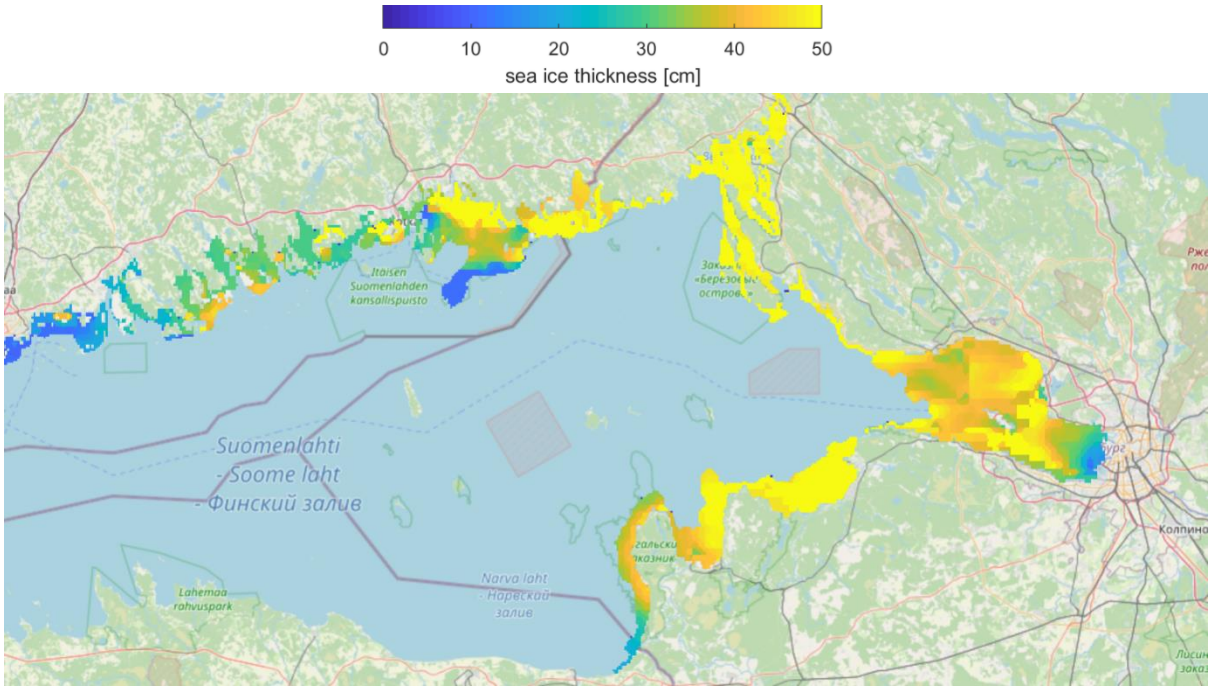

Figure 2-3 Ice conditions on eastern Gulf of Finland on March 9th 2021.

Operational conditions on the Saimaa Lake and canal can be considered easy. Wind and wave conditions are mild compared to Gulf of Finland. For instance, at Pyhäselkä (largest open part of lake Saimaa with dimensions of 23km x 6km) the significant wave height with 20 m/s wind speed reaches only 0.85 meters (Suhonen 2020). As the ship operates in other parts of lake Saimaa that are more narrow and less open, the significant wave heights in those regions would be much less than in Pyhäselkä. Same applies for the Saimaa canal as well.

The monthly mean significant wave height in Gulf of Finland is illustrated in *Figure 2-4*. The mean varies between 0.5m – 1.5m. What is interesting to note is that the mean is at the lowest during summer months and significantly increases towards the end of the year. The mean height increases to 2-3 times larger compared to the summer months. In the beginning of the year some data is missing due to the ice conditions.

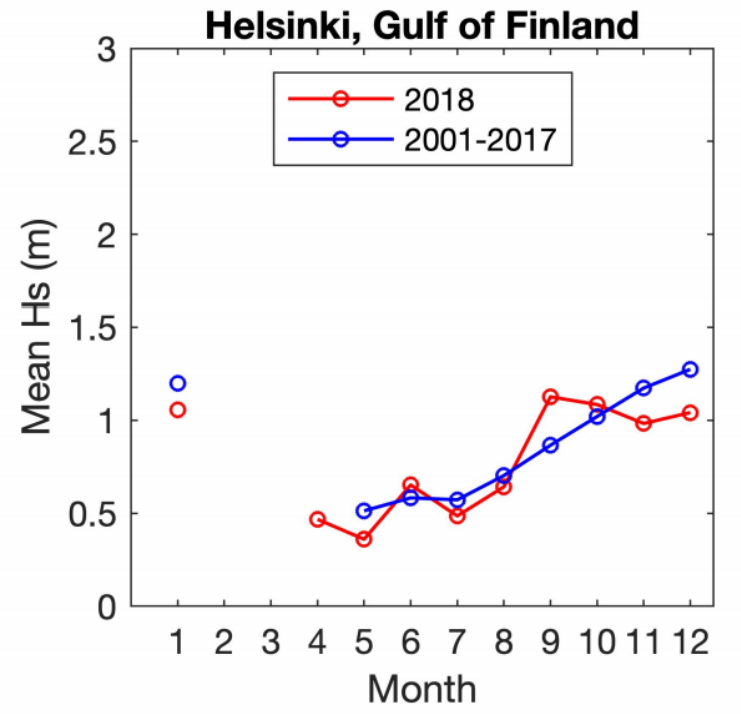

Figure 2-4 Mean significant wave height in Gulf of Finland. (Helcom 2019).

Highest significant wave height ever measured at Gulf of Finland is 5.2 meters (2001 and 2012). Individual waves may reach up to 9 meters. These can be considered extreme conditions for the region. Highest significant wave heights are illustrated in *Figure 2-5*.

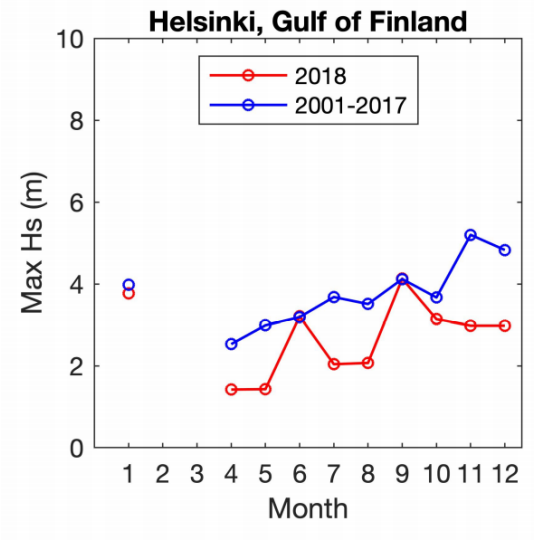

Figure 2-5 Max significant wave height in Gulf of Finland. (Helcom 2019).

The waves are usually travelling along the shoreline at Gulf of Finland. Therefore, the waves are usually travelling towards west, but they may also travel towards south-west according to Ilmatieteen laitos.

Three different wave cases are illustrated in Appendix 1. The illustration includes the worst-case scenario, where the significant wave height is 5.2 meters and wave length equals to ship waterline length.

The annual mean wind speed at height of 10 meter around Gulf of Finland is illustrated in *Figure 2-6*. At the height of 10 meters, the mean wind speed is around 7 m/s in Gulf of Finland. Lower wind speeds are seen in the Saimaa lake/connected lakes (5-6 m/s) and in the canal (2-4 m/s). In the summer months the mean wind speed is at the lowest (same pattern as with wave heights).

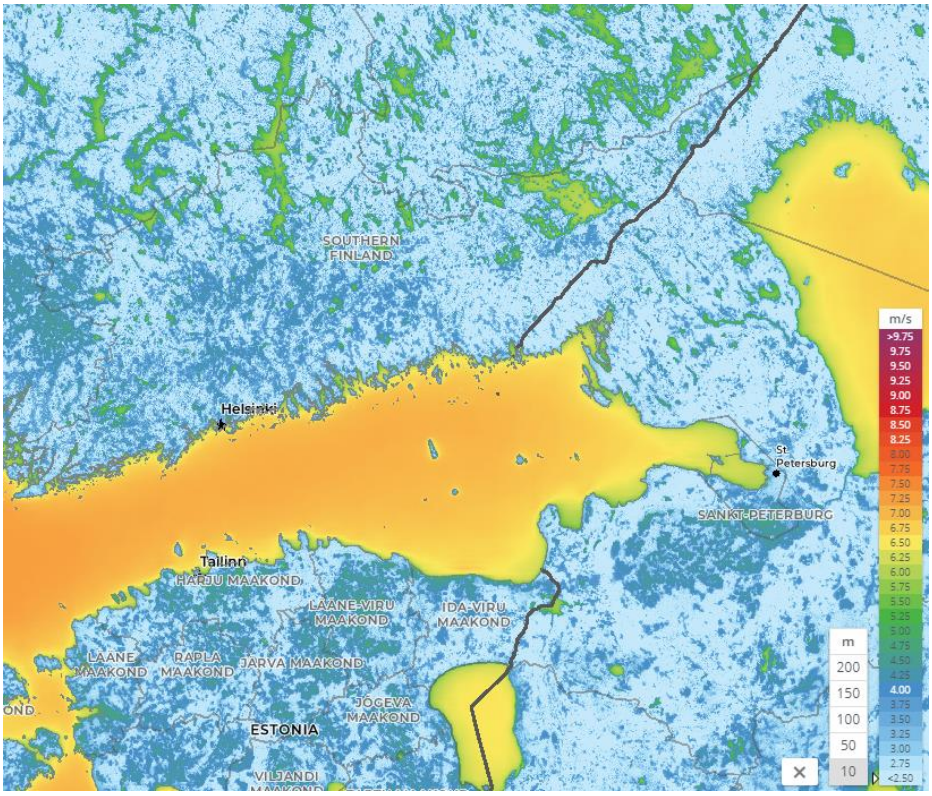

Figure 2-6 Mean annual wind speed at height of 10m. (Global Wind Atlas).

Data collected by Ilmatieteen laitos (Finnish Meteorological Institute) indicates that over 20 m/s windspeeds are encountered on average 27 times a year in the coastal areas of Finland (see *Figure 2-7*). It is worth noting that this includes data from all over the coastal area of Finland. This means that the expected number of days is even lower at the eastern Gulf of Finland. Also, it must be remembered that individual gusts may reach much higher wind speeds than the average. A chart of average number of storm days by months is also presented below. The data is average between years 2006-2020.

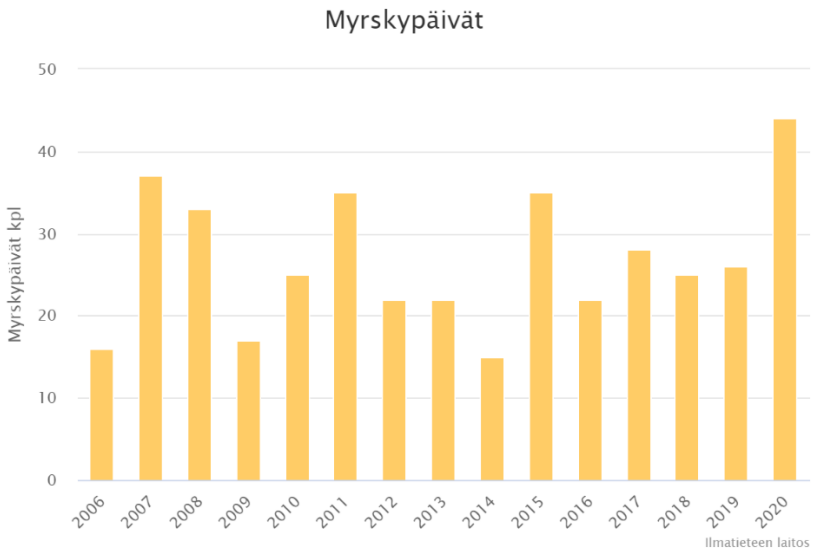

Figure 2-7 Number of storm days (wind speed > 20m/s) in the coastal area of Finland. (Ilmatieteen laitos).

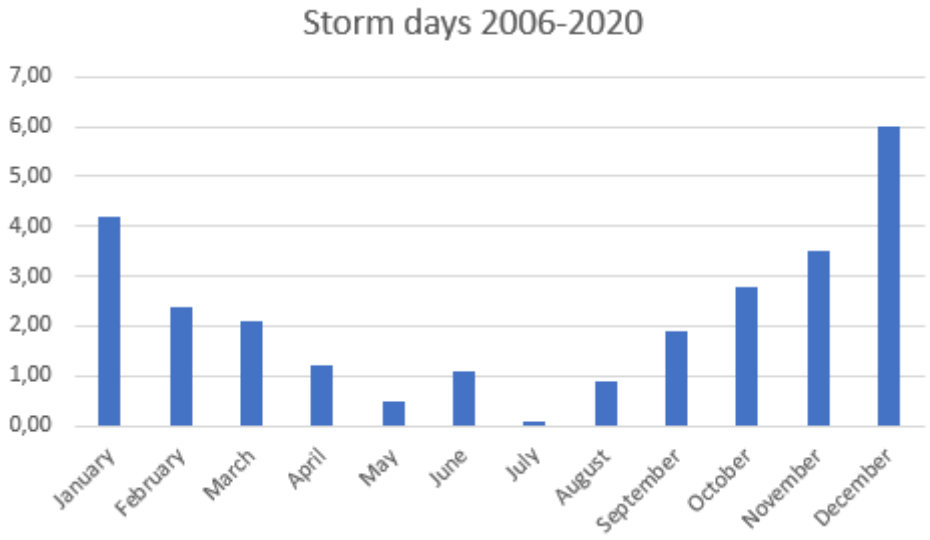

Figure 2-8 Seasonal average number of storm days between 2006-20 (Ilmatieteen laitos).

Occurrence of high wind speeds in Finnish coastal areas are presented in a table below. The data is from Ilmantieteen laitos.

Average wind speed (m/s)	**Occurrence**
21	27 days / year
25	5 days / year
28	once every 2 years
29	once every 3 years
30	once every 5 years
31	once every 14 years
32	once every 50 years
33	never measured

3 DHI Metocean Data portal

The website (DHI 2020) provides different plots of the metocean and wind data around the world from different resources. The dataset adopted for reporting the wave characteristics in this section is DHI global wave model dataset (GWM). This dataset is generated by DHI's 3rd generation MIKE 21 Spectral Wave Model (DHI), which is based on a high accuracy global CFSR wind dataset from NCEP/NOAA. The NOAA dataset is regarded as a perfect basis for both global and regional wave modelling. In addition, for ensuring an adequate accuracy, the data was calibrated against various offshore buoy and satellite data.

Figure below represents the correlation between wave directions, significant wave height and probability of occurrence (frequency) within a time-span of 40 years (1979 to 2019) in a random point at Baltic Sea close to Gulf of Finland. It can be observed that the major wave approaches from 247.5 degree (west direction), while the other directions are less frequent.

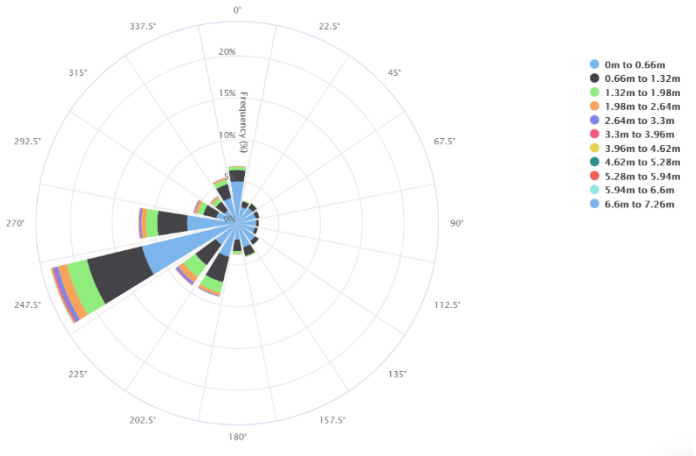

Figure 3-1 The frequency of wave direction and significant wave height from 1979 to 2019

It is noteworthy that, the most frequent wave height is from 0 to 2.64, with very slight sea states exceed this value.

Figure 3-2 indicates the correlation between H_s and time throughout the last 3 years in the same location. The limit of the free metocean data is just 1 year/chart, therefore, 3 charts are extracted, a chart for each year. The figure clearly indicates that the worst sea states usually happen in winter.

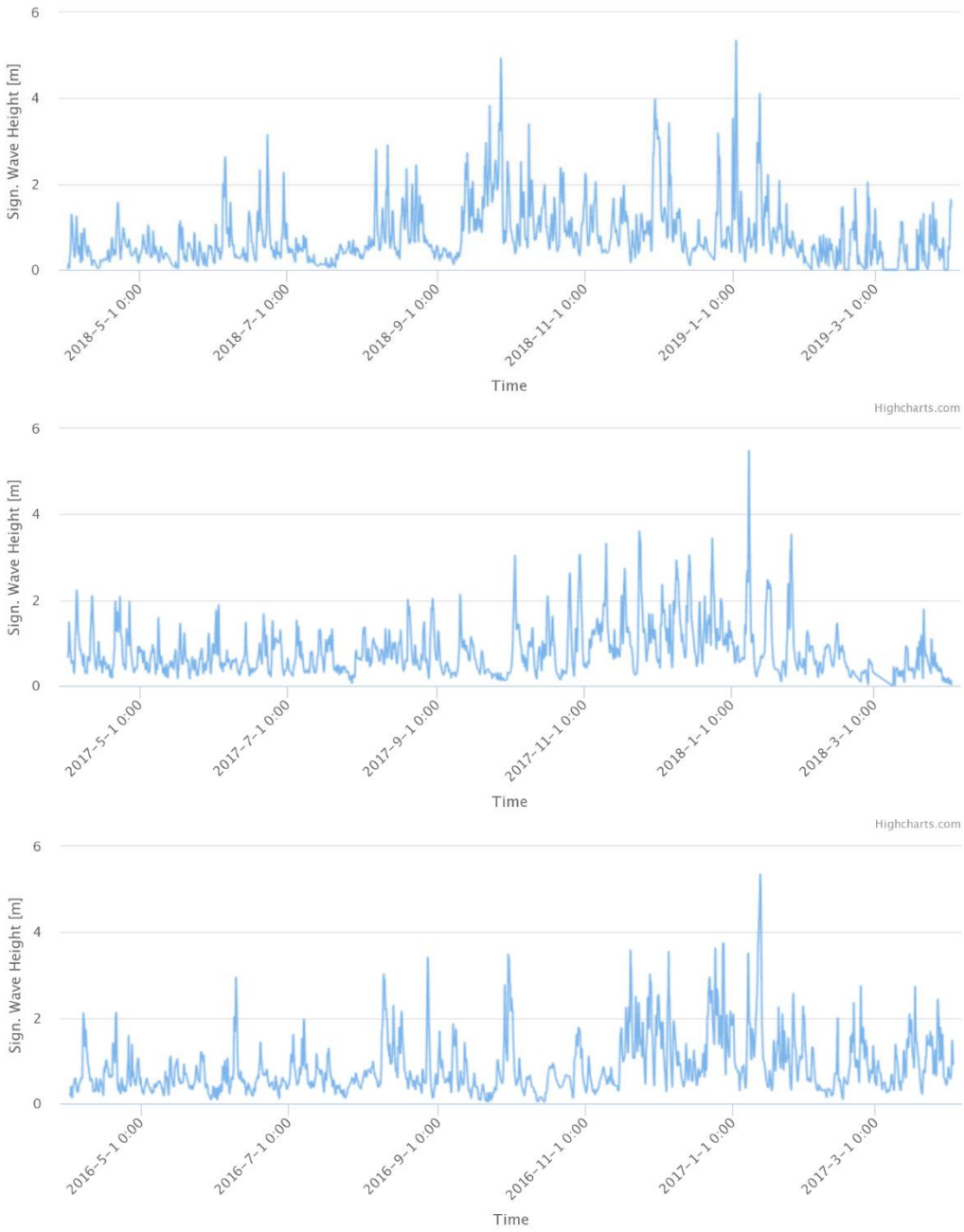

Figure 3-2 Wave height throughout the last 3 years

Just defining the significant wave height of each sea state is not enough for the further load processing and hydrodynamic response analysis. Therefore, zero-crossing period data is essential for fully describing each sea state. *Figure 3-3* illustrates the wave period corresponding to the above-mentioned wave heights.

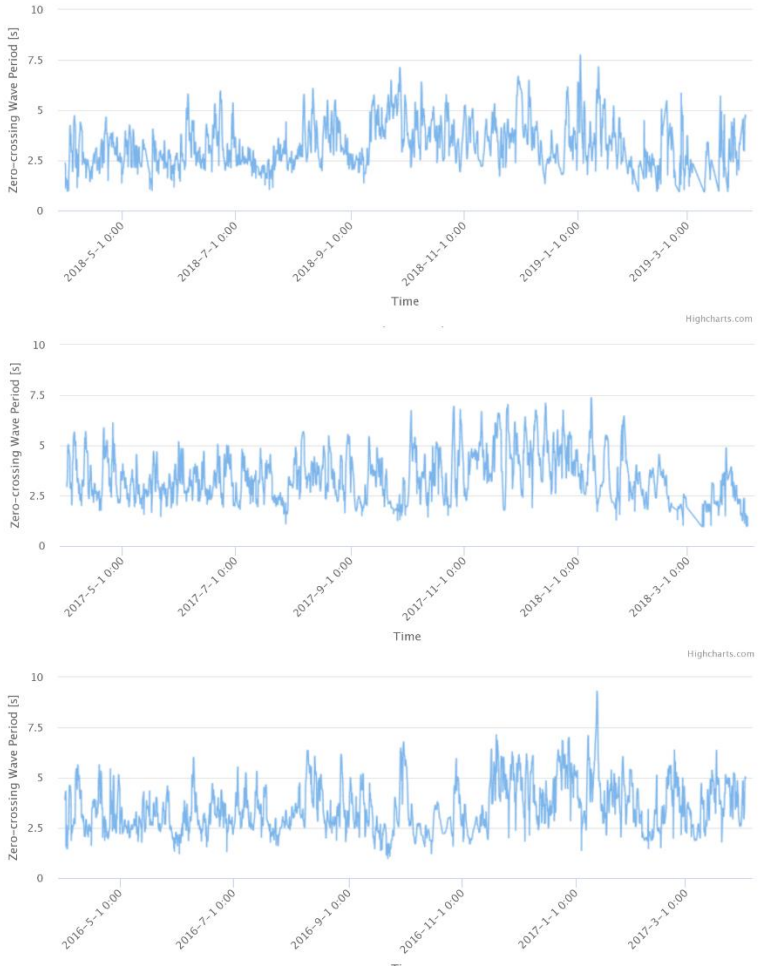

Figure 3-3 Zero-up-crossing period in the last 3 years

It is noteworthy that, within a sea state, the worst structural response or motion usually happens when the wave frequency has the natural frequency of the offshore structure, the wave height in this case will be considerably effective. The frequency of the sea states described by the zero-crossing period and Sign wave height is illustrated in Figure below

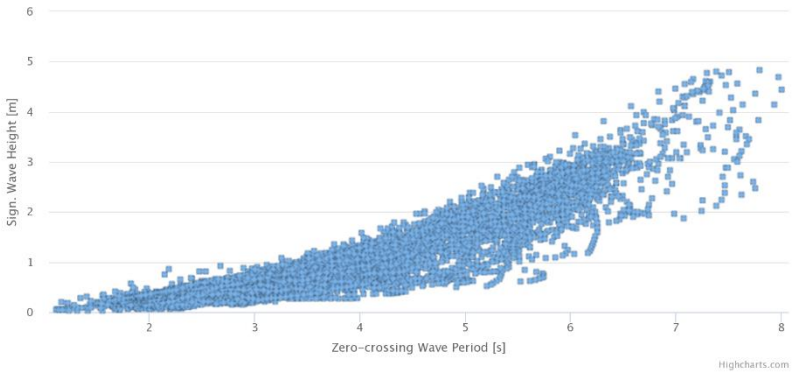

Figure 3-4 The frequency of sea states described by the zero-crossing period and Sign wave height.

4 Wave scatter diagram in literature

Kahma et, al, (Kahma, Pettersson, and Tuomi 2003) have illustrated the wave scatter of the northern parts in Baltic Sea based on data recorded by offshore buoys throughout nine years. The statistics collected by the offshore buoys are usually affected by the ice season (Kahma, Pettersson, and Tuomi 2003). This phenomenon can be observed clearly in figure below where in winter it is difficult to forecast the wave height. There are four methods can be adopted to analyze the waves in those areas that have ice in a specific time of the year, direct statistics (measured data only is considered without any correction), formal statistics (zero wave height in presence of ice), Ice-free season statistics (consider only ice-free season) and Hypothetical "no ice" statistics (No ice considered throughout the year). The statistics of Kahma et, al, (Kahma, Pettersson, and Tuomi 2003), in table below, is based on Direct statistics from Northern Baltic Proper 59°15.0 N 21°00.0 E. recorded from September 1996 to September 2000.

The statistics in the table below can be called a wave scatter diagram which defines the probability of occurrence of the different sea states. Here the scatter diagram considers the peak periods, T_p in sec, and the significant wave height, H_s in m, to define each sea state. In Other scatters may replace the peak period by the zero-crossing period. This scatter can be represented by Weibull distribution.

The scatter diagram in table below was selected to represent the long-term description of the wave climate in the considered operational area. The periods in the table represent the midpoints. That means the observed wave periods of a sea state lie between T_p +0.5 sec and T_p - 0.5 sec

Table 4 Recorded data from Northern Baltic 59°15.0 N 21°00.0 E. September 1996 — September 2000..

Significant wave height [m]	peak wave period [s]											
	2	3	4	5	6	7	8	9	10	11	12	Tot
7.75 : 8.00	0	0	0	0	0	0	0	0	0	0	0	0
7.50 : 7.75	0	0	0	0	0	0	0	0	0	0	0	0
7.25 : 7.50	0	0	0	0	0	0	0	0	0	2	0	2
7.00 : 7.25	0	0	0	0	0	0	0	0	0	0	2	2
6.75 : 7.00	0	0	0	0	0	0	0	0	0	4	3	7
6.50 : 6.75	0	0	0	0	0	0	0	0	1	4	1	6
6.25 : 6.50	0	0	0	0	0	0	0	0	4	2	0	6
6.00 : 6.25	0	0	0	0	0	0	0	0	7	10	2	19
5.75 : 6.00	0	0	0	0	0	0	0	0	9	5	0	14
5.50 : 5.75	0	0	0	0	0	0	0	2	11	9	2	24
5.25 : 5.50	0	0	0	0	0	0	0	11	17	11	0	39
5.00 : 5.25	0	0	0	0	0	0	1	5	16	1	2	25
4.75 : 5.00	0	0	0	0	0	0	0	4	10	5	0	19
4.50 : 4.75	0	0	0	0	0	0	10	40	41	8	1	100
4.25 : 4.50	0	0	0	0	0	1	4	29	8	4	0	46
4.00 : 4.25	0	0	0	0	0	1	36	58	38	7	0	140
3.75 : 4.00	0	0	0	0	0	9	72	84	39	9	1	214
3.50 : 3.75	0	0	0	0	1	12	138	121	42	4	0	318
3.25 : 3.50	0	0	0	0	2	54	197	85	21	1	0	360
3.00 : 3.25	0	0	0	0	5	114	212	67	21	2	0	421
2.75 : 3.00	0	0	0	0	15	147	229	47	13	1	0	452
2.50 : 2.75	0	0	0	1	104	436	344	90	7	1	1	984
2.25 : 2.50	0	0	0	4	196	413	192	42	2	1	0	850
2.00 : 2.25	0	0	0	32	492	686	221	43	4	0	0	1478
1.75 : 2.00	0	0	0	115	846	559	187	37	3	1	0	1748
1.50 : 1.75	0	0	6	596	1288	586	157	35	11	1	0	2680
1.25 : 1.50	0	0	60	1371	1175	334	95	11	1	0	0	3047
1.00 : 1.25	0	0	366	1579	745	163	75	16	0	0	0	2944
0.75 : 1.00	0	64	1791	2008	624	159	62	10	2	0	0	4720
0.50 : 0.75	1	700	2264	1100	352	111	35	4	0	0	0	4567
0.25 : 0.50	274	1859	1589	744	370	136	16	4	20	1	0	5013
0.00 : 0.25	212	419	377	291	406	113	5	5	8	1	0	1837
Total	487	3042	6453	7841	6621	4034	2288	850	356	95	15	32082

5 Joint distribution of significant wave height and period.

The different joint environmental data models can be adopted to predict the metocean data and values of wave height and periods during the extreme weather conditions in any location around the world. The best available models are Maximum Likelihood Model (MLM) (Prince-Wright 1995) and the Conditional Modelling Approach (CMA) (Bitner-Gregersen and Haver 1991). In this report only CMA, which is recommended by DNVGL (DNVGL-CG-0130 January 2018), is reported. The significant wave height Hs is described by a 3-parameter Weibull probability density function.

$$f_{H_s}(h) = \frac{\beta_{Hs}}{\alpha_{Hs}}\left(\frac{h-\gamma_{Hs}}{\alpha_{Hs}}\right)^{\beta_{Hs}-1} \exp\left\{-\left(\frac{h-\gamma_{Hs}}{\alpha_{Hs}}\right)^{\beta_{Hs}}\right\}$$

While the zero-crossing wave period conditional on H_s is modelled by a lognormal distribution

$$f_{T_Z|H_s}(t \mid h) = \frac{1}{\sigma t\sqrt{2\pi}} \exp\{-\frac{(\ln\ t-\mu)^2}{2\sigma^2}\}$$

where the μ and σ can be described by the significant wave height (Bitner-Gregersen and Haver 1991) . As was stated by DNVGL (DNVGL-CG-0130 January 2018) the following equations of μ and σ can give reliable estimation of the wave periods.

$$\mu = E[\ln\ T_z] = a_o + a_1 h^{a_2}$$
$$\sigma = \text{std}\ [\ln\ T_z] = b_0 + b_1 e^{b_2 h}$$

The values of those parameters are given in table below for a wide range of nautical zones in figure below. The considered zone in this report is area 5.

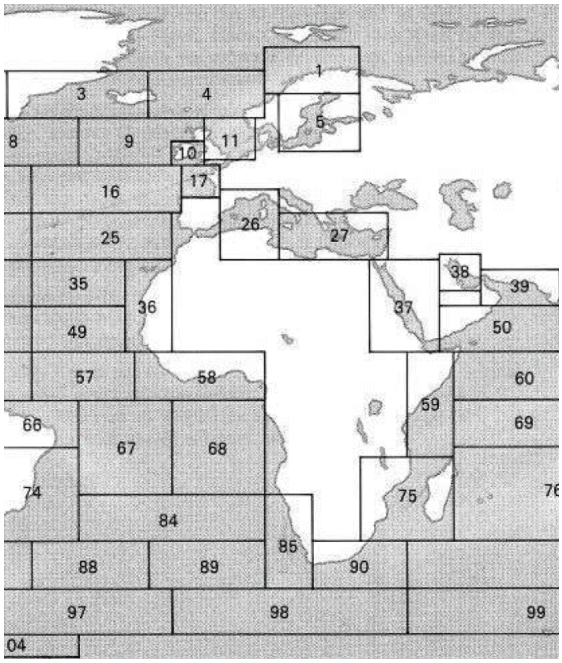

Figure 5-1 Nautical zones (DNVGL-CG-0130 January 2018)

Table 5 Weibull parameters of the long-term sea states scatters by DNV

Table C-1 2-parameter Weibull parameters and Log-Normal distribution parameters for H_S and T_Z ($\gamma_S = 0$)													
Area	α_s	β_s	a_1	a_2	b_1	b_2	Area	α_s	β_s	a_1	a_2	b_1	b_2
1	2.33	1.33	0.974	0.205	0.1263	-0.0201	53	2.56	1.93	1.188	0.129	0.1041	-0.0091
2	1.96	1.34	0.994	0.175	0.1414	-0.0238	54	2.45	2.19	1.176	0.168	0.1097	-0.0091
3	2.74	1.35	1.127	0.160	0.1255	-0.0912	55	1.83	1.96	1.046	0.143	0.1542	-0.0191
4	2.84	1.53	1.125	0.150	0.0978	-0.0074	56	2.40	2.18	1.157	0.157	0.1067	-0.0169
5	1.76	1.59	0.828	0.167	0.3449	-0.2073	57	2.17	2.19	1.083	0.214	0.1202	-0.0173

5.1 Conditional Modelling Approach (CMA) in area 5

Long-term statistics gathers data for a longer time span (years), to include time variations of seaway energy. The Conditional Modelling Approach is adopted to predict the metocean data and values of wave height and periods that may be helpful for further long-term analysis. This Weibull distribution of the wave heights is illustrated in the figure below (using **Matlab**). As we can see from the Figure the distribution of wave heights does follow Rayleigh distribution not Weibull distribution. That may be specific for the area of the operation, while different areas will give different shapes of distribution.

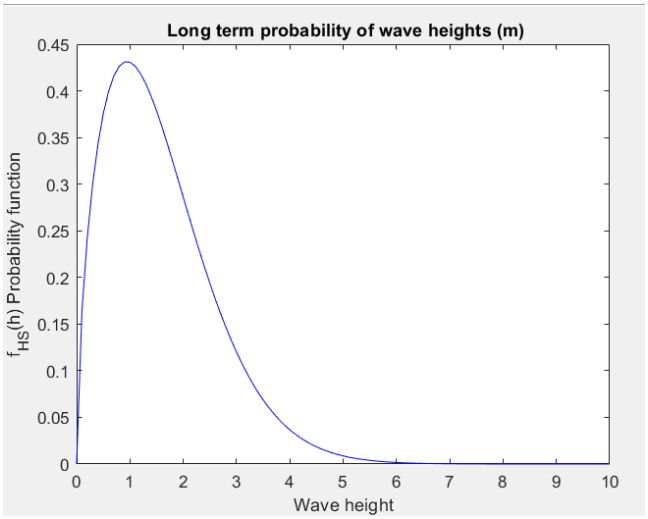

Figure 5-2: Weibull distribution of significant wave height (CMA)

6 Selection of wave spectra

Wave spectrum represents the wave energy (or wave amplitude) distribution of individual wave frequencies in a stationary sea state (frequency domain). There are a large set of standardized wave spectra available in the design standards. However, the most suitable spectra for floating structures are the two-parameter Pierson–Moskowitz (PM) spectra (DNVGL-CG-0130 January 2018), equation (1), and Jonswap (Joint North Sea Wave Project) wave spectra, equation (2) (Hasselmann et al. 1973), which has a sharper peak and applies to the growing waves in continental-shelf waters.

$$S_{PM}(\omega) = \frac{5}{16}.\ {H_s}^2\ .{\omega_p}^4.\omega^{-5}\ .\exp\left(-\frac{5}{4}\left(\frac{\omega}{\omega_p}\right)^{-4}\right) \qquad (1)$$

$$S_J(\omega) = A_\gamma S_{PM}(\omega).\gamma^{\exp\left(-0.5\left(\frac{\omega-\omega_p}{\sigma\,\omega_p}\right)^2\right)} \quad (2)$$

where:

ω wave frequency in rad/sec

γ is non-dimensional peak shape parameter

ω_p spectral peak frequency = $\frac{2\pi}{T_P}$, T_P is the wave peak period

For $\gamma = 3.3$, $T_p = 1.286T_z$; and $T_1 = 1.073T_z$; T_1 is the mean wave period; T_z is the zero up-crossing period.

For $\gamma = 1$, $T_p = 1.405T_z$; and $T_1 = 1.087T_z$.

Otherwise, equation (3) can be adopted to estimate the relation between peak period and γ

σ spectral width parameter; $\sigma_a \; for \; \omega \; \leq \omega_p, \sigma_b \; for \; \omega > \omega_p$.

A_γ is a normalizing factor = $1 - 0.287.\ln(\gamma)$.

$$\frac{T_z}{T_p} = 0.6673 + 0.05037\gamma - 0.006230\gamma^2 + 0.0003341\gamma^3 \quad (3)$$

The wave data collected during the Jonswap experiment show that average values for the γ and σ are $\gamma = 3.3$, $\sigma_a = 0.07$, $\sigma_b = 0.09$. While for $\gamma = 1$, the Jonswap spectrum becomes equal to the PM wave spectrum. In case no particular values are given for the peak shape parameter, γ, Equation **(4)** can be used (DNVGL-CG-0130 January 2018).

Figure below indicates the P-M and Jonswap wave spectrum at $H_s = 3.5$ m and $T_z = 8.5$ sec. It can be observed that T_p varies with different γ values as in equation (3).

$$\begin{aligned} \gamma &= 5 && \text{for} \quad T_p/\sqrt{H_s} \leq 3.6 \\ \gamma &= \exp\left(5.75 - 1.15\frac{T_p}{\sqrt{H_s}}\right) && \text{for} \quad 3.6 < T_p/\sqrt{H_s} < 5 \\ \gamma &= 1 && \text{for} \quad 5 \leq T_p/\sqrt{H_s} \end{aligned} \quad (4)$$

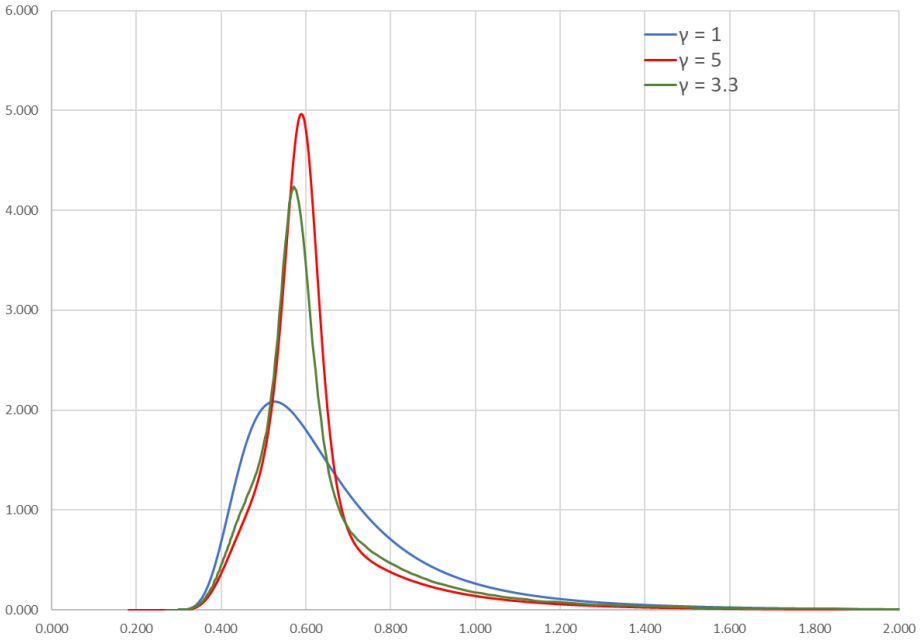

Figure 6-1 Wave spectra for H_s = 3.5 m and T_z = 8.5 sec

For a given sea state (i) a spreading function may be introduced to include the wave spreading (Guedes Soares 1995).

$$m_{ni} = \int_0^\infty \sum_{\theta-\frac{\pi}{2}}^{\theta+\frac{\pi}{2}} f_S(\theta') \cdot \omega^n \cdot S_\sigma(\omega|H_s, T_z, \theta) d\omega \tag{5}$$

where the spreading function is modelled using the cosine-squared approach:

$$f_s(\theta') = \begin{cases} \frac{2}{\pi}\cos^2(\theta'), & \theta - \frac{\pi}{2} \leqslant \theta' \leqslant \theta + \frac{\pi}{2} \\ 0, & \text{otherwise} \end{cases} \tag{6}$$

7 Maneuvering equipment

The maneuvering equipment generally have two coupled tasks to perform. The geometric task and the dynamic task. The geometric task means that the ship has to be able to follow the desired curve or path. This being the route from Lappeenranta to St. Petersburg. The dynamic task is to maintain the desired speed or achieve desired acceleration along the path. The dynamic task in our case is quite advanced since the route involves multiple locks along the path. (Skjetne 2003).

7.1 Propulsion

The ship has single-screw fixed pitch propulsion. The propeller is four-bladed. The propeller diameter was chosen to be 2.5 m based on available space from the centre of the shaft to the keel level with enough clearance. The propeller was chosen to be fixed because of the efficient

revolution controllability of the electric propulsion motors. The total power of main propulsion motors is 1600 kW according to Finnish-Swedish ice class 1C. The ice class rules require 1517 kW and we can assume that the efficiency from motor output shaft through one gearbox and 5 bearings ending at end of the propeller shaft line, is close to 95 %.

The maneuvering at port and locks requires also a bow thrusting equipment, so the ship has one bow thruster. The projected windage area for beam wind is approximately 1000 m^2. According to Wärtsilä (2020), the power of the bow thruster is usually 0.6-0.8 kW/ m^2, so we will choose a bow thruster with power of 600-800 kW. Wärtsilä CT/FT 125 H would be one reasonable candidate. It has power of 614 kW and propeller diameter of 1.25 m.

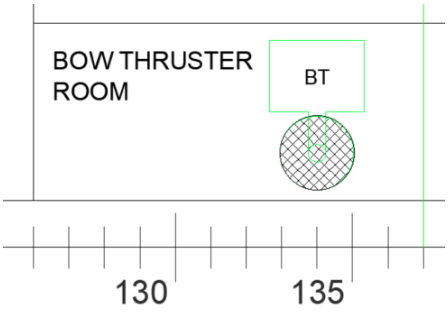

Figure 7-1. Side view of the bow thruster arrangement on Deck 1.

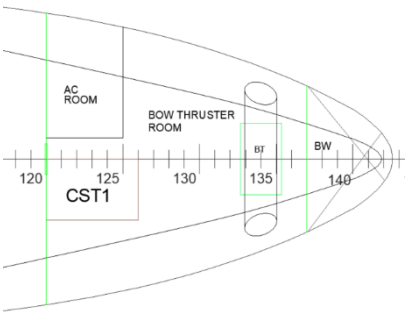

Figure 7-2. Deck view of the bow thruster arrangement on Deck 1.

7.2 Steering

The steering is conducted with one semi-balanced rudder. The steering gear system is placed in steering gear room on Deck 2. Due to the hull form, the steering gear system is placed on bare hull behind the aftmost part of Deck 2.

The minimum projected area of the rudder is calculated with Equation 1. (Rawson & Tupper, 2001).

$$A_R = \frac{T \cdot L_{PP}}{100} \cdot \left(1 + 25\left(\frac{B}{L_{PP}}\right)^2\right) \tag{1}$$

$$A_R = \frac{4.45\ m \cdot 89.13\ m}{100} \cdot \left(1 + 25\left(\frac{12.6\ m}{89.13\ m}\right)^2\right) = 5.95\ m^2$$

We have chosen rudder area of 6.9 m^2 so it is approximately 16% larger than the minimum. Rudder dimensions are 2.4 m x 3.6 m.

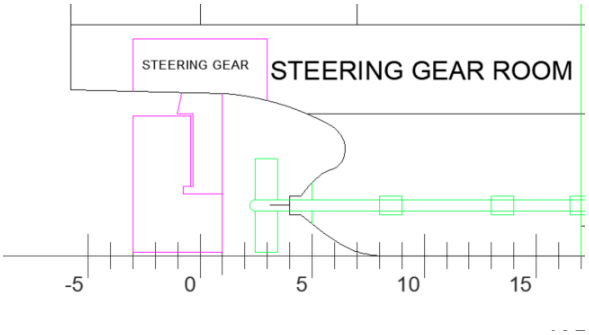

Figure 7-3. Side view of the steering gear and rudder arrangement.

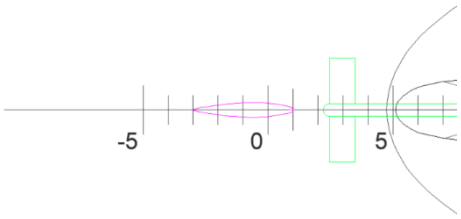

Figure 7-4 Deck view of the rudder arrangement.

8 Saimaa Hybrid Dynamic behavior

There are different parameters that affect the ship dynamics of Saimaa Hybrid. The ship main dimensions have the major contribution in defining the dynamic behavior of the ship. The main particulars that considerably impact on the dynamic behavior refer to the ship length, breadth, draft, L/B ratio, B/T ratio in addition to the hull form coefficient as block coefficient and prismatic coefficient.

The longitudinal, vertical and transverse center of gravity together with the ship displacement have a remarkable effect on the dynamic behavior of our vessel as it affects the radius of gyration and inertia.

8.1 Ship length

Ship length is the main parameter that affects the behavior of ships in heading seas. The worst structural response happens when the ship length equals the wavelength. The max hogging and sagging occur when the ship length is stationary or stabilized on wavelength equals the ship length. When there is a crest at amidships the buoyancy at the midship is larger than the buoyancy at the ends of the ship which causing maximum hogging moment amidship. While maximum sagging when the ship has a trough amidships, hence the ship will gain buoyancy at the forward and aft part and loses buoyancy amidships which in consequence will cause sagging moment. The sagging moment is usually more dangerous than the hogging because the added buoyancy from fine stern and bow is usually larger the lost buoyancy in hogging, assuming that the change of the ship has parallel middle body amidship, see *Figure 8-1*.

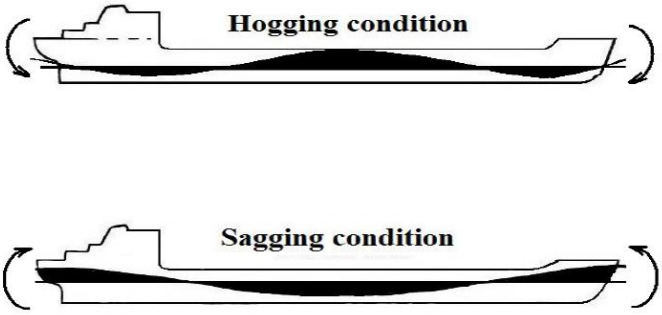

Figure 8-1 Worst structural response in head seas.

8.2 Ship breadth

Ship breadth considerably affects the rolling motion of the ship. Hence in beam seas the most effective parameter is the ship breadth. Dumbing the excessive rolling motions by increasing the ship breadth or using passive and active tank stabilization, fin stabilizer or bilge keel is sometimes essential to prevent capsizing of the vessel. Therefore, when the ship sails in sea states that contains large probability of wave lengths near the natural rolling frequency, the ship master should avoid these beam waves as possible, otherwise the vessel may be lost.

Figure 8-2 illustrates the response of the ship in different wave conditions. It can be overserved that the maximum response in head seas is at wave length equals to the ship length while the worst response in beam seas occurs in very small wave periods near the rolling natural frequency.

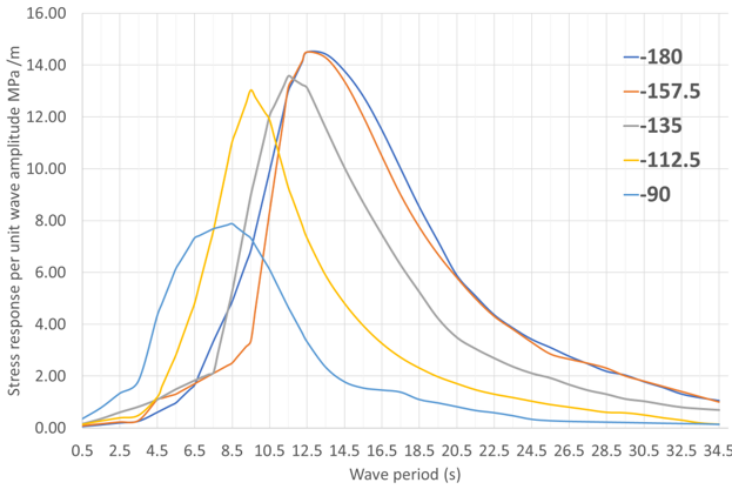

Figure 8-2 ship response of a tanker ship in different wave heading conditions (Ship length =240m breadth = 43 m).

8.3 Block coefficient

The block coefficient is an important parameter that highly affect the vertical bending moment and heave motions. The higher the block coefficient, the higher the induced wave bending moment as can be observed in the figure below. It can be observed that the vertical bending moment is almost tripled due to an increment of the block coefficient from 0.45 to 1. While the heave motions RAOs is significantly reduced with increasing the ship block coefficient.

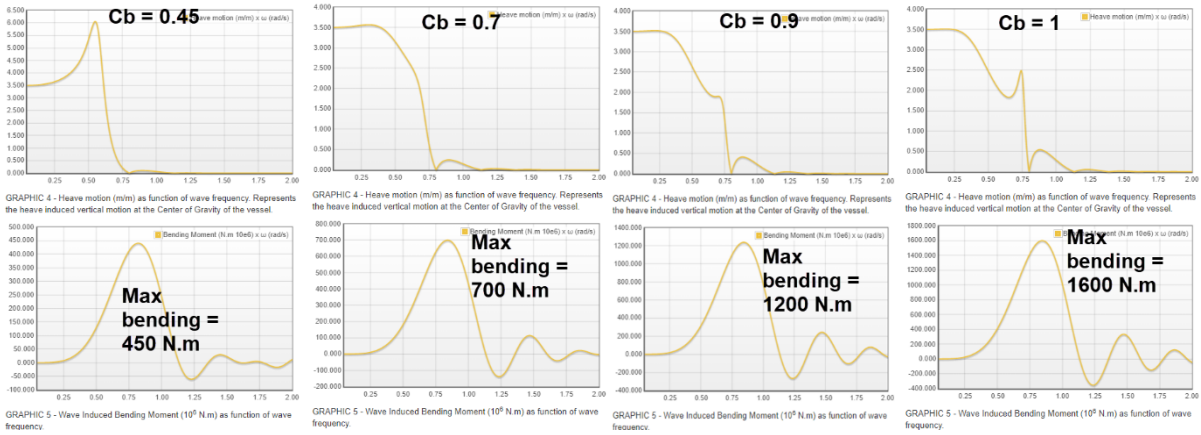

Figure 8-3 Heave motions as a function of wave amplitude and vertical bending moment as a function of wave frequency for 3 different block coefficients with the same length, breadth and displacement. (shiplab.hials.org)

8.4 Bow and stern shape

The shape of the bow and stern have considerable impact on the slamming loads and in consequence the springing and the whipping loads. The slamming loads originate mainly from the heaving and pitching motions (usually in head seas) due to the continuous in and out motion of the bow and stern from the water. It is highly affected by the forward speed and the shape of the bow and also the stern. The flat bottom near the forward part increases the impact of slamming.

The slamming load is a nonlinear phenomenon that is highly sensitive to the ship motions and contact angle between the ship and the free surface. The period of slamming impact is very short and therefore it only can be studied using the hydroelasticity theory, which considers the hull deformation due to impact of slamming loads.

There are 4 main types of slamming loads:

- Bottom slamming: due to the impact of flat bottom with the free surface. See *Figure 8-4*
- Bow-flare slamming due to the relative motions between the bow flare and the free surface. This phenomenon will occur in Saimaa Hybrid due to its flare bow
- Breaking wave impacts are type of slamming; these impacts loads occur when the ship breaks encountering waves. The superposition of the bow waves and the incident waves represent the breaking wave impacts.
- Stern slamming is similar to bottom slamming, occurs when the ship stern hits the free surface. As Saimaa Hybrid has transom stern, this type of slamming is expected
- Wet deck slamming, usually happens in catamaran when the free surface hits the deck between the hulls. It is not important in our case.

Figure 8-5 illustrates the increment of wave induced loads due to slamming effect. It can be distinguished from the regular bending moment in waves by its short period. Therefore, the slamming impact increases the maximum bending moment and should be considered in the ultimate strength analysis.

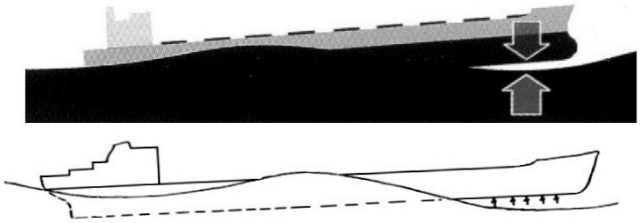

Figure 8-4 Bottom slamming.

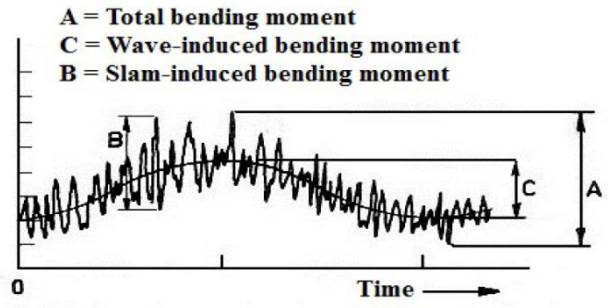

Figure 8-5 Increase in range of wave bending stresses due to slam-induced stresses.

9 Numerical investigation of the hydrodynamic loads and the stress response

The most common numerical tools for obtaining the hydrodynamic response of a large volume structure in waves is the three-dimensional panel method which is based on fluid potential theory (Li et al. 2016). ANSYS Aqwa uses that concept to solve a set of linear algebraic equations to obtain the harmonic response of the body to regular waves.

Another crucial and simple method is the Strip theory which is a frequency-domain method. The main advantage of employing this method is the reduction of the computation time considerably. However, the method generally becomes limited to computing the linear vessel response. The vessel is divided into a number of transverse two-dimensional sections to compute its hydrodynamic characteristics. The coefficients for the sections are then integrated along the length of the hull to obtain the global coefficients of the equations of motion of the whole vessel. Finally, the coupled equations of motion are solved (Bentley Systems 2018). Both methods, panel method and strip theory, can be employed in Maxsurf Motion to predict the motion of the vessel.

(Li et al. 2016) investigated the short-term vertical wave-induced bending moment of a container ship (4250 TEU) using ANSYS Aqwa. The long-term wave bending moment corresponding to different probabilities of exceedance was obtained based on the long-term statistics of the North Atlantic Ocean. They validated the numerically estimated wave induced vertical bending moment RAOs, for different forward speed in the frequency domain by comparing it with the experimental results of lee et, al. (Lee et al. 2011). The numerical results were fitted well with the model tests as shown in *Figure 9-1* (Li et al. 2016). Moreover, the numerical wave vertical bending moment corresponding to 10^{-8} probability of exceedance was almost equal to the long-term wave bending moment of DNV Classification Rules (Veritas 2009).

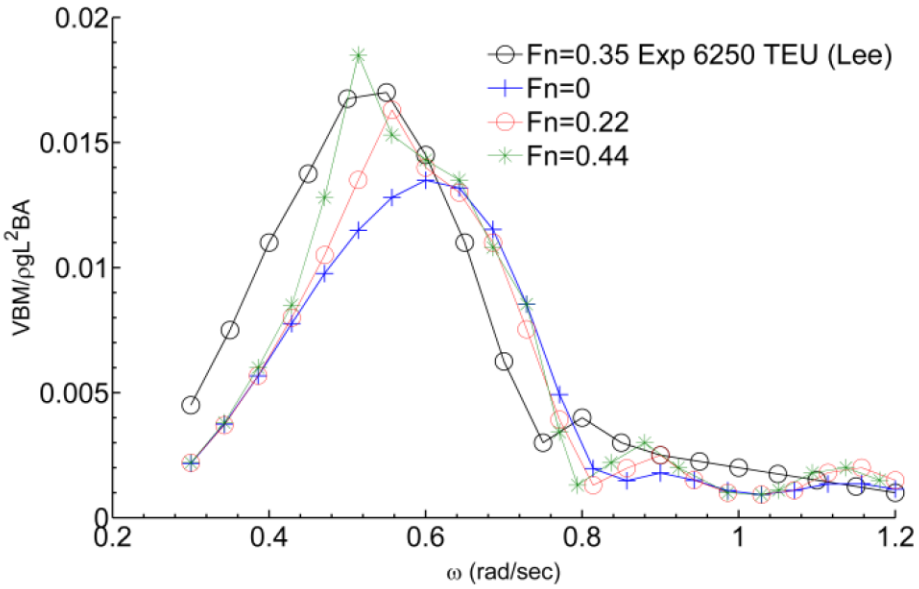

Figure 9-1 the correlation between bending moment at different forward speeds and the experimental values by Lee et al., (2011).

Aqwa also has been used in a wide application for transferring the hydrodynamic pressure to the finite element model for further structural analysis. Wallnöfer (2015) has assessed the global structural strength of a semi-submersible according to classification society rules and guidelines using ANSYS AQWA and Ansys Mechanical. The analysis procedure is divided into two main steps; hydrodynamic analysis to obtain the RAOs and the design waves, and mapping of the hydrodynamic loads on the structural model for evaluating the stress response. For the hydrodynamic analysis, the author modelled the external hull surface in SolidWorks and imported it to ANSYS modeler via Parasolid. The element size is chosen to depict the geometry of the outer hull properly for hydrodynamic analysis in Aqwa. The highest obtained wave frequency in Aqwa, which is based on the element size, was 2.2 Hz. As the element shape is very important for the diffraction analysis, attention was paid to stay within the element growth rate and warping limits. The structural steel parts are modelled as beam and shell elements. The tank items were modelled in the FE model as point masses on the nodes of the tank's boundary structural shell elements. The results of the hydrodynamic diffraction analysis, RAOs, were compared with the results given in the tank model tests. The results generally are in good agreement with the measured data; especially for the relevant motions of heave, roll and pitch, the agreement was excellent. Finally, the hydrodynamic pressure was mapped on the finite element structural model and the stress response was investigated as illustrated in *Figure* 8.

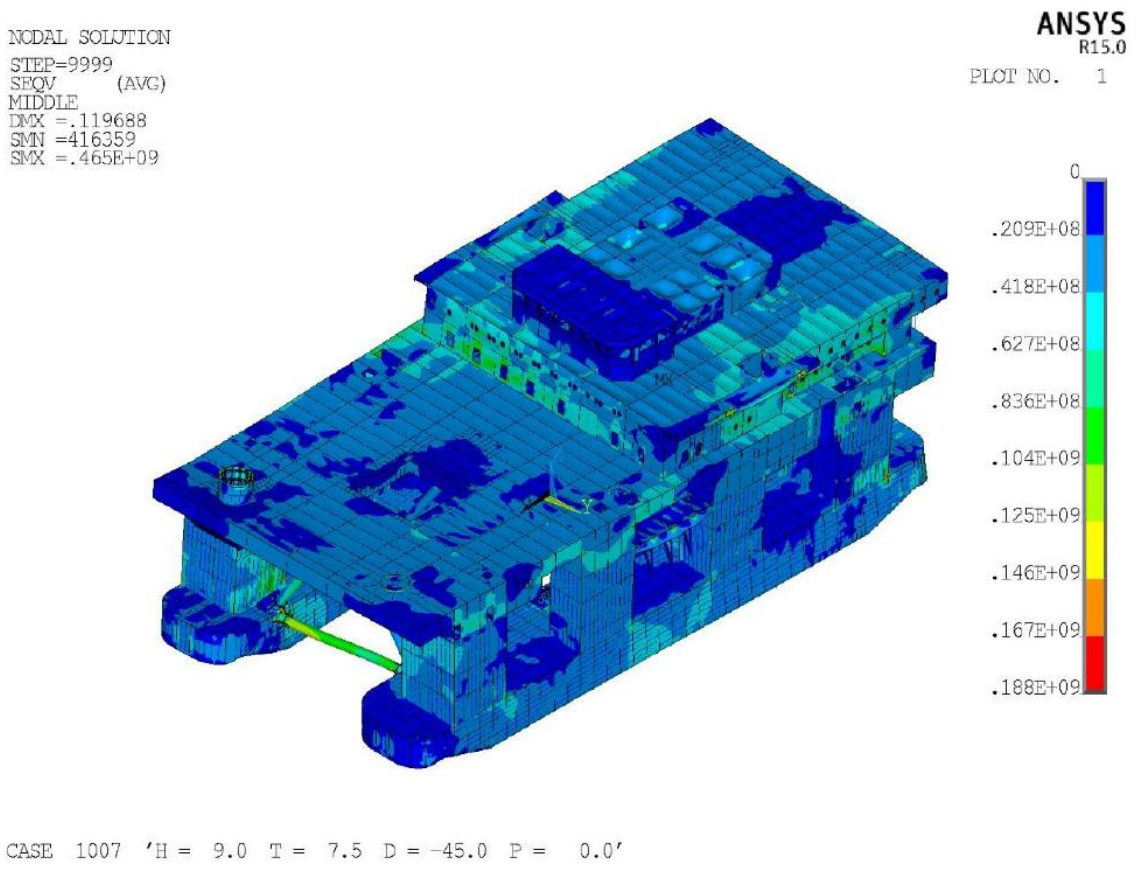

Figure 9-2 equivalent stress results of the global finite element model.

9.1 Hydrodynamic software

The available hydrodynamic or seakeeping software in the market focuses on the prediction of ship response in a predefined sea condition using different hydrodynamic theories. Examples of such software are MAXSURF motions, MOSES motions, SACS motions (Bentley Systems 2018), ANSYS Aqwa (ANSYS 2013) and in addition to some software programs developed by classification societies, specifically for offshore and ship structures, such as FD Waveload by Lloyd's Register (LR 2020) and Hydrostar by Bureau Veritas (2020a) and Sesam by Det Norske Veritas Germanischer Lloyd (2020b). The features of such software differ from one to another. Such software can calculate the ship motions, Response Amplitude Operators RAOs, panel pressures, drift forces, wave forces, added mass, damping, etc. ANSYS Aqwa, which is vastly used in the offshore industry.

9.2 Bilge-Keel Influence

As stated previously, the ship will frequently operate in wave conditions. The article "Bilge-Keel Influence on Free Decay of Roll Motion of a Realistic Hull" by Jiang et al. 2014 presents a method for evaluating the roll motion characteristics with bilge keels with different spans on a ship hull. The research simulated two-dimensional floating bodies.

The stability of the ship is directly connected to its roll motion and the natural period of roll is designed to be away from the period of the higher energy of the wave spectrum. The effect of the bilge keel is based on formation and shedding of vortices. The vortices significantly affect the roll damping and the evolution of the roll response of the ship.

The research evaluated four different bilge keel span lengths and it was found that a larger bilge keel generates stronger counter-rotating vorticity pairs resulting in stronger damping effect. The effect transfers the more energy to the surrounding flow the larger the span length is.

In Saimaa Hybrid's case, the bilge keel might be the most relevant roll-damping system since it would be highly maintenance-free and inexpensive to build. The wave height of the route of the Saimaa Hybrid is relatively small compared to other common routes of Baltic Sea.

10 Maneuvering in shallow water

Paper called "Maneuvering in Shallow and Confined Water" by Vantorre et al. (2017) discusses the shallow water effects. Big portion of our design route is covered in the shallow waters of the Saimaa canal. The water depth to draft ratio affects the ship's maneuverability. The effects are very significant in shallow water ($1.2 < h/T < 1.5$) and the effects completely dominate the behavior in very shallow water ($h/T < 1.2$) (Vantorre et al. 2017). The water depth to draft ratio in our case falls under these two categories, so it is only logical to study and assess the effects of the shallow water. Different h/T ratios for our ship are presented in meters in the table below.

Depth	**Meters**
Deep	> 13.4 m
Medium deep	6.7 m – 13.4 m
Shallow	5.3 m – 6.7 m
Very shallow	< 5.3 m

The pressure distribution around the hull can change notably in shallow waters causing increased hydrodynamic forces. This will increase the ship's resistance and also decrease the maneuverability (Vantorre et al. 2017). This negative effect on the maneuverability is quite critical since the canal is very narrow already. This inevitably leads to slower speeds in order to be able to operate safely. The canal has graduated speed limit based on the draft. Most likely the negative effects of shallow waters have been considered.

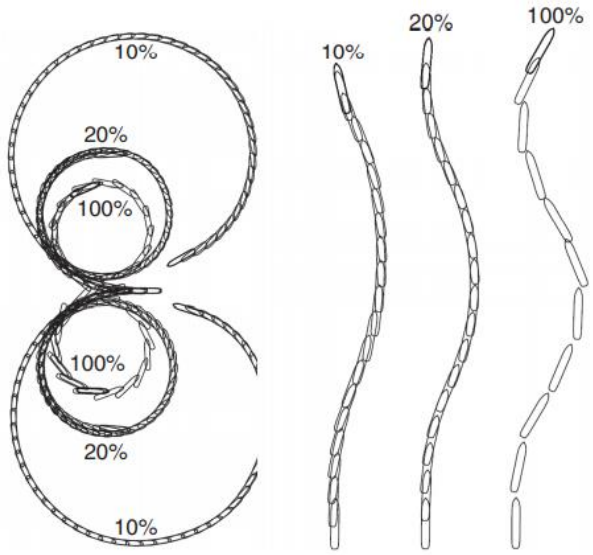

Figure 10-1 Effect of under-keel clearance on turning radius and on zigzag maneuver (Vantorre et al. 2017)

The effect on turning radius and directional stability is illustrated in the figure above. Here the under-keel clearance (UKC) is represented as percentage of the draft. From the figure we can observe that the effect on the turning radius is overwhelming when operating in shallow waters. The turning radius increases significantly at lower UKC. Decreasing UKC from 20% to 10% increases the turning radius considerably more than decreasing UKC from 100% to 20%. On the other hand, we can observe a beneficial effect during zigzag maneuver. The course-checking ability of the ship is improved, and the overshoot angles have become smaller. According to Vantorre et al. (2017) the maneuvering characteristics can differ for certain ship types. During the zigzag maneuver, the overshoot angles can increase instead of decrease in medium water depth ($1.5 < h/T < 3.0$). In some cases, even the turning circle can get smaller. This implies that full-scale or model-scale tests have to be performed in order to fully understand the behavior in shallow waters. The typical behavior shown in the figure is not always the case.

10.1 Bank effects

The narrow Saimaa canal portion of the route will introduce bank effects. Confined waters have an impact on the pressure field around the hull, which then affects the hydrodynamic forces and moments acting on the hull. Typically bank effects can be seen when the ship is operating in asymmetric area with respect to the trajectory. In symmetric canal the ship will only see increased resistance. (Vantorre et al. 2017). The former case relates to our route and therefore bank effects are introduced.

In the asymmetric area, the flow around the hull will also cause an asymmetric pressure field. This pressure field will create lateral force and yawing moment. The flow velocity on the nearest bank side is greater than on the other side. According to Bernoulli's law, this will result in smaller pressure and therefore decrease the water level more on the bank side. The resulting force pushes the ship towards the bank. This effect is known as "bank suction". (Vantorre et al. 2017).

On top of that, there are differences at the stern and bow areas of the ship. Often the pressure is lower at the stern. Now the bank suction is accompanied by yawing moment. As a result, the stern is getting closer to the bank and the bow away from the bank (bow-out moment). (Vantorre et al. 2017).

Noting these effects is of great importance from the safety perspective. As mentioned previously in chapter 2.2, the water depths are very shallow in the canal. The water depth can decrease significantly when deviating from the path. Since our under-keel clearance is on average ~15%, this can quickly lead into grounding.

11 Description of sea states

In the 1968 article by Walter H Michel titled "Sea Spectra Simplified" the content was reviewed and reflected against the project ship for Saimaa Ferry. The scientific text articulates the pertinent factors to developing sea spectrum and illustrates the differences between different wave theories by summarizing the different experiments that have been executed in the previous decades.

The main takeaway from the article is that the sea is irregular and does not produce uniform waves of constant height and length and as such there are mathematical approaches to approximating the impact on a vessel, but one must know the topics that are important for each

problem. Wave spectrum is defined as the distribution of energy throughout the sea of a defined area [Michel 1968] and there are several classical approaches to defining the probability of a wave of certain size depending on several factors, such as wind speed, wave height, significant wave period, and significant wave height. The oldest and earliest way that waves were specified is Neumann's spectrum and is shown below in equation (2).

Neumann's spectrum (*the* classic).

$$2h^2(\omega) = 400/\omega^6 e^{-725/V_k^2\omega^2} \tag{2}$$

and the area

$$H_s^2 = 1.9V_k^5/10^5$$

After presenting Neumann's spectrum, the article shows the weaknesses of this approach and postures several other approaches that are relevant to understanding the ways in which waves are developed [Michel 1968]. In order to understand the forces on a ship at sea the region with environmental properties must be considered but even once the factors are considered, the randomness and simplifications that are chosen can either make the prediction good or not useful and without verification, it is difficult to have confidence for all conditions. The article states that the best philosophy to adopt to think about mathematical prediction is the ISSC formula and the most practical formula is the Bretschneider's spectrum. Both of these are shown below.

Bretschneider's spectrum. Which is derived on the premise that the wave period follows a Rayleigh distribution, as does the wave height.

$$2h^2(\omega) = 4200H_s^2/T_s^4\omega^5 e^{-1050/T_s^4\omega^4} \tag{3}$$

ISSC Spectrum. The International Ship Structures Congress' modification of the Bretschneider form:

$$2h^2(\omega) = 2760H_s^2/T_s^4\omega^5 e^{-690/T_s^4\omega^4} \tag{4}$$

where

H_s = significant wave height (average of the one-third highest waves)

T_s = "significant period," actually the average period of the significant waves

The reason why the ISSC spectrum is the best philosophy is that it averages waves from different regions and prevents super specific predictions that could be correct but generally not useful for the main structural requirement calculations or stability/roll designs. The most practical is stated as the Bretschneider's because it uses the wave height instead of the significant wave height. The significant wave height is a calculated by recording the wave heights of a given area and then taking the tallest 33% of the waves and using this for spectra calculations [Michel 1968]. Other methods are shown in figure 28 below for how others have attempted to quantify the value of sea wave heights.

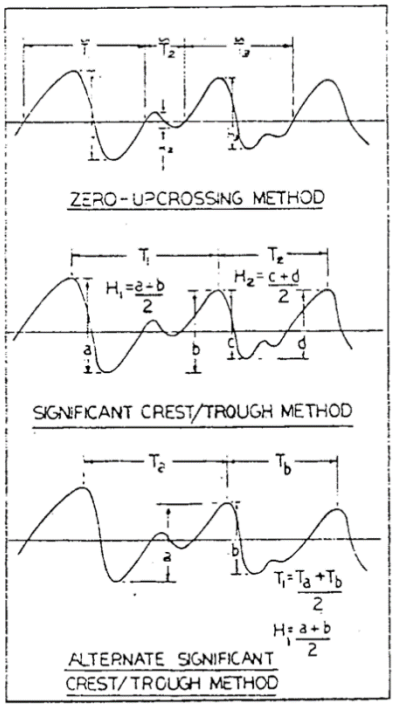

Figure 11-1*: Wave Analysis Methods*

The impact of this article is that with better knowledge of the important factors for wave forming theories, better decisions can be made in terms of preparations for wave loading with the maneuvering equipment and internal structures. Saimaa Ferry is not anticipated to experience the worst wave loading conditions, but it is good to understand that if the mission changes or increased operational area is desired then these calculations may need to be revisited.

12 Equations of motion

12.1 Theory behind equations of motion

The ship equation of motion in regular waves is presented below.

$$(a + m)\ddot{x} + b\dot{x} + cx = F_0 \sin(\omega t)$$

Where term a is related to added mass, m to structural mass, b to hydrodynamic damping, c to stiffness and $F_0 \sin(\omega t)$ to sinusoidal excitation.

The left-hand side of the equation of motion represents the dynamic properties of the ship. Thus, it also represents the forces on the ship when forced to oscillate in still water conditions. The right-hand side of the equation of motion represents the forces on the ship when restrained from motion and is a subject to regular waves.

Hydrodynamic forces are provided due to effects of hydrodynamic damping and added mass. They are due to pressure distribution around the oscillating hull. The hydrodynamic forces needed to obtain the coefficients for equations of motion are radiation forces/moments, incident wave or Froude – Krylov forces/moments and diffraction forces/moments. Radiation forces/moments occur as the ship is assumed to oscillate in still water. From this, the hydrodynamic added inertia and damping coefficients are determined. Incident wave or Froude – Krylov forces/moments occur as the wave is considered in the absence of ship. The

corresponding wave forces or moments acting on the ship are determined from this. The diffraction forces/moments where the effects of presence of the ship on waves are considered. From this, the corresponding diffracted wave forces/moments are determined.

The coupled motions of heave – pitch and sway – roll – yaw can be examined separately during seakeeping analysis for a ship with port-starboard symmetry. Heave, pitch and roll have a restoring force or moment, while sway does not.

Naturally, the total mass of the ship consists of the structure, cargo, equipment, passengers etc. Mass distributions couple with global ship motions and local actions such as sloshing liquid in tanks and openings like swimming pools. Added mass relates to the motion of fluids along with the ship and represents the amount of total fluid accelerated by the object. Damping is loss of energy that is caused by ship-induced waves that decay at some certain distance away from the ship. Damping can be controlled by appendices.

12.2 The main components associated to equations of motions of the ship

The main components affecting the equations of motions are present whenever the ship is moving and under non-calm weather conditions. The ship is moving with the effect of propulsion equipment and changes its direction with steering equipment. Propulsion and steering affect mainly the surge, sway and yaw motions.

As the ship proceeds in waves, the heave, pitch and roll motions have a greater part in the equations of motion compared to operation in calm weather.

The change of deadweight has an effect to equations of motion. In Saimaa Hybrid, the greatest added mass will be gained when the ship is loaded with cargo along the passengers. The ship has a cargo capacity of 950 tonnes, so the difference between cargo loaded and unloaded condition is over 25 % of the displacement. The effect of varying amount of passengers is less significant.

The operational safety has to be considered more carefully when the ship is fully loaded. The speed of the ship combined with fully loaded condition has greater effect on equations of motions.

12.3 GA, hull form & operational profile effect on equations of motion

The features of the General Arrangement (Appendix 2) affect the equations of motion of the ship via the mass distribution. As the righting lever (GZ) depends on ship's weight distribution, the General Arrangement defines a significant part of the effect. Placing heavy objects on the lower decks will bring the ship's center of gravity lower, thus increasing the metacentric height (GM). If the GM is very high, excessive accelerations may occur that decrease safety. Regarding our ship, the GM value is somewhat low, so excessive accelerations should not occur. The tanks located at double bottom and Deck 1 may experience e.g. sloshing, and thus affect the equations of motion. The free-surface effect has been attempted to be minimized by dividing the tanks into smaller individual compartments.

The hull form of the ship has an effect to the hydrodynamic forces. The breadth of the ship has a great effect to the righting lever. The breadth of Saimaa Hybrid is close to a likely appearing wave length in operational area.

As can be seen in Figure , the operational profile follows mainly two different operation speeds. The speed of 4.5 knots is used in the canal and maximum of 12 knots is used at sea.

13 Simplifications of seakeeping analysis methods

Level of idealization for forward speed hydrodynamic solutions are divided into 6 different levels as presented in the figure below. Level 1 is the linear method while Levels 2-6 are non-linear methods.

Figure 13-1 Level of idealization for forward speed hydrodynamic solutions. Figure from course notes.

13.1 Simplifications of linear seakeeping analysis methods

Seakeeping analysis is mainly a three-part challenge as the likely environmental conditions (wave spectra), response characteristics of the ship and the criteria used to assess the ship's seakeeping behavior need to be solved and specified. Strip theory and panel methods are used to obtain the needed forces.

For linear strip theory, many basic assumptions are made.

Fluid is inviscid
Viscous damping is mainly ignored or used independently with an empirical coefficient related to roll damping
Ship hull is rigid – no flexure of the hull
Small motions or linear with wave amplitude at least
Speed is moderate and there is no planing lift
Ship is slender meaning that L >> B or T. Beam is also much less than the wave length
Hull sections are wall-sided
Deep water wave approximations are used meaning that water depth >> wave length
Presence of the hull does not effect the waves

Panel method requires lots of computing time. Green's function is needed to solve the unknown source strengths. Especially the forward-speed version of the Green's function is very time consuming. Thus, it is important to use the most suitable Green's function related to water depths and wave lengths.

13.2 Simplifications of non-linear seakeeping analysis methods

Methods for non-linear seakeeping analysis are more complex and slower than the linear ones.

Froude-Krylov (Level 2)	- Moderately fast computations - Disturbance potential determined similarly as in Level 1 -
Body non-linear (Level 3)	
Body exact (Level 4)	
Smooth waves (Level 5)	
RANS (Level 6)	

Level	Description	Key features	Additional comments
1	Linear	• The wetted body surface is defined by the mean position of the hull under the free surface • The free surface BC are applied in way of the internment wetted body surface • Hydrodynamics are solved in FD by strip theory or BEM using a range of GFM	• Computations are fast • Viscous forces are not part of the solution and must be obtained by other methods, if important or required • The boundary integral methods cannot handle breaking waves, spray and water flowing onto and off the ship's deck.
2	Froude–Krylov NL	• The disturbance potential is determined as in Level 1 • Incident wave forces evaluated by integrating incident wave and hydrostatic pressures over the wetted hull surface • The wetted hull surface is defined by the instantaneous position of the hull under the incident wave surface • Hydrodynamics are solved in FD or TD by GFM and convolution integrals are used for memory effects	• Computations are moderately fast • NL modification forces can be included in addition to Froude–Krylov and restoring forces to account for slamming and green water
3	Body NL	• The disturbance potential is calculated for the wetted hull surface defined by the instantaneous position of the hull under the mean position of the free surface.	• Computations are slow since re-gridding and re-calculation of the disturbance potential for each time step is required.
4	Body exact	• The disturbance potential is calculated for the wetted hull surface defined by the instantaneous position of the hull under the incident wave surface • The disturbed, or scattered waves, caused by the ship are disregarded when the hydrodynamic boundary value problem is set up • The scattered waves are considered small compared to the incident waves and the steady waves	• Computations are mathematically complex and slow. This is because common CFM satisfies the free surface condition on the mean free surface and not on the incident wave surface.
5	Smooth waves	• Scattered waves are no longer assumed to be small, and they are included when the boundary value problem is set up. • In MEL methods the Eulerian solution of a linear boundary value problem and the Lagrangian time integration of the nonlinear free surface boundary condition is required at each time step. • Wave breaking or fragmentation of the fluid domain is ignored.	• Computations are typically forced to stop based on a wave breaking criterion. • The stability of the free surface time-stepping can cause numerical problems
6	Fully NL	• The water/air volume is normally discretised, and a finite difference, finite volume or a finite element technique is used to establish the equation system. • Particle methods, where no grid is used, can be applied to solve the Navier–Stokes equations. Examples are the Smoothed Particle Hydrodynamics (SPH), the Moving Particle Semi-implicit (MPS) and the Constrained Interpolation Profile (CIP) methods, with the latter believed to be more suitable for violent flows.	• Mathematics and computations are complex • There is no unification in the approaches used to solve sea-keeping problems, hence extensive efforts for validation of solution and the benefits of practical implementation are necessary.

14 Numerical estimation of ship motion

As mentioned earlier, the most common numerical tools for obtaining the ship motions and different hydrodynamic responses in waves are the strip theory, panel method and the three-dimensional panel method which is based on fluid potential theory (Li et al. 2016). Maxsurf and NAPA use both strip theory and panel method to obtain the motion and loads response. ANSYS Aqwa uses the later concept to solve a set of linear algebraic equations to obtain the harmonic response of the body to regular waves. It is intended to use ANSYS AQWA. Here it is intended to use the 3 mentioned software to solve and compare between the results, especially, the Maxsurf and Napa may be affected by the dynamic damping rolling coefficient of the system which is not common in AQWA.

The Strip theory used in NAPA and Maxsurf is a frequency-domain method. The main advantage of employing this method is the reduction of the computation time considerably. However, the method generally becomes limited to computing the linear vessel response.

14.1 NAPA

In NAPA, seakeeping analysis can be done using strip-theory or panel method. In the strip-theory, the solution for the added mass and the damping coefficients are based on the assumption of ship slenderness. This means that there is no flow generated lengthwise. This allows the wetted hull to be divided longitudinally into cylindrical segments. In the panel method the surface is covered with planar facets (Figure *14-1*). The panels have constant source strength, which is solved using boundary conditions.

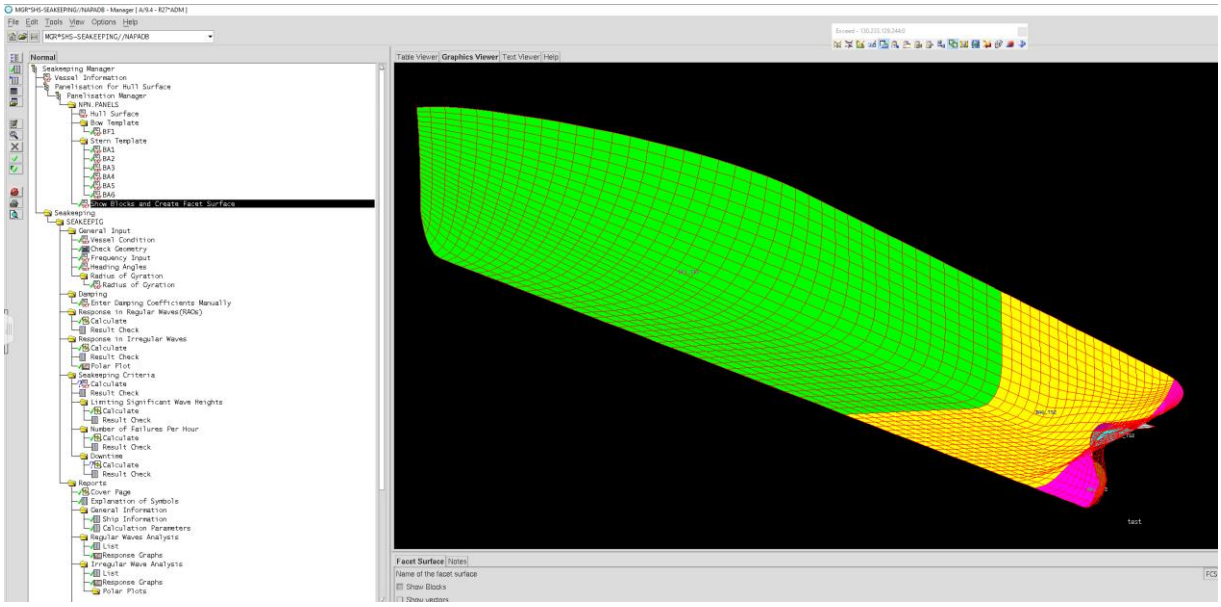

Figure 14-1 Seakeeping analysis using panel method

In general, the equations of motions are solved by generating a small, sinusoidal, oscillating pressure on the hull. This generated hydrodynamic force is then divided into parts which are in phase with the acceleration and velocity of the vessel. These represent the added mass and the damping seen in the equations of motion. The excitation force can be solved with direct calculation from the pressure induced by the wave or derived from the added mass and damping coefficients (depends on the method). Finally, the motions are calculated for each degree of freedom by transposing the coefficient matrices. As a result, Response Amplitude Operators (RAO's) are obtained (see figure below), which are functions of frequency. It is worth mentioning that the damping is often nonlinear and requires nonlinear methods to be solved accurately. The strip theory and the panel method both use linear methods to approximate the damping. Nonlinear, one-degree of freedom roll equation exists in NAPA, which can be used to solve roll amplitude for beam seas.

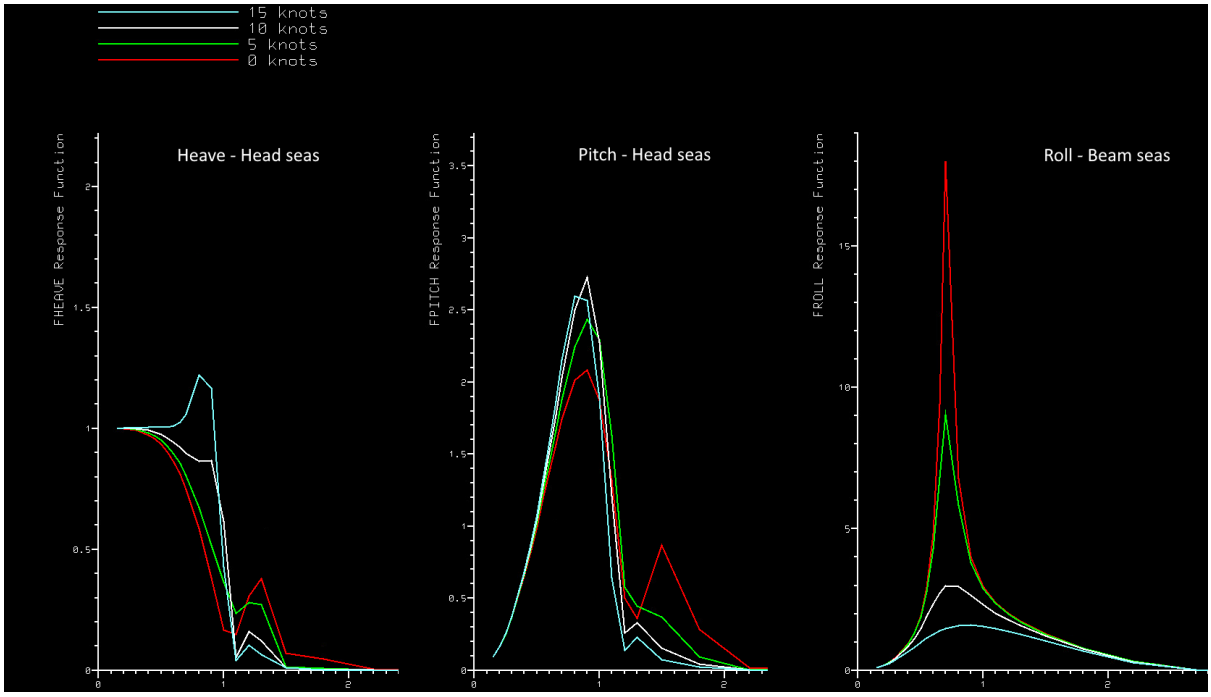

Figure 14-2 Response Amplitude Operators for heave, pitch and roll motions

14.1.1 NAPA parameters & results

For the seakeeping analysis, the panel method was used to obtain all six degrees of motion. What this essentially means is that we have to define the panelisation of the hull, radius of gyration and damping coefficients to obtain the response amplitude operators. After that, the motions can be defined with the help of wave spectrum.

The hull surface was divided into panels as shown in Figure 14-1. The bow section (green) and the aft section (yellow and pink) consists of 950 and 800 panels respectively, resulting in total of 1750 panels. This division should give reasonably accurate results with acceptable computational time. For the radius of gyration, the default settings of NAPA were used, so that the roll gyradius is defined as 40% of the breadth, pitch and yaw gyradius as 25% of the length. With specific loading conditions, more accurate gyradii can be obtained. Finally, the damping coefficient was defined using linear roll damping coefficient as a fraction of critical roll damping (default setting in NAPA). The resulting main response amplitude operators are shown in Figure *14-2 Response Amplitude Operators for heave, pitch and roll motions*. For the final motions in irregular seas, Pierson-Moskowitz spectrum was selected (see Chapter 6.) with significant wave height of 1 meter. The reason behind this wave height is the assumption that the responses are linear. To get the response in different wave heights, the results may be simply multiplied by the chosen wave height (according to NAPA manuals). The results for speed of 0 and 5 knots are shown in Figure 14-3 and Figure 14-4 respectively. It should be noted that NAPA plots the results against zero crossing period instead of frequency in rad/s. The axis can be converted by dividing 2pi with the crossing period.

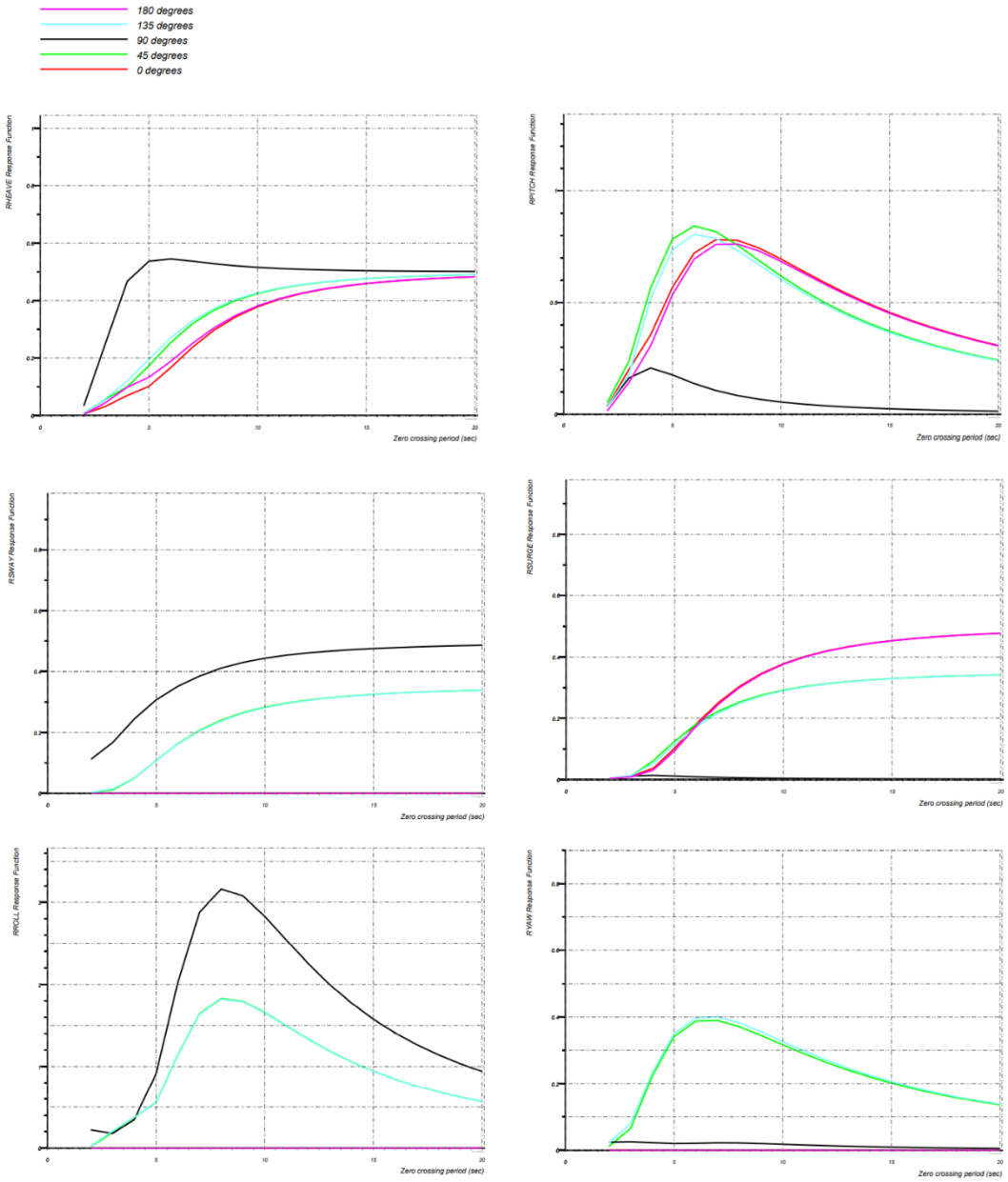

Figure 14-3 Response in irregular seas for all 6 degrees of freedom in different headings (significant wave height of 1m, ***speed 0 knots****)*

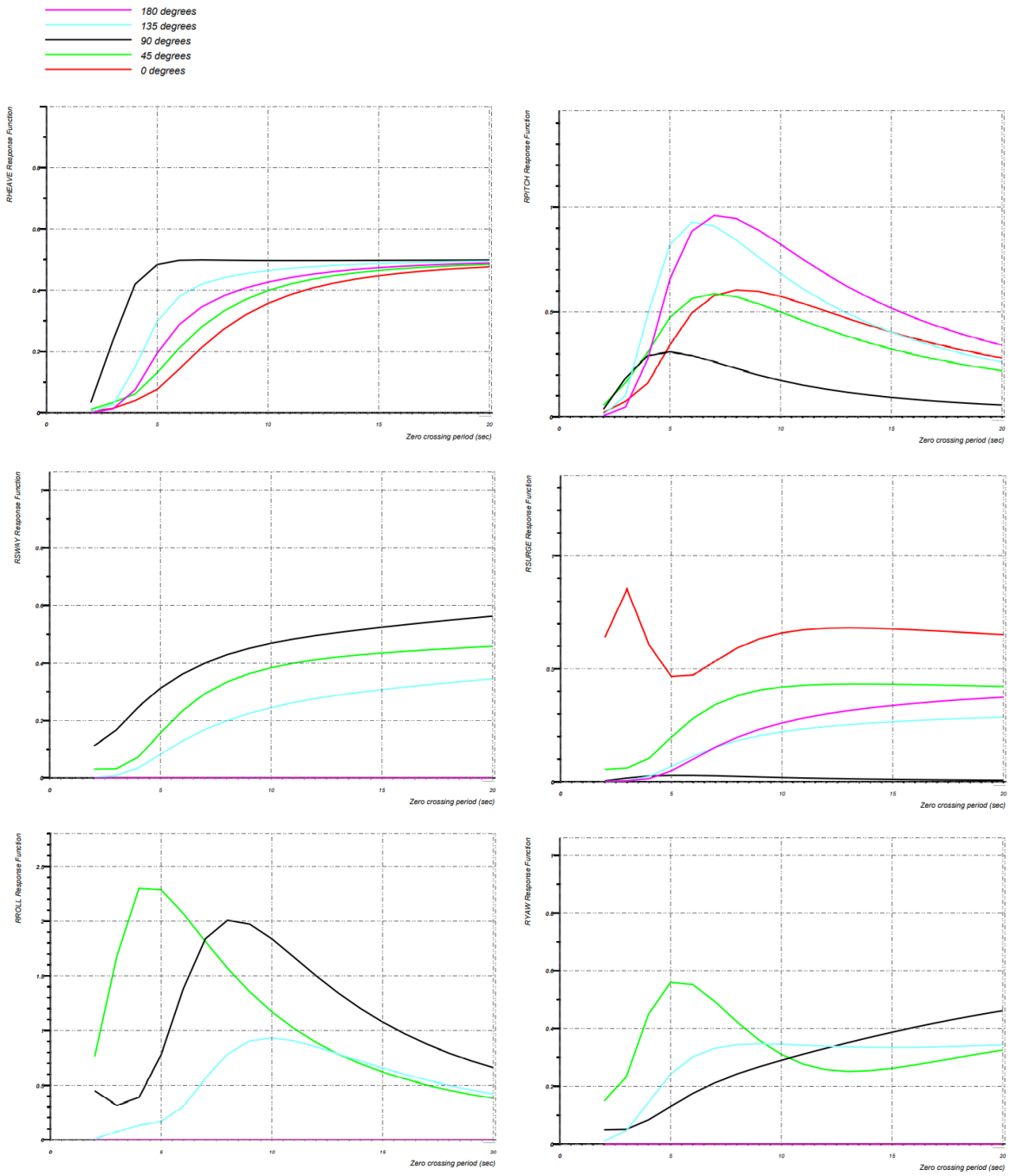

Figure 14-4 Response in irregular seas for all 6 degrees of freedom in different headings (significant wave height of 1m, ***speed 10 knots****)*

The roll, pitch and heave motions could be argued to be the most important ones, and thus we will focus on them. The results indicate that in the worst sea conditions the vessel can encounter (5m significant wave height):

- With zero forward speed, the roll response is around 16 degrees (3.2 deg for 1m wave height). This response should fall under the acceptable limit.
- Pitch of 5 degrees in head seas with forward speed of 10 knots.
- In heave, we can observe motions of 2.5 meters

NAPA was also used to estimate the wave-induced bending moment and shear force. The maximum speed of 12 knots was used in the estimations.

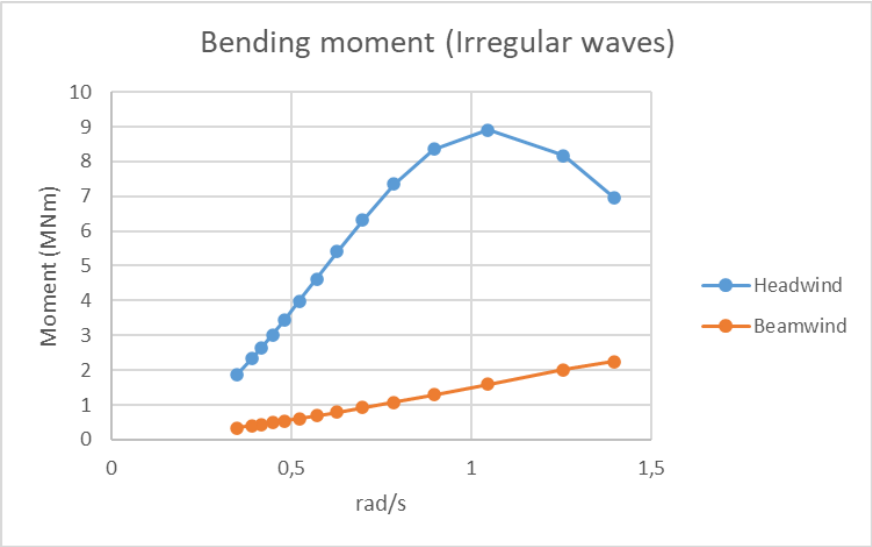

Figure 14-5 Bending moment in irregular waves (NAPA)

Figure 14-5 shows an estimation of the bending characteristics of the vessel in irregular waves with heading of 180° and 90°. As can be seen, the maximum bending moment is reached approximately at the wave period of 1 rad/s when proceeding on headwind.

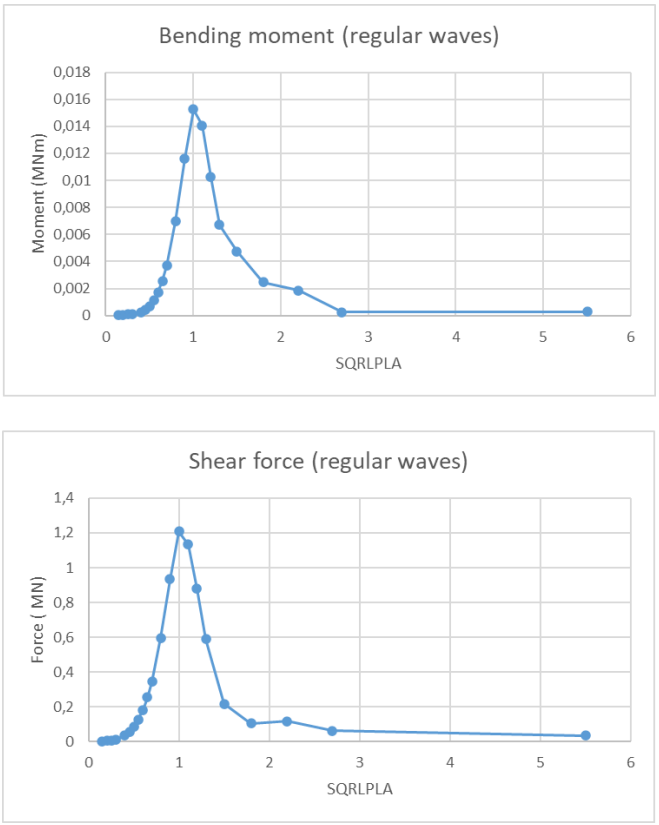

Figure 14-6 Bending moment and shear force in regular waves (NAPA)

The bending moments and shear forces in regular waves are presented in *Figure 14-6*. They are present as a function of square root of L_{pp} per wavelength. The estimation is for headwind.

The results for bending moments and shear forces from AQWA can be seen in Chapter 14.2.10. The results from both programs seem reasonable.

NAPA manuals state that the error in these response amplitudes can be around 10-15% compared to full scale measurements. This is especially the case with the roll motion. The roll damping is often nonlinear, and since these results are obtained using linear methods, the results should be taken with care.

14.2 Other seakeeping software

The hydrodynamic response analysis was also conducted using Maxsurf, Aqwa and Hydrostar in order to validate the results obtained from NAPA, and also to practice using this software.

Starting with Maxsurf, two motions theories can be adopted, Strip Theory and Panel Methods. The linear strip theory method, developed by Salvesen et al. 1970 [79]; unlike more advanced methods, is relatively simple and not too computationally intense. The main shortcoming of this method is it can only calculate the response of heave and pitch motions, Maxsurf can still predict the roll motion using the hydrostatic characteristics of the vessel and a predefined value of rolling coefficient. The main assumptions in the strip theory method are:

- Linear strip theory method to predict the vessels heave and pitch response.
- Roll response is estimated assuming that the vessel behaves as a simple, damped, spring/mass system and that the added inertia and damping are constant with frequency [83].
- The fluid is inviscid which means that, viscous damping is ignored.
- The ship is slender (i.e. the length is much greater than the beam or the draft, and the beam is much less than the wavelength).
- The hull is rigid so no flexibility is taken into account.
- The speed is moderate so there is no dynamic lift.
- The motions are small (or at least vary linearly with wave amplitude).
- The ship hull sections are wall-sided, the effect of nonlinearity was ignored.
- The water depth is much greater than the wavelength so that deep water wave approximations may be applied. No confined water.
- Frequency domain analysis. Which means the principle of superposition is used to compute the response of the vessel to irregular waves. This means that the contributions to the motions of the individual regular waves making up the irregular sea spectrum may be summed to obtain the total response of the vessel to the irregular seas.
- Hence the main source of uncertainties and shortcoming of the strip theory in Maxsurf are:
- As the solver is linear, the emergence or submergence of the bow or stern induces some level of inaccuracy.

- Flare (non-wall sidedness) of the hull at the waterplane.
- Submergence of the bow or stern overhangs in a vessel.
- 3D flow effects and flow interaction in longitudinal direction along the hull including dynamic lift at high speed.
- Modelling wave diffraction / radiation and the Kelvin wave pattern at forward speed.

14.2.1 3D model

The model, that is already created in NAPA modeller, was transferred to Maxsurf as an .iges file. Then we cured the faults that occurred in the transferring process, as some surface bondages were lost. Grid lines, sections, buttocks and waterlines were defined and the reference point was set at the aft perpendicular at the keel. The model is illustrated in the figure below:

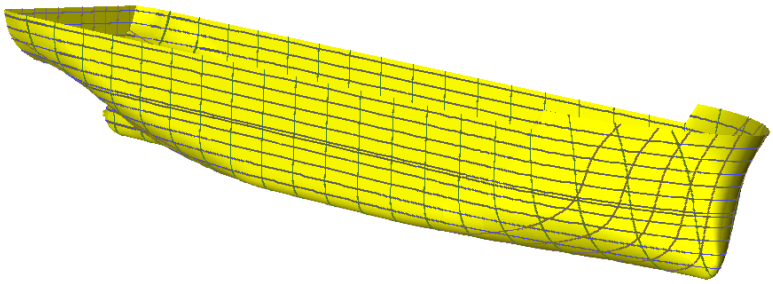

Figure 14-7 Transferred model from NAPA to Maxsurf for strip theory seakeeping analysis

14.2.2 Section mapping

Strip Theory requires to split the vessel into a number of transverse sections, we used here 41 sections to represent the overall ship geometry for seakeeping analysis. Each of these sections is then treated as a two-dimensional section for which the hydrodynamic characteristics are computed. Refer to figure below for section mapping.

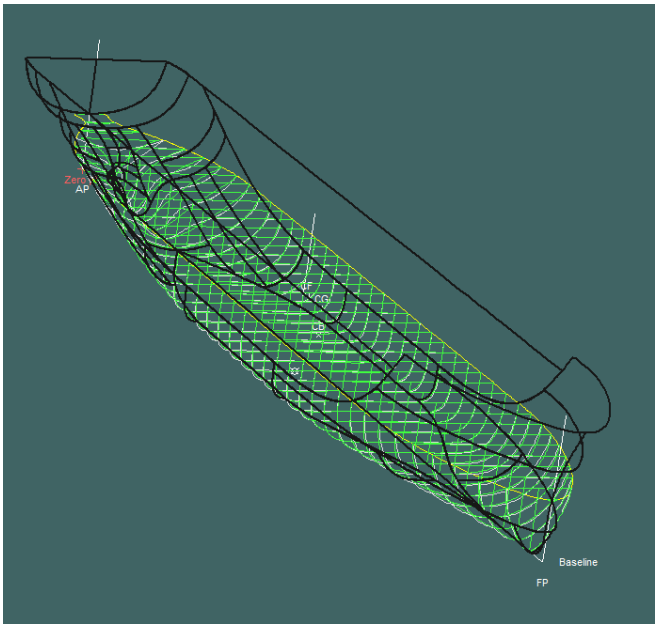

Figure 14-8 Section mapping

14.2.3 Gyradii

Evaluation of motions require the pitch, yaw and roll gyradii of the vessel. The effect of mass distribution (weight of the cargo, light ship weight and other weight components) on the ship motions can be defined by these gyradii:

These parameters can be defined as:

Roll gyradius (40% Breadth)

Pitch gyradius (25% Length over all Loa)

Yaw gyradius (25% Loa)

Vertical Center of Gravity (defined from NAPA)

Mass value (Calculated based on the equilibrium DWL)

Another method to evaluate the Gyradii accurately by using the following equation:

$$K = \sqrt{\frac{I}{M}}$$

Where I is the inertia of mass around center of gravity and M is the vessel mass. The inertia can be calculated after defining the load distribution accurately, which could be possible to evaluate in the next assignments.

14.2.4 Hydrodynamic damping coefficients

Heave/Pitch inviscid damping can be calculated accurately by Maxsurf.

The roll response can be calculated in Maxsurf based on the vessel's hydrostatic properties (which defines the roll stiffness, the roll gyradius and the roll damping). Typical values for most vessels are between 0.05 and 0.1. Lewis 1988 gives a value of **0.075** for typical ships with bilge keel.

14.2.5 Frequency range

The frequency range is defined to include all the expected gravitational waves the vessel may encounter. From the wave scatter diagram, see figure below, the peak period ranges from 2 to 12 sec, while the defined wave frequency/period in Maxsurf ranges from 0.21 sec to 31 sec corresponding to 0.2 rad/sec to 30 rad/sec.

Significant wave height [m]	peak wave period [s]											
	2	3	4	5	6	7	8	9	10	11	12	Tot
7.75 : 8.00	0	0	0	0	0	0	0	0	0	0	0	0
7.50 : 7.75	0	0	0	0	0	0	0	0	0	0	0	0
7.25 : 7.50	0	0	0	0	0	0	0	0	0	2	0	2
7.00 : 7.25	0	0	0	0	0	0	0	0	0	0	2	2
6.75 : 7.00	0	0	0	0	0	0	0	0	0	4	3	7
6.50 : 6.75	0	0	0	0	0	0	0	0	1	4	1	6
6.25 : 6.50	0	0	0	0	0	0	0	0	4	2	0	6
6.00 : 6.25	0	0	0	0	0	0	0	0	7	10	2	19
5.75 : 6.00	0	0	0	0	0	0	0	0	9	5	0	14
5.50 : 5.75	0	0	0	0	0	0	0	2	11	9	2	24
5.25 : 5.50	0	0	0	0	0	0	0	3	14	8	0	39
5.00 : 5.25	0	0	0	0	0	0	1	5	16	1	2	25
4.75 : 5.00	0	0	0	0	0	0	3	11	9	5	0	19
4.50 : 4.75	0	0	0	0	0	0	10	40	41	8	1	100
4.25 : 4.50	0	0	0	0	0	1	4	29	8	4	0	46
4.00 : 4.25	0	0	0	0	0	1	26	58	38	7	0	140
3.75 : 4.00	0	0	0	0	0	9	72	84	39	9	1	214
3.50 : 3.75	0	0	0	0	1	12	138	121	42	4	0	318
3.25 : 3.50	0	0	0	0	2	54	197	85	21	1	0	360
3.00 : 3.25	0	0	0	0	5	81	226	67	21	2	0	421
2.75 : 3.00	0	0	0	0	15	147	229	47	13	1	0	452
2.50 : 2.75	0	0	0	1	104	436	344	90	7	1	1	984
2.25 : 2.50	0	0	0	4	196	413	192	42	2	1	0	850
2.00 : 2.25	0	0	0	32	432	526	221	43	4	0	0	1478
1.75 : 2.00	0	0	0	115	846	559	187	37	3	1	0	1748
1.50 : 1.75	0	0	6	596	1288	586	157	35	11	1	0	2680
1.25 : 1.50	0	0	60	1371	1175	334	95	11	1	0	0	3047
1.00 : 1.25	0	0	366	1579	745	163	75	16	0	0	0	2944
0.75 : 1.00	0	64	1791	2008	624	159	62	10	2	0	0	4720
0.50 : 0.75	1	700	2264	1100	352	111	35	4	0	0	0	4567
0.25 : 0.50	274	1859	1589	744	370	136	16	4	20	1	0	5013
0.00 : 0.25	212	419	377	291	406	113	5	5	8	1	0	1837
Total	487	3042	6453	7841	6621	4034	2288	850	356	95	15	32082

Severe sea state 5

Severe sea state 4

Severe sea state 3

Severe sea state 2

Severe sea state 1

Figure 14-9 Wave scatter diagram and the considered severe sea states.

14.2.6 Environmental parameters and forward speed.

Four forward speeds for seakeeping analysis were studied. Zero, 5. 10 and 15 knots. This speed corresponding to maximum Froud number 0.27 (lower than the limit of Strip theory in Maxsurf 0.7).

Nine wave directions were defined, starting from head sea 180 degree to following sea 0 degree with 22.5-degree interval. See figure below.

	Name	Heading [deg]	Analyse
1	head seas 180	180.0	☑
2	157.5	157.5	☑
3	Oblique 135	135.0	☑
4	112.5	112.5	☑
5	Beam 90	90.0	☑
6	67.5	67.5	☑
7	Oblique 45	45.0	☑
8	22.5	22.5	☑
9	Following seas 0	0.0	☑

Figure 14-10 Defined wave headings

Five severe sea states were selected from the wave scatter diagram in *Figure 14-9* with highest significant wave height of 5.5 m. This significant wave height may induce uncertainties due to the nonlinear effect of these high amplitudes waves, however, it may be possible to give an overview of the max linear response of the system in these severe sea states.

14.2.7 Panel method in Maxsurf, Ansys Aqwa and Hydrostar

The second method is the panel method can be employed in computing the vessel motions in six degrees of freedom, surge, heave, pitch, sway, roll and yaw motions. It is also applied to a wider range of vessel geometries than the linear strip theory. In Aqwa and Hydrostar the theory can be applied for small forward speed, while in Maxsurf only zero speed is applicable. The same definition of the environmental parameters as in the strip theory are followed in the panel method for the three software. The following figures indicates the 3D diffracted panels. Only he panels below the DWL will be used to estimate the seakeeping characteristics of the vessel.

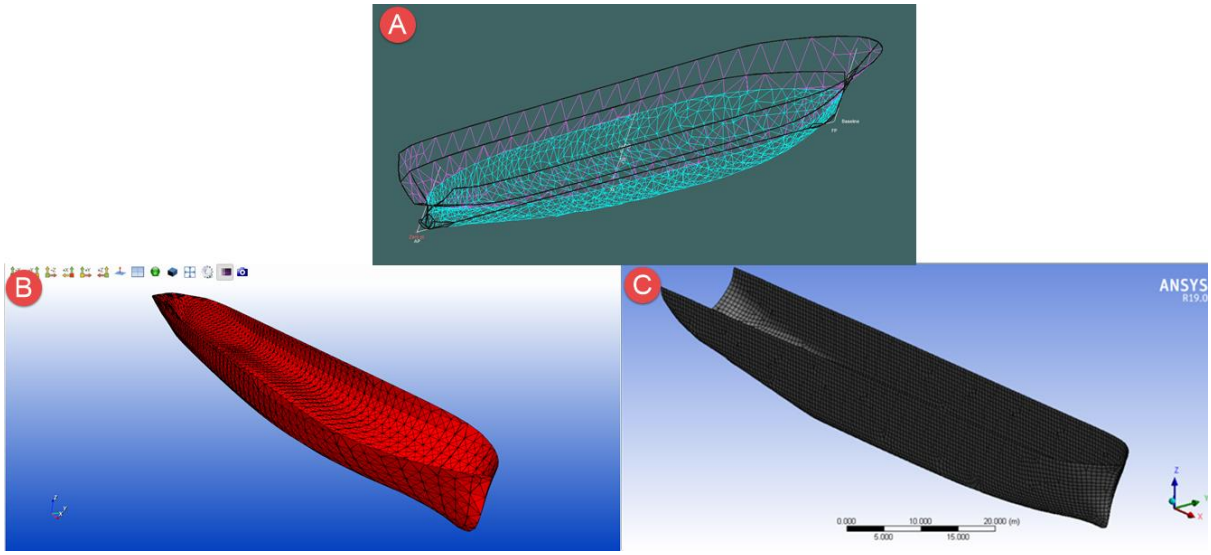

Figure 14-11 3D diffracted Panels used in the seakeeping analysis, (A) Maxsurf, (B) Hydrostar, (C) Aqwa

14.2.8 Results

The aim of the seakeeping analysis is to obtain the Response Amplitude Operator RAO of the vessel. They are also referred to transfer functions which describe the behavior of the vessel in waves. This is normally non-dimensionalised with wave height or wave slope.

Figure below indicates the heave motion of our vessel of 3 different software, they are quite in good agreement.

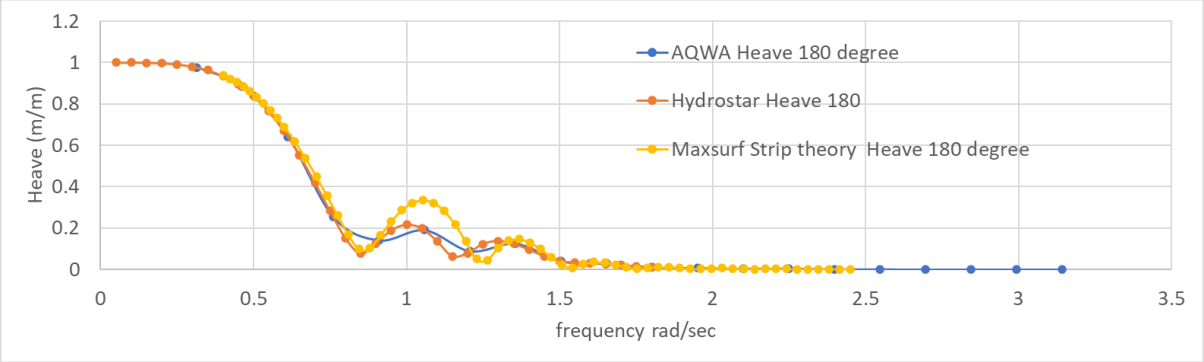

Figure 14-12 Heave motion of Saimaa-Hybrid

The pitch motion transfer function is illustrated in the figure below, it also shows that the Hydrostar and AQWA give the same results as will be observed in all the following figures for the other motions.

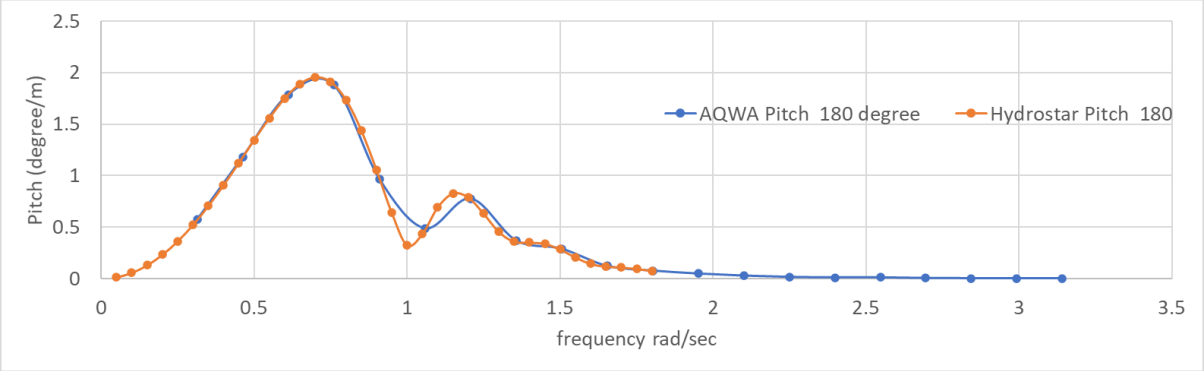

Figure 14-13 Pitch motion of Saimaa-Hybrid (Heading 180 degree)

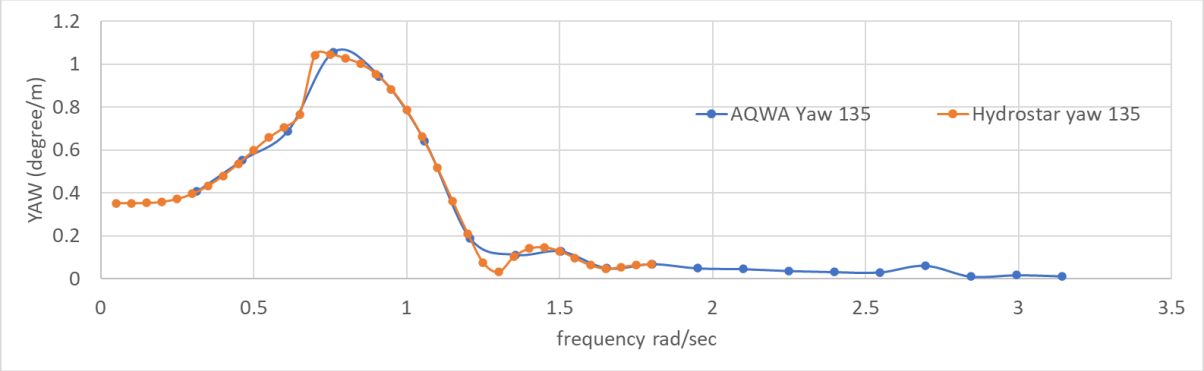

Figure 14-14 Yaw motion of Saimaa-Hybrid (Heading 135 degree)

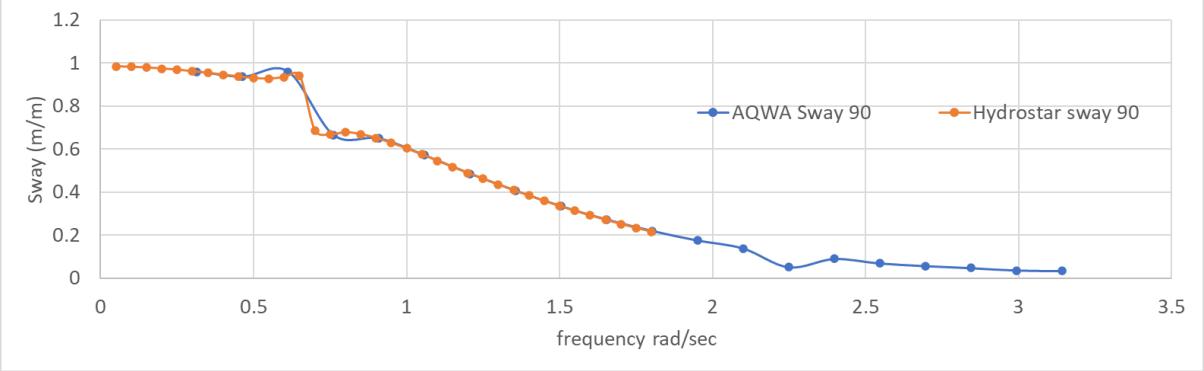

Figure 14-15 Sway motion RAO of Saimaa-Hybrid (Heading 90 degree)

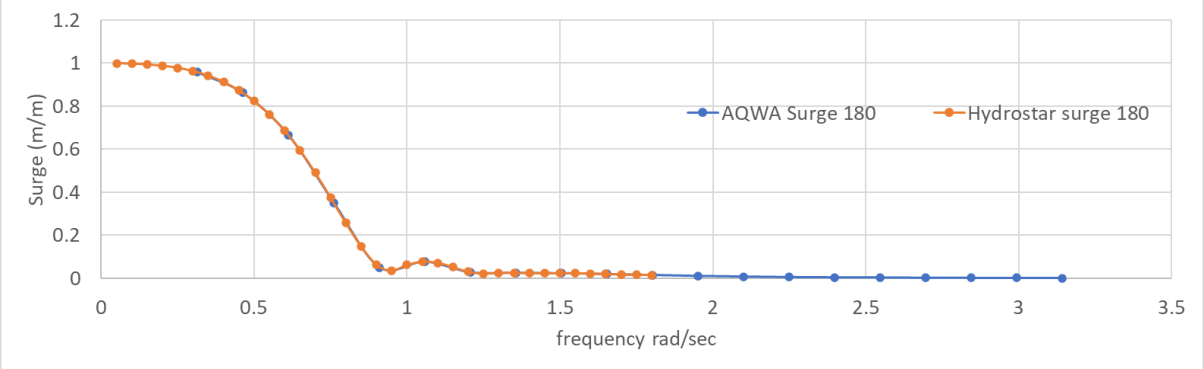

Figure 14-16 Surge motion RAO of Saimaa-Hybrid (Heading 180 degree)

The roll motion of the vessel shows a big difference between the different software, as can be observed in the figure below. This difference is mainly due to the errors in the roll damping coefficient. For instance, Maxsurf has 2 different results for two different roll damping coefficients 0.01 and 0.075, both are quite different. Therefore, it is essential to investigate the roll damping coefficient by experiment or by using numerical software as AQWA.

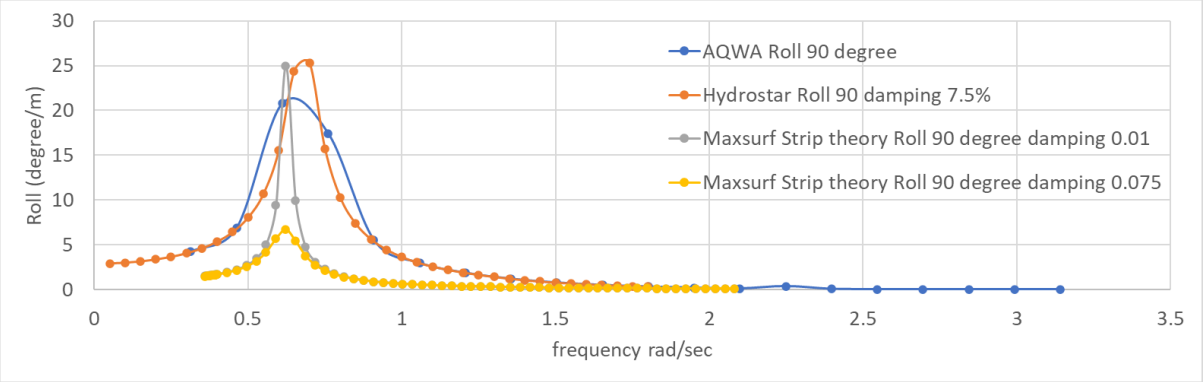

Figure 14-17 Pitch motion of Saimaa-Hybrid (Heading 180 degree)

14.2.9 RAOs in different wave headings

Figure below indicates, the roll motion has a maximum peak in oblique heading and also in beam seas, while in head seas there is no roll motion (based on the linear analysis).

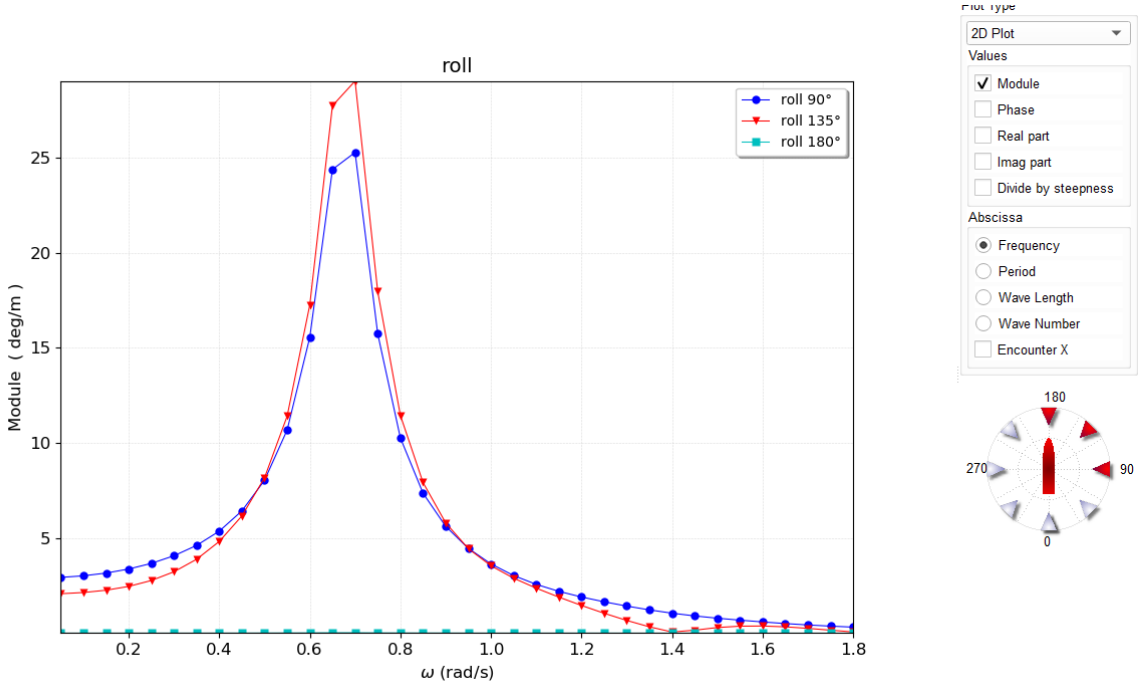

Figure 14-18 Roll motion of Saimaa-Hybrid in 3 headings (Hydrostar)

Heave motion has a peak in 90 degree heading as can be shown in the figure below, while nearly same results in oblique and head seas

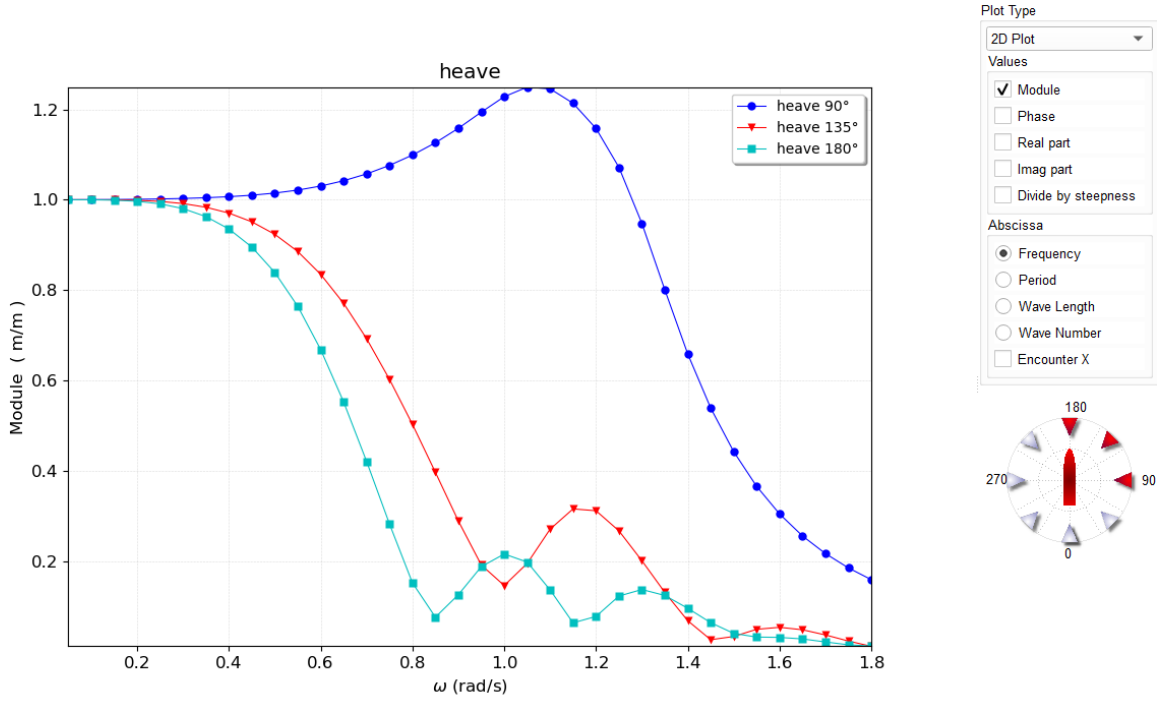

Figure 14-19 Heave motion of Saimaa-Hybrid in 3 headings (Hydrostar)

The figure below shows considerable pitch motion in the head and oblique seas while in beam seas the pitch motion is small as predicted.

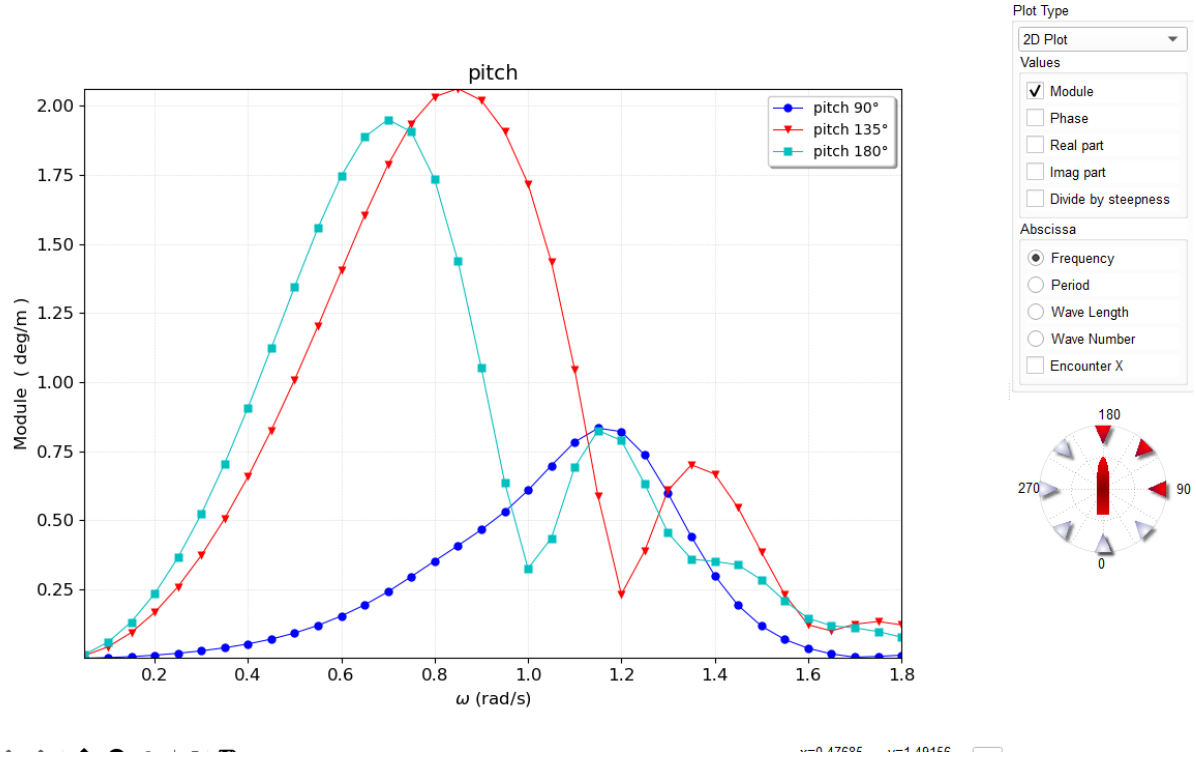

Figure 14-20 Pitch motion of Saimaa-Hybrid in 3 headings (Hydrostar)

On the other hand, yaw motion is significant in oblique seas and almost zero in heading seas.

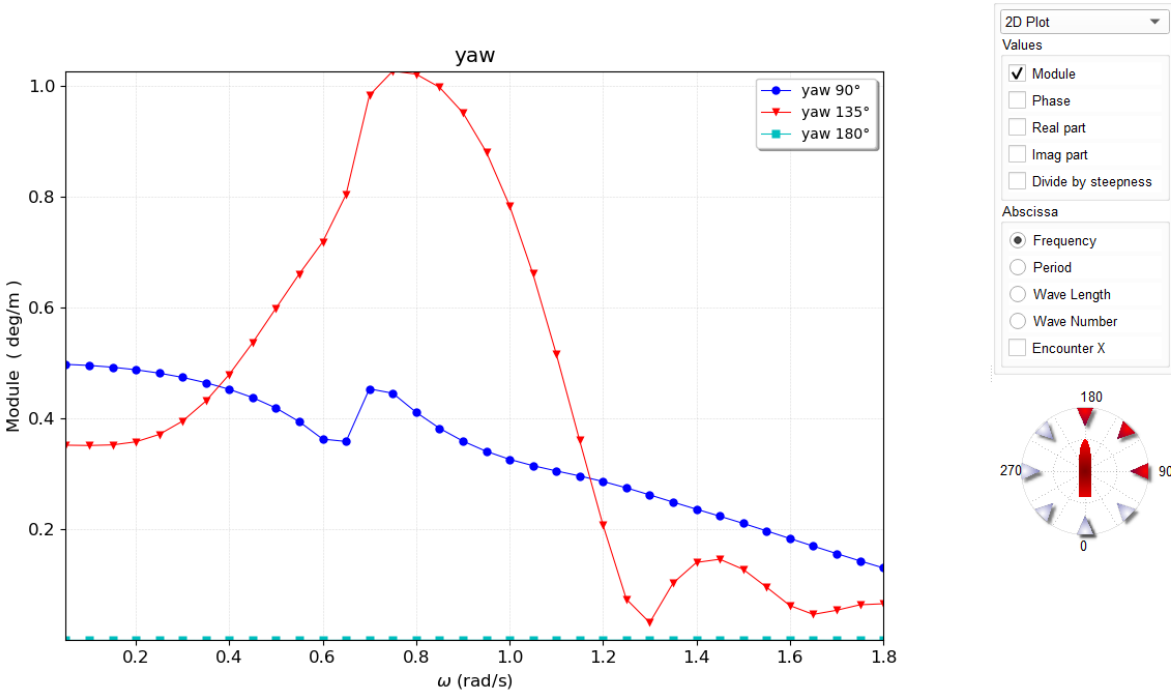

Figure 14-21 yaw motion of Saimaa-Hybrid in 3 headings (Hydrostar)

However, surge motion is not usually important in normal operation, the figure below indicates the surge is negligible in beam seas comparing with the heading and oblique seas

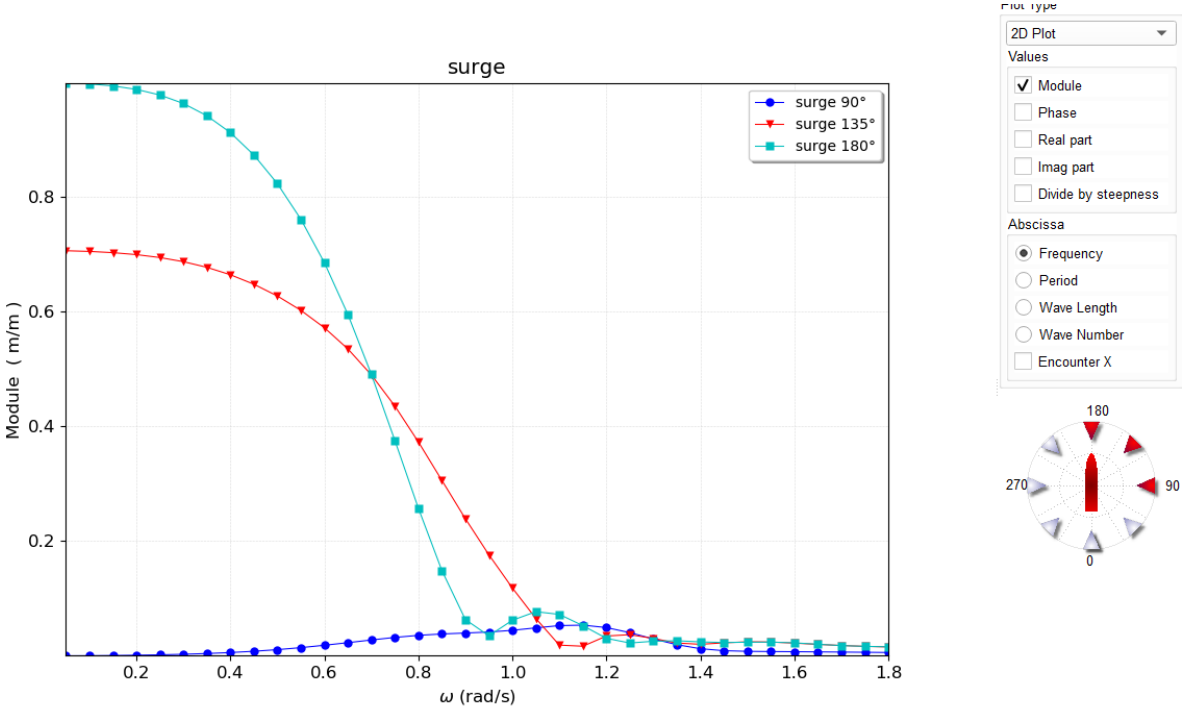

Figure 14-22 surge motion of Saimaa-Hybrid in 3 headings (Hydrostar)

It can be observed that at high frequency, or low period, in all figures the response tends to be zero since the effect of many very short waves cancels out over the length of the vessel. Typically, the vessel will have a peak greater than unity due to resonance which occurs close

to the vessel's natural frequency. RAO values greater than unity indicate that the vessel's response is greater than the wave amplitude (or slope).

14.2.10 Wave induced bending moment and shear force

The wave induced bending moment RAO as a function of wave frequency and unit wave amplitude is obtained using AQWA. As can be seen in the figure below the moment reaches plateaus at wave frequency near the ship length which is predicted and validate the results of wave induced bending moment.

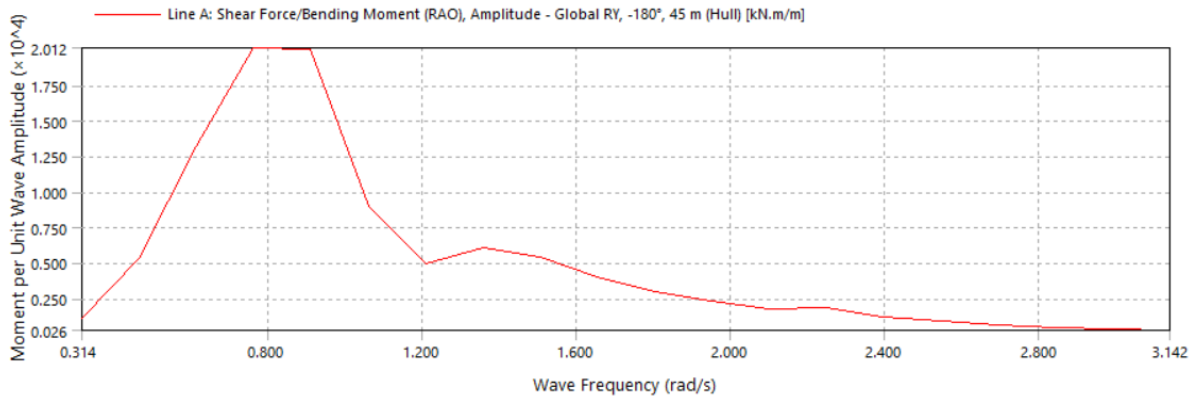

Figure 14-23 Bending moment RAO amidship(AQWA)

while the wave induced bending moment is also obtained using Jensen and Mansour (2002) formula, equation below. It is a frequency response function of the vertical wave induced vertical bending moment amidships ΦM.

$$\frac{\Phi_M}{\rho g B_0 L^2} = \kappa \frac{1-\boldsymbol{k}T}{(k_e L)^2}\left[1-\cos\left(\frac{k_e L}{2}\right)-\frac{k_e L}{4}\sin\left(\frac{k_e L}{2}\right)\right] F_V(Fn) F_C(C_b) \times \sqrt[3]{|\cos\ \beta|}$$

where B_0 is the maximum waterline breadth, κ is the Smith correction factor is approximated by: $\kappa = \exp(-k_e T)$, $\boldsymbol{k}$ is the wave number $k=2\pi/\lambda$ where $\lambda = (\boldsymbol{g}T\_w\text{^}2)/\boldsymbol{2\pi}$ in deep water; the effective wave number: $k_e = |\boldsymbol{k}\ cos\ \beta|$, β is the heading angle (180º corresponding to head sea), Froude number $Fn = V/\sqrt{gL}$.

The correction factor for the block coefficient is:

$$F_C(C_b) = [(1-\vartheta)^2 + 0.6\alpha(2-\vartheta)]$$

$$\vartheta = 2.5(1-C_b) \qquad \text{where} \qquad C_b = max(0.6, C_b)$$

$$\alpha = 1 - Fn\sqrt{\boldsymbol{k}L}\cos\ \beta$$

The speed correction factor (validated for Fn < 0:3, only):

$$F_V(Fn) = 1 + 3Fn^2$$

As this is a linear equation that relates bending moment with the wave heigh, it may show considerable inaccuracy due to the non-linearities effect.

Figure below indicates the resultant bending moment RAO, comparing with the AQWA results there is good agreement between both curves.

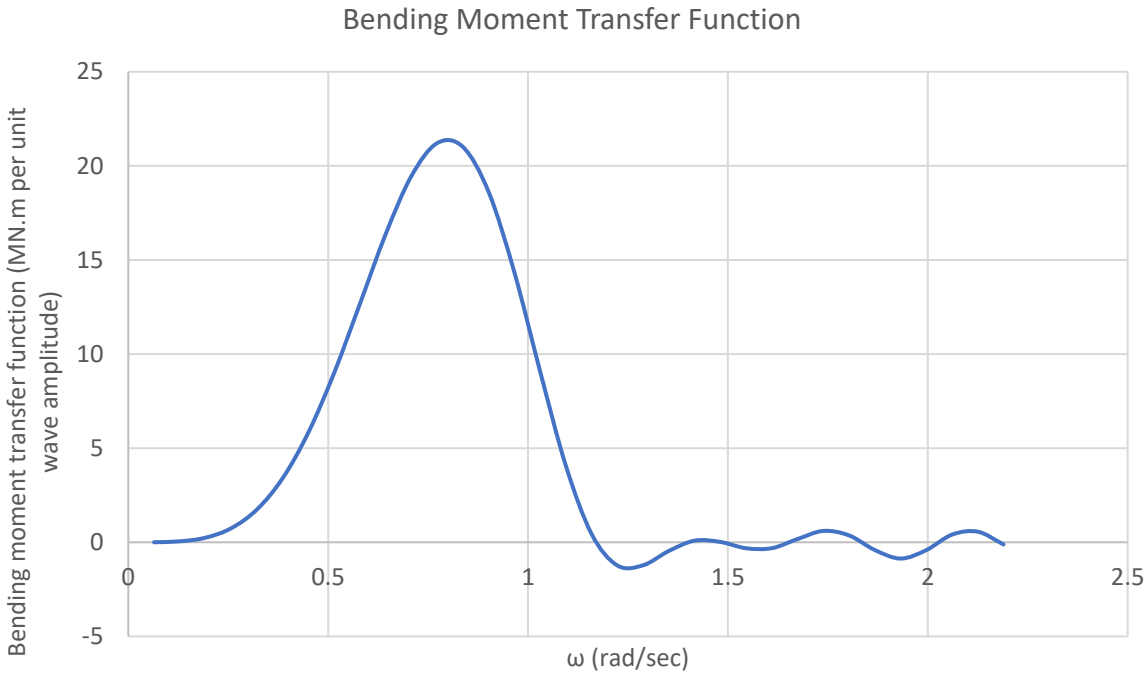

Figure 14-24 bending moment RAO using closed formula

The shear force from waves is also obtained from AQWA as can be seen in the figure below.

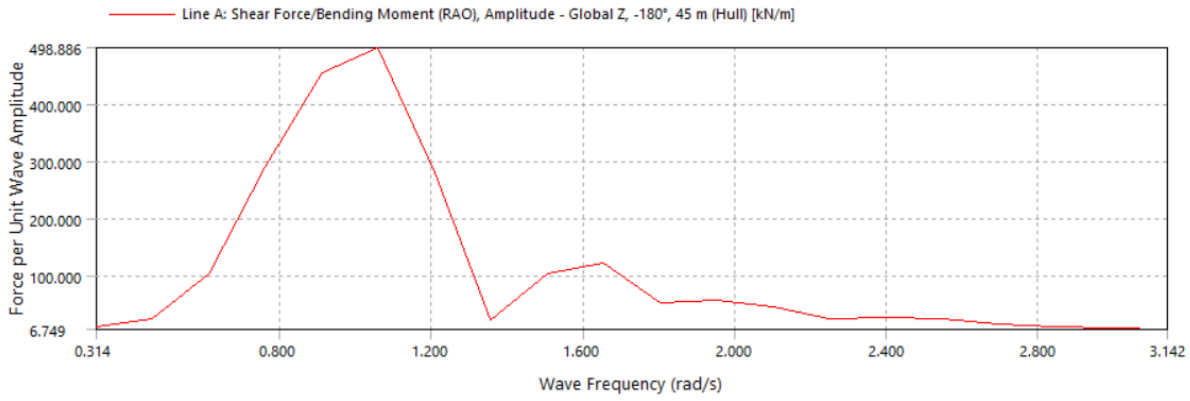

Figure 14-25 Shear force RAO using AQWA

14.2.11 Spectral density response

The marine environment can be described by the wave spectrum which describes the energy (or amplitudes) of wave components (or regular waves) of different frequencies that compose the irregular sea state. This is a random stochastic process, and we cannot predict the value of response x(t) at a time instant t in future. The usage of Fourier series is not always practical because the periodic requirement $f(t)=f(t+T)$ is always violated; the Fourier integral also does not converge. On the other hand, spectral density converges, therefore, it is always considered. Using the spectral density, we can get the response power spectral which describes the component frequencies of the response. By this way, we can amend the system to omit certain frequency to reduce the response, or even study the maximum by matching the peaks of load spectral and the RAO of the structure.

The application of the spectral method is much easier than its derivation, actually its derivation is considerably complicated. The response spectral density $S_{yy}(\omega)$ can be obtained by squaring the response amplitude operator of the system $H_{yy}(\omega)$ (which may be stress, load or motion) and multiply it by the wave spectrum.

$$S_{yy}(\omega) = \left|H_{yy}(\omega)\right|^2 S_{xx}(\omega)$$

Assuming linear ship response, the ship's RAOs depend only on the vessel's geometry, mass distribution, speed and heading. Therefore, the spectrum for a particular vessel motion at a particular sea spectrum can be derived from the estimated transfer function RAOs [83].

Here we have used Hydrostar to obtain the spectral density response in a sea state of period 3 hours. The sea state is the worst condition that our vessel may encounter during sailing in Gulf of Finland. It is described by Johnswap spectrum with 5 m significant wave height and zero up-crossing period equals 8 sec. As can be observed in the figure below, the red curve represents the wave spectrum while the response in heave, surge and pitch are plotted as a function of wave frequency.

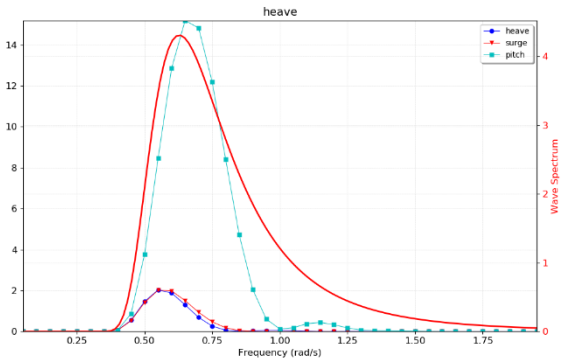

Figure 14-26 Response spectrum of heave, surge and pitch (Johnswap wave spectrum of 180 degree heading and Hs= 5.5 m, T_z = 8 sec, no spreading)

The effect of wave spreading following is also investigated using cosine-squared approach:

$$f_s(\theta') = \begin{cases} \frac{2}{\pi}\cos^2(\theta'), & \theta - \frac{\pi}{2} \leqslant \theta' \leqslant \theta + \frac{\pi}{2} \\ 0, & \text{otherwise} \end{cases} \quad (1)$$

Figure below illustrates the effect of spreading on the previous demonstrated response.

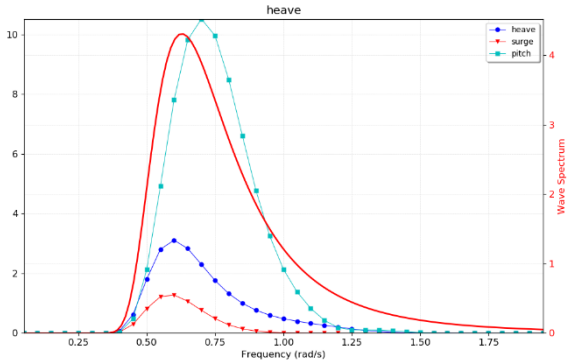

Figure 14-27 Response spectrum of heave, surge and pitch (Johnswap wave spectrum of 180 degree heading and Hs= 5.5 m, T_z = 8 sec, with spreading cos2 approach)

The response spectrum in beam seas is dominated by the excessive roll motion as can be observed in the figure below.

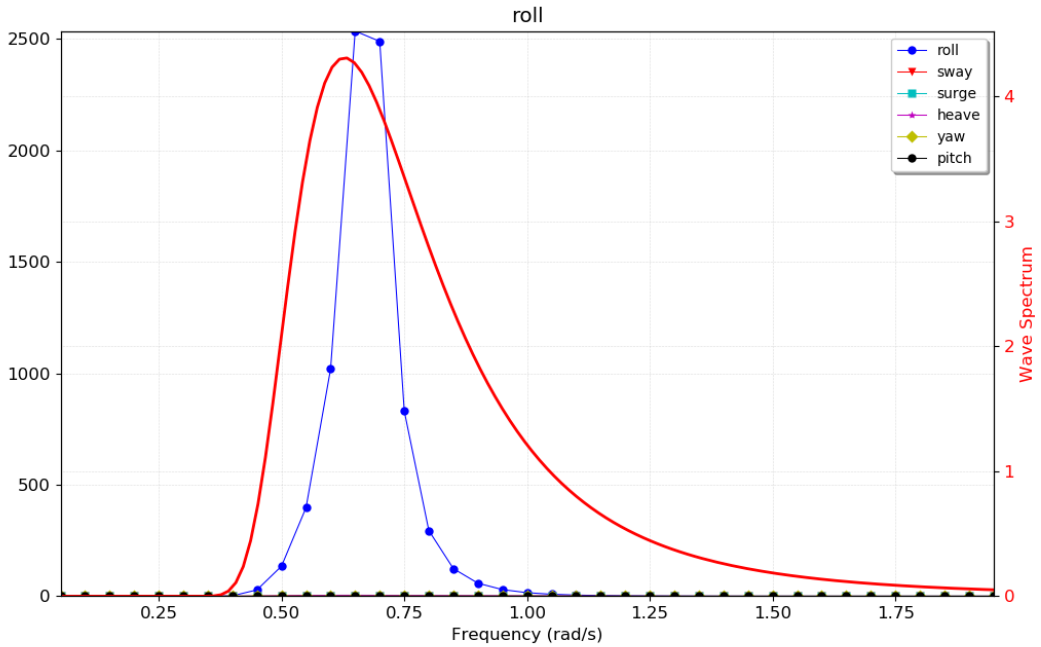

Figure 14-28 Response spectrum of Roll (Johnswap wave spectrum of 90 degree wave heading and Hs= 5.5 m, T_z = 8 sec, no spreading)

The effect of spreading on the roll motion response spectrum is illustrated in the figure below

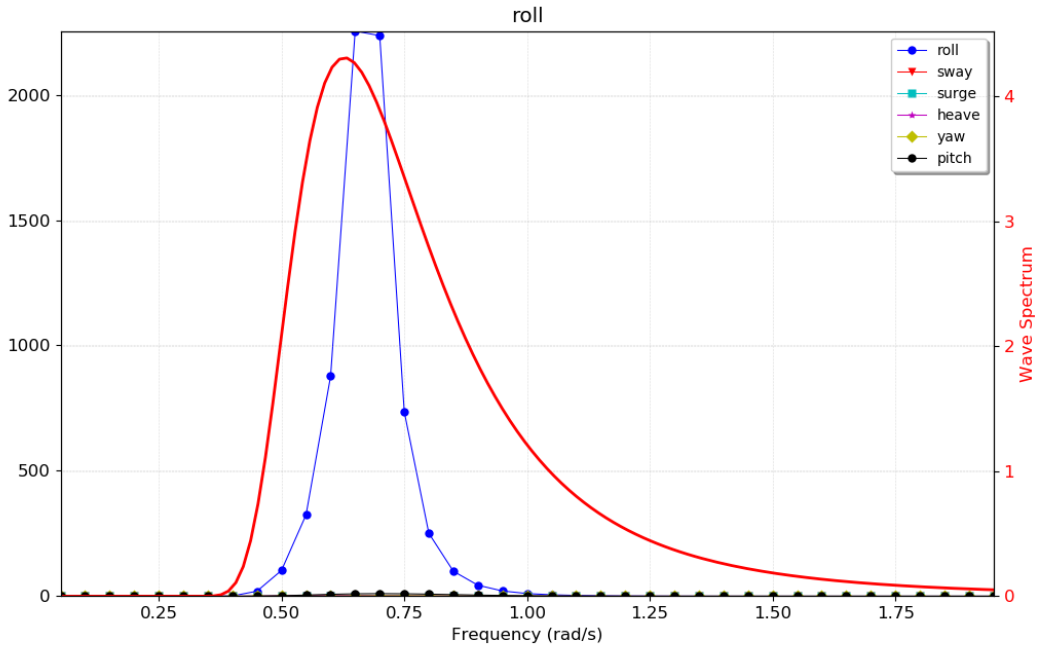

Figure 14-29 Response spectrum of Roll (Johnswap wave spectrum of 90 degree wave heading and Hs= 5.5 m, T_z = 8 sec, with spreading)

Also, the response of roll motion in time domain is illustrated in the figure below for 6 minutes. It can be observed that there is an excessive roll motion (nearly 40 degree) the ship may experience if it operates in such sea states. The results here reflect the important of studying the comfortability of the passengers on board to make sure that the vessel can operate in such severe sea states.

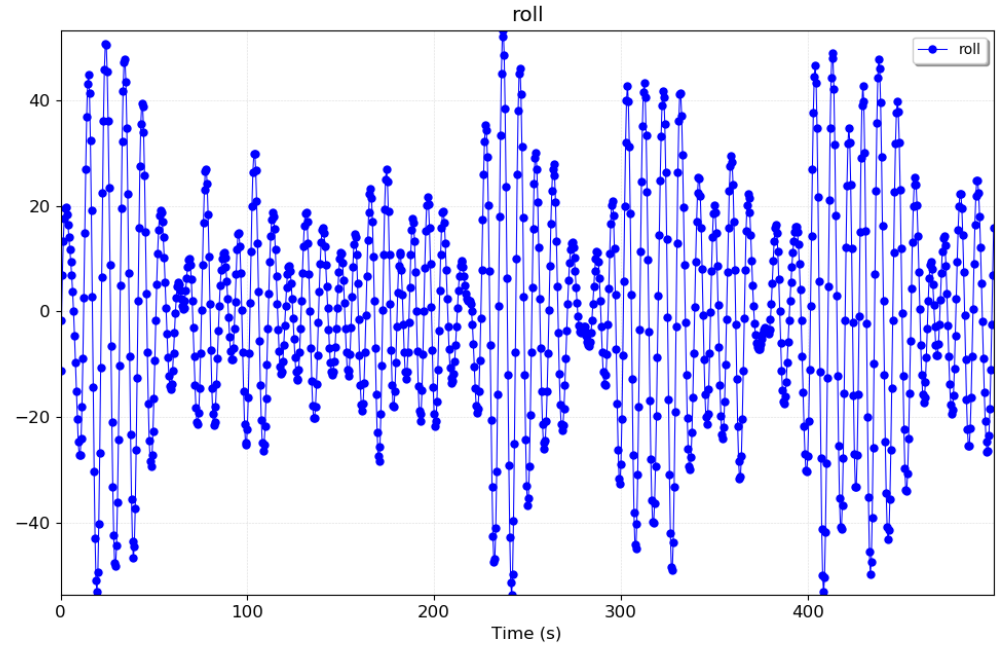

Figure 14-30 Time domain response of Roll motion

The response of pitch motion in time domain is illustrated in the figure below

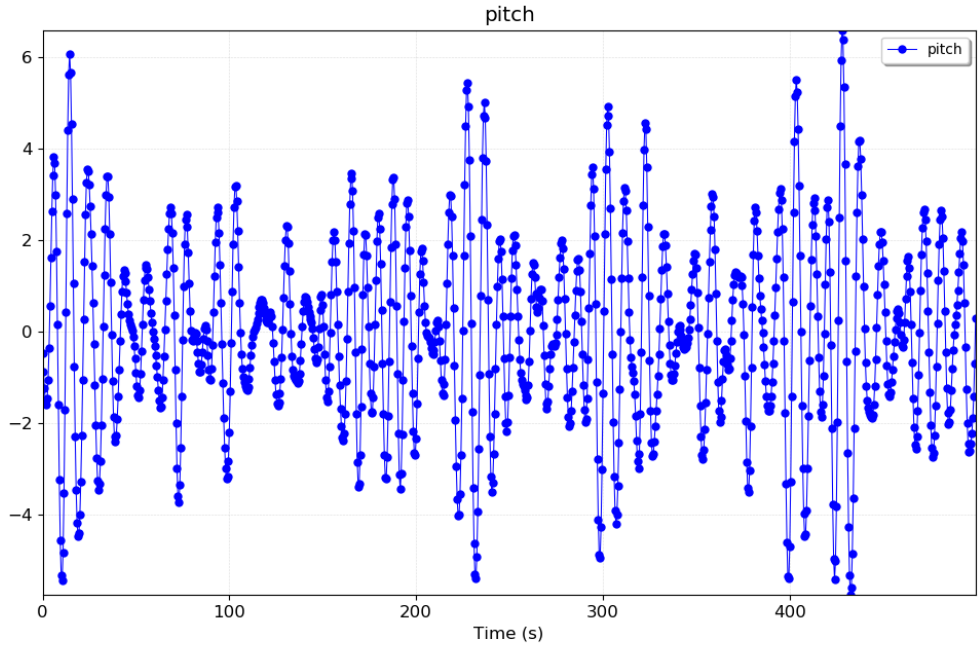

Figure 14-31 Time domain response of pitch motion

14.2.12 Visual representation of ship motion and severe sea state.

For visual purpose, the marine environment was rendered using Hydrostar. Severe sea state represented by Johnswap spectrum of 5.5 Hs and 8 sec zero up crossing period is used to model the surrounding marine environment. The contours on the hull represent the hydrodynamic pressure on the hull surface form the irregular waves.

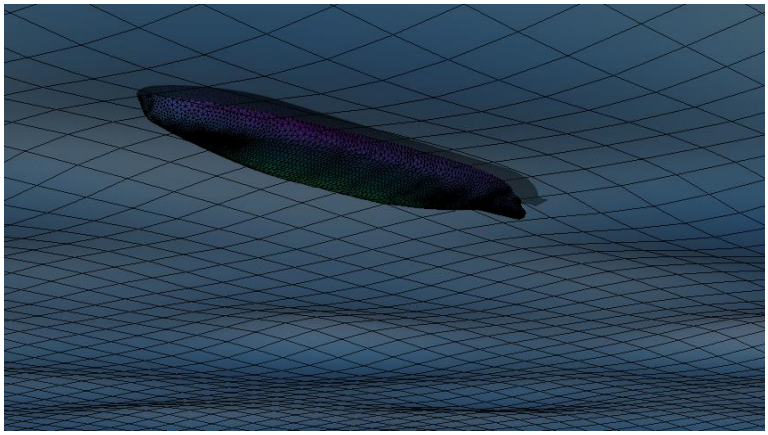

Figure 14-32 Visual representation of the ship motion in severe sea state

15 Stress response

In the structure report we have obtained the scantling from the DNVGL. We have modelled the full structural model with many simplification in order to get the stress response in waves. Figure below illustrate the structural model used in the analysis.

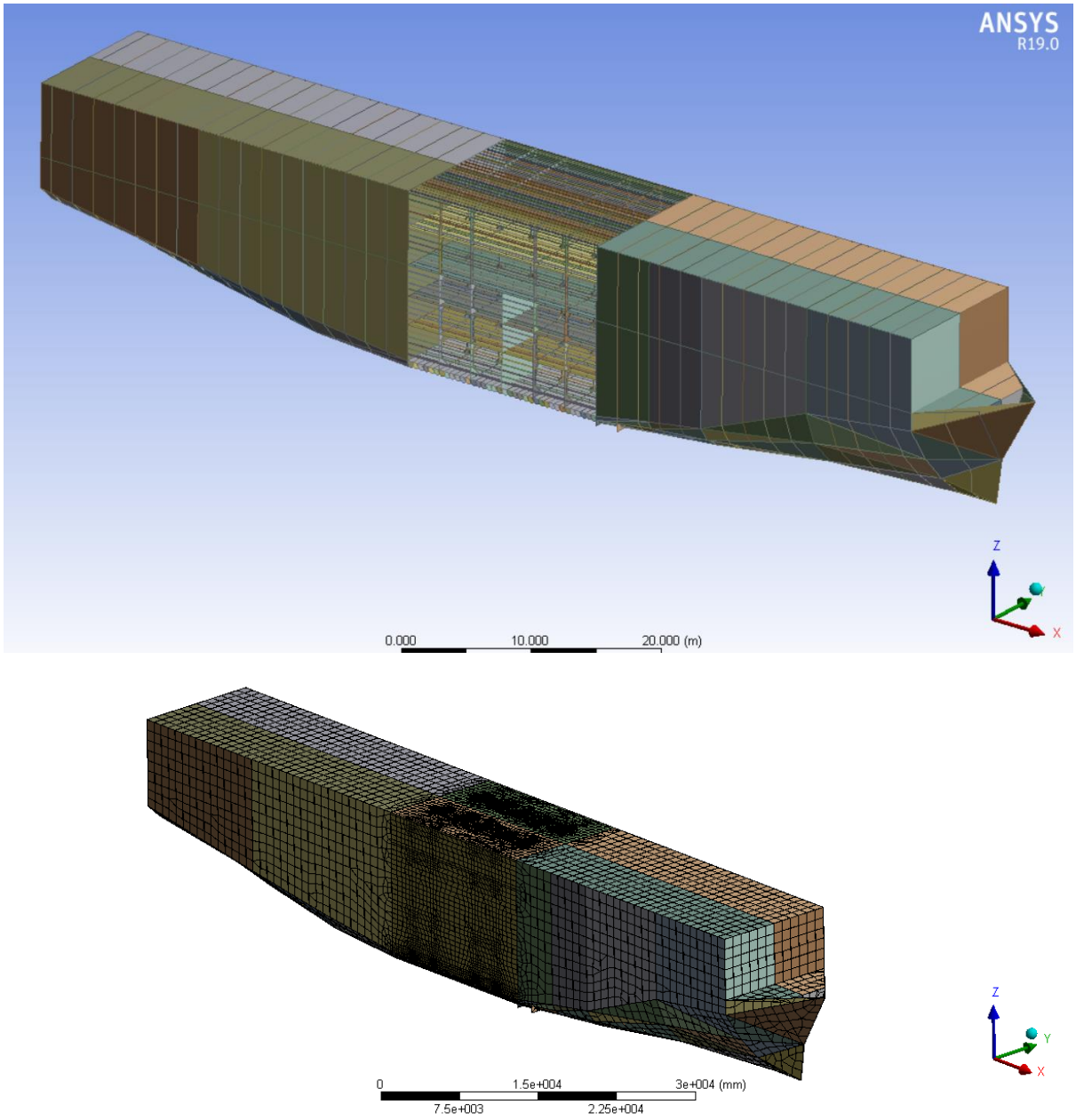

Figure 15-1 Finite element model and typical mesh employed in this study after simplification

It can be observed that the model has quite coarse mesh near the forward and aft parts. While slightly fine mesh near the amidship where the structural details are modelled accurately and with high care. In this study, simplified model of the vessel were created. The model consists of several planar surfaces, while the vessel has the same main hydrostatics characteristics of the NAPA model. hence, the *simplified model should* maintain the same motions, displacement and other principal characteristics of the original vessel at least with enough accuracy for this application.

The mass summary that is important for conducting the dynamic analysis is summarized in the figure below.

```
********** PRECISE MASS SUMMARY **********

TOTAL RIGID BODY MASS MATRIX ABOUT ORIGIN
        Translational mass            |  Coupled translational/rotational mass
 0.36746E+07   0.0000      0.0000     |   0.0000      0.17087E+08   3.8504
 0.0000      0.36746E+07   0.0000     |  -0.17087E+08   0.0000      0.14846E+09
 0.0000      0.0000      0.36746E+07  |  -3.8504      -0.14846E+09   0.0000
 ------------------------------------ | ------------------------------------
                                      |       Rotational mass (inertia)
                                      |  0.13681E+09   140.44      -0.67572E+09
                                      |    140.44      0.70060E+10  -7.0855
                                      |  -0.67572E+09  -7.0855      0.69178E+10

TOTAL MASS = 0.36746E+07
The mass principal axes coincide with the global Cartesian axes

CENTER OF MASS (X,Y,Z)=   40.400     -0.10478E-05   4.6500

TOTAL INERTIA ABOUT CENTER OF MASS
  0.57356E+08  -15.118      0.14596E+08
   -15.118      0.92898E+09  -24.990
  0.14596E+08  -24.990      0.92023E+09
```

1.1 Hydrodynamic model and analysis

The hydrodynamic seakeeping analysis was conducted by ANSYS AQWA (ANSYS 2013). AQWA only requires the geometry of the external hull, in addition to the ship's displacement, its center of gravity and mass moment of inertia. Those data are described in the figure above. The hull model was obtained from the structural model, only the external hull shell. Then it the diffracted panels and environmental condition are defoined before running the seakeeping analysis. The main results from the seakeeping analysis is the pressure on each panel. We have transferred the pressure from AQWA to ANSYS using a script we wrote/amended based on the instruction in AQWA manual.

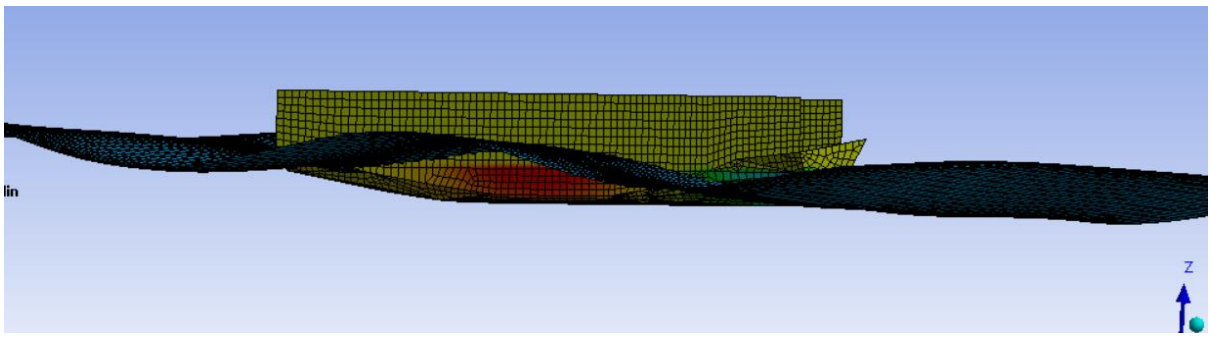

Figure 15-2 Worst seakeeping results in AQWA and the corresponding pressure distribution 3

1.2 Pressure mapping

Mapping the hydrodynamic loads to the structural model is one of the functions of the ANSYS software package. Once the hydrodynamic diffraction analysis is performed; wave loading can be transferred to the FEM model by two methods. The first method transfers the loads seamlessly using the Hydrodynamic Pressure Mapping ACT Extension. This method is simpler than the second method which involves writing script code for each wave frequency and direction. However, the second method was employed in the current work.

The mapped pressure represents the hydrodynamic pressure of a single wave with a specified frequency, direction and phase angle. The mapping is conducted for multiple wave phase angles with a small interval in between. twelve phases were selected in each finite element analysis range between zero and 330 degrees with 30-degree interval; therefore, the maximum and minimum stress can be checked at each wave phase. The mapping procedure can be conducted using the interpolated method. The pressures are interpolated from the centre of the hydrodynamic mesh elements onto the nodes of the structural mesh. This principle is illustrated in below; where first the hydrodynamic pressures (P) at the nodes (N) of the hydrodynamic mesh are estimated from the panel pressures. Then, the node pressures of the hydro mesh are interpolated onto the structural mesh nodes. Finally, the finite element nodal pressures are computed from weighted averaging of hydrodynamic nodal values (ANSYS 2013).

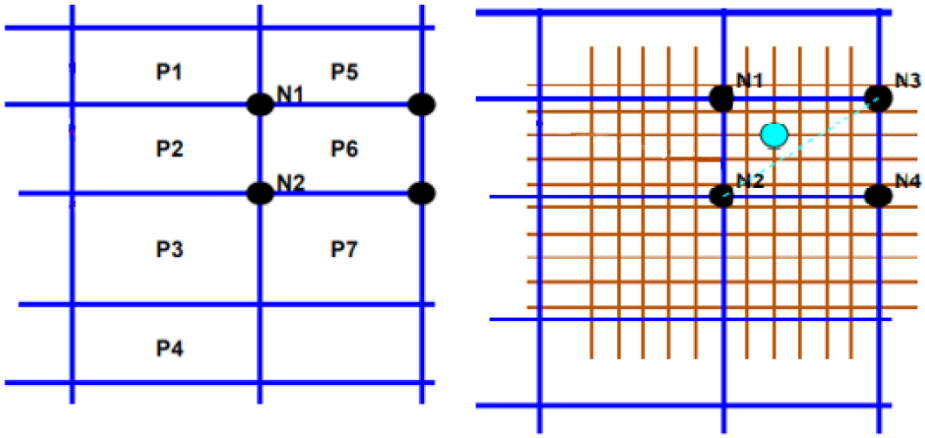

Figure 15-4 Mapping of the hydrodynamic pressure into the structural model

1.3 Structural analysis results

Mapping was conducted successfully for a wave height of 6 m and length equals to the ship length. This wave represent the worst scenario we may experience during operation in Gulf of Finland. The stress response is illustrated below. The maximum observed stress is nearly 113 MPa and occurred on the deck stiffeners. This stress from the waves should be added to the stress in still water to have the total stress. Therefore, the total stress will not exceed 130 MPa; comparing with max permissible stress of 170 MPa we are still have slightly lower stress from the permissible. As we are using coarse mesh we can not estimate accurately the stress concentration at many of the structural details, therefore, the obtained stress is quite good taking into account it may increases at the structural discontinuity due to the stress concentration.

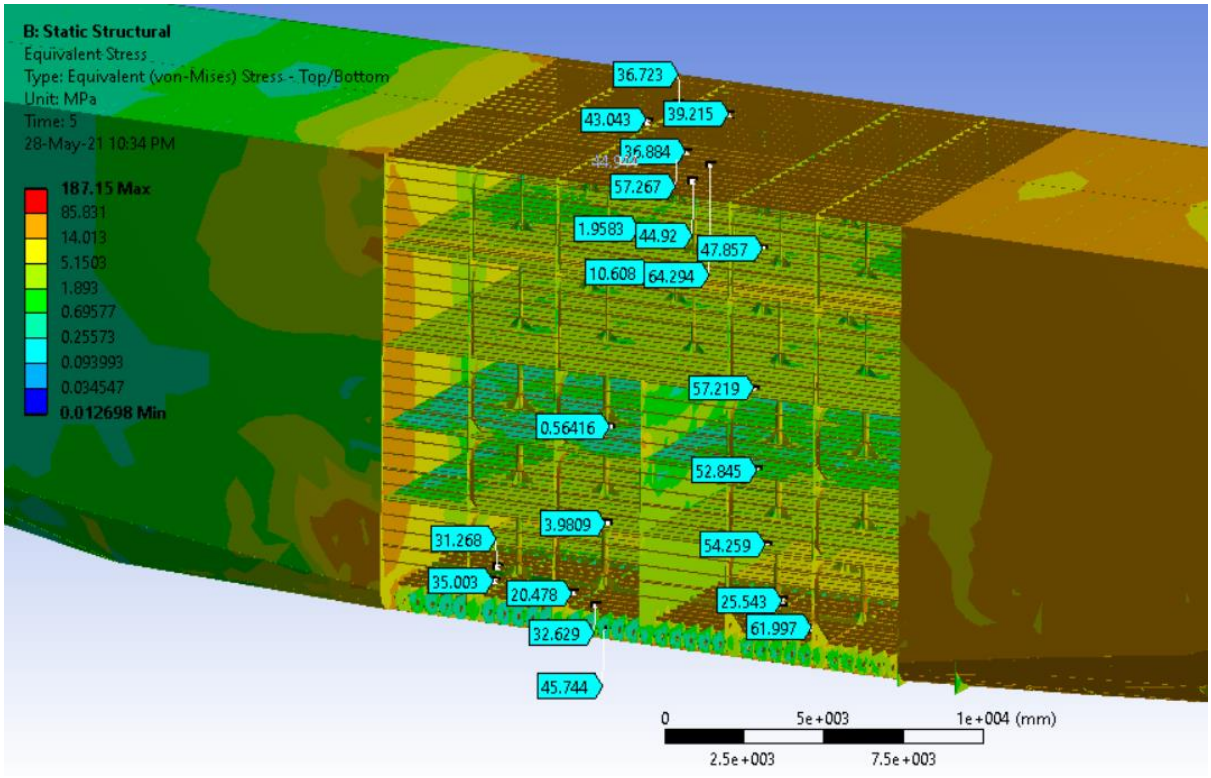

Figure 15-5 Von Mises stress contour and some stress response gauges

The fluctuation of the stresses from sagging to hogging and vice versa is presented in the figures below. The contour represent the normal stress in x direction. The phase shift between both figures is 180 degree phase shift.

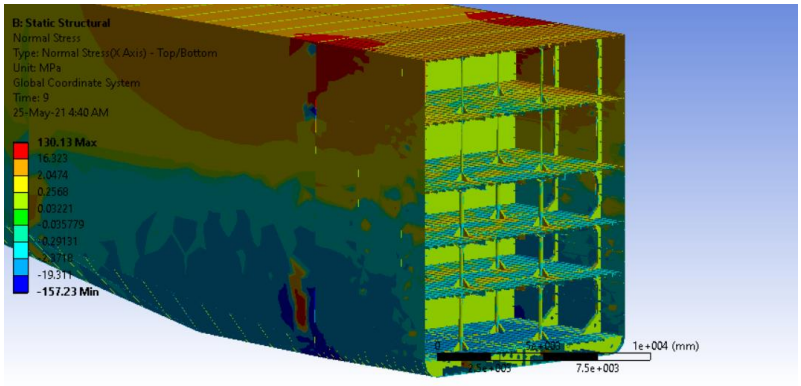

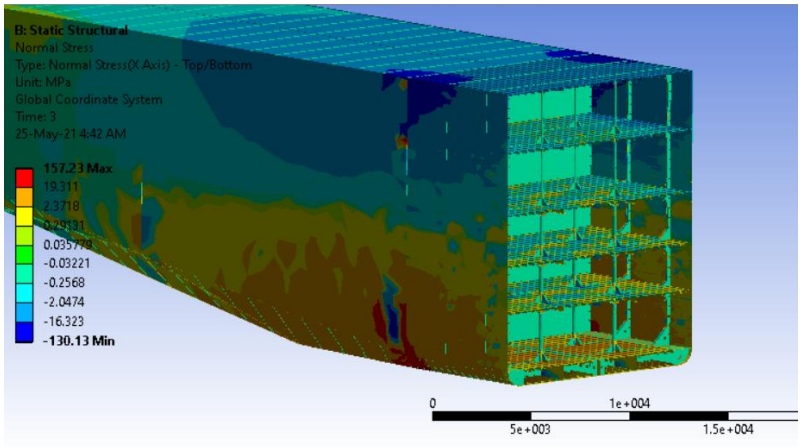

Figure 15-6 Hogging and sagging normal (x-direction) stress

We can not say that the above analysis is accurate, but it can be improved and optimized to obtain much accurate results. The improvement may include improving the mass distribution in the structural model to get much more accurate response. It is noteworthy that, in this study the total mass distribution in the structural model is represented by only one point mass.

The coarse mesh , lower structural details of the forward and aft part and simplified hull form may have an impact on the results. However, all these approximations still acceptable to have satisfactory results for this assignment.

16 Hydroelastic effect, current developments and future directions

Design of ship safety has not implemented latest technology advancements in ship motion prediction programs as ships have gotten larger. More accurate assessment of loading and motions is possible with new programs, and there is a need to evaluate current standards to make sure they are still adequate. This paper assesses current standards and looks at recent work to use FSI and other non-linear hydromechanics models.

The paper discussed current state of assessing wave-induced loads and ship responses and the specific avenues that are being pursued currently with reasons why and some preliminary interpretations of results. Loads previously were evaluated under low-frequency domain and ultra-low frequency domain and rely on linear rigid-body ship hydrodynamics but larger ships have shown that there is a needed shift to look at vibration loads as well as springing and whipping (Hirdaris 2010). The figure below shows the linear and non-linear vertical bending moments as well as the whipping effects, and the context is that the effects of non-linear and whip can grossly increase the amount of cyclic loading a structure endures.

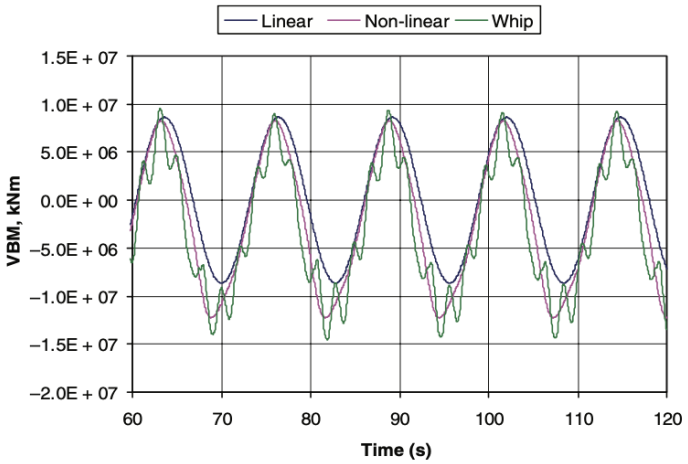

Figure 16-1 time history of amidships VBM of a container ship

Hydrodynamic tools such as PRECAL and FD-WAVELOAD solve the flow potential in six degrees of freedom and a time domain simulation helps represent the non-linearity in ship responses to the environment, FD-WAVELOAD considers fluids in tanks such as LNG carriers and models the tank effects of sloshing liquids, which it does quite well. Sloshing in ship tanks is under further review due to the increased use of liquified natural gas carriers which have very large fuel tanks that start near full with minimal sloshing and by the end of the mission have either half the tank empty or even more space for sloshing (Hirdaris 2010). Further study is being carried out with water or other fuels to correlate and improve the modeling but loads encountered in moderate sea states produce the maximum sloshing and not the most severe states. Strength assessment of a physical system that feeds back into an FEA simulation has been performed and is a promising avenue to further characterize these complex loads and responses from the systems they are installed within.

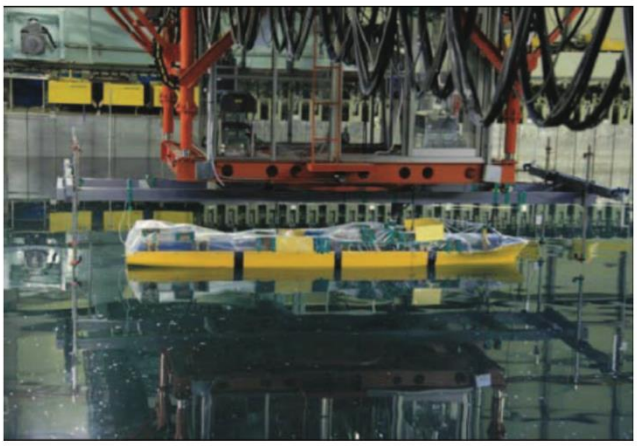

Figure 16-2 Elastic tank testing model

Recommendations from the article are that the culture needs to change and improve the interaction between academic community and industry to improve technological solutions, and promote a new school of thinking towards assessing novel engineering problems through

fundamentals analysis instead of collecting data without thought of reasons why the loads are what they are, and the need to develop technologies, products, and services that raise the standards of safety at sea and protect the environment

The relevance to this project is such that as the proficiency and skills of the Saimaa design team improves, this information is useful to know that the design spiral later steps can impact earlier design cycles, particularly when predicting the maximum bending moment in the estimated sea spectra.

17 Seakeeping criteria

Seakeeping characteristics and evaluation against the available recommendation is quite important for passenger vessel. As Saimaa Hybrid is classified as a passenger vessel, it is important to evaluate the seakeeping characteristics in waves to ensure safe and convenient operation of the vessel in normal and short severe sea states. The excessive uncontrolled motions of the vessel maybe harmful to the passenger and also the vessel itself. These harmful effects may include vomiting, headache, dizziness and lose of balance. The anxious, hungry, smells, reading and alcoholic drinks exacerbate the motion sickness. Hence it is essential to follow the seakeeping criteria to avoid these harmful effects and to provide the best comfortability to the passengers. Usually, the symptoms of the seasickness disappear after a few days at sea, however, unfortunately, each journey of Saimaa-Hybrid may not exceed 2 days. Therefore, we believe that we should keep the motion as low as possible in by avoiding severe weather and installing the necessary devices to damp the motions, especially, rolling motions. This can be achieved by installing active or passive tanks, bilge keel, or stabilizing fins. The probability of the excessive and severe sea states is very small, so we don't expect to have excessive motions and therefore only bilge keel is enough for our vessel.

In Saimaa Hybrid the vertical acceleration is the main source of seasickness, as other motions are not essentially high and don't affect the seasickness remarkably.

17.1 Criteria check

There is a big variation between individuals about the effect of motions on them. Even a single person may feel uncomfortable in a specific sea state while repeating this sea state not necessarily mean the same person will experience the same feeling of comfortability. This reflect that there are many parameters that can affect the feeling of individuals rather than the motion itself. Therefore, we cannot judge the seasickness using deterministic approach, while, the statistical approach seems to be more realistic. Many criteria are available to judge the influence of motion on the people onboard. In this report MSI are adopted and executed on Maxsurf motions in different remote locations as follows.

17.2 MSI Motion Sickness Incidence

Motion Sickness Incidence MSI is a tool to measure and evaluate the seasickness and comfortability of passengers on board. It is the percentage of subjects who vomit in the specified time that subjects are exposed to the motions. The data were derived from test on healthy, young, males' students who were subjected to vertical motions for a period of up to two hours. Thus, extrapolation to other demographics or longer durations of exposure can be difficult. In this report, two different ways are used to define motion sickness incidence as follows.

17.2.1 ISO 2631/3 1985 and BS 6841:1987

In this method, the likely discomfort can be gauged by how close the acceleration curves approach the defined acceleration limits suggested by these rules. This MSI acceleration depends on the magnitude of the vertical acceleration at the point of interest on the vessel. This is computed by integrating the power spectrum density PSD $S_{\text{vert accel}}$ over a one third octave range centred about the frequency of interest:

$$MSI(\omega_{e\,\text{centre}}) = \int_{\omega_{e1}}^{\omega_{e2}} S_{\text{vert accel}}(\omega_e)\, d\omega_e$$

17.2.2 MSI after 2 hours exposure

The motion sickness incidence derived from the formulation original 1974 paper of O'Hanlon and McCauley is calculated for a fixed exposure time of 2 hours. Here in Maxsurf Motions, the MSI is estimated based on the method described in Lloyd 1998, pages 304 to 306.

$$\text{MSI\%} = 100 \times \Phi\left\{\frac{\log\left(\frac{|\ddot{s}_3|}{g}\right) - \mu_{\text{MSI}}}{0.4}\right\}$$

where Φ(x) is the cumulative normal distribution function up to x for a normal distribution with zero mean and unity standard deviation. This can be evaluated using excel sheet easily by the excel function =NORMDIST(x, 0, 1, TRUE). And Lloyd factor μ_{MSI}:

$$\mu_{\text{MSI}} = -0.819 + 2.32(log\ \omega_e)^2$$

And the frequency in rad/sec $\omega_e = \sqrt{\frac{m_4}{m_2}}$ and the and the acceleration $\left|\ddot{s}_3\right| = 0.798\sqrt{m_4}\ .\ m_2$ and m_4 are the second and forth moment of the acceleration spectrum density function.

17.3 Subjective Magnitude

It is a measure of comfortability of the crew and the influence of motions on ability to work effectively. The calculation of the Subjective Magnitude follows the method described in Lloyd 1998:

$$\text{SM} = A\left(\frac{\ddot{s}_{30}}{g}\right)^{1.43}$$

where A depends on the encounter frequency:

$$A = \left\{1 - \exp\left(-1.65\omega_e^2\right)\right\}\left\{75.6 - 49.6\ln\omega_e + 13.5\left(\ln\omega_e\right)^2\right\};$$

and the vertical acceleration $\ddot{s}_{30}$ can be evaluated from the vertical motion spectrum:

$$\ddot{s}_{30} = 2\sqrt{m_4}$$

Subjective magnitude is on a scale of zero to 30 where:

0 – 5 Moderate
5 – 10 Serious
10 – 15 Severe: necessary to “hang on”
15 – 20 Hazardous
20 – 30 Intolerable

17.4 Remote locations

Different remote locations are defined in Maxsurf motions to predict the accelerations that are likely to be experienced in these locations. We included many places where the crew, passenger and cargo are situated. The locations included in the seasickness analysis are the bridge, accommodation areas throughout the ship length, café, buffet, sundeck, Sauna, cargo compartment and machinery spaces and hydrogen fuel tanks, see figure below.

Name	Long. Pos. [m]	Offset [m]	Height [m]	Long. Pos. from	Offset from CG	Height from CG	MII slide friction coeff.	MII tip fore/aft. stance coeff.	MII tip side/side. stance coeff.	Exposure time for MSI [min.]
Bridge	81.00	0.00	16.00	32.97	0.00	11.35	0.70	0.17	0.25	120
Sundeck FWD	70.00	0.00	14.00	21.97	0.00	9.35	0.70	0.17	0.25	120
Second floor forward cabins	70.00	5.00	13.00	21.97	5.00	8.35	0.70	0.17	0.25	120
Cafe	22.00	0.00	13.50	-26.03	0.00	8.85	0.70	0.17	0.25	120
Puffet	31.00	0.00	13.50	-17.03	0.00	8.85	0.70	0.17	0.25	120
SAUNA	10.00	0.00	13.50	-38.03	0.00	8.85	0.70	0.17	0.25	120
first floor forward cabins	70.00	5.00	10.00	21.97	5.00	5.35	0.70	0.17	0.25	120
first floor aft cabins	10.00	5.00	10.00	-38.03	5.00	5.35	0.70	0.17	0.25	120
amidship cabins first floor	45.00	5.00	10.00	-3.03	5.00	5.35	0.70	0.17	0.25	120
Forward cargo compartment	70.00	0.00	7.00	21.97	0.00	2.35	0.70	0.17	0.25	120
amidship cargo compartment	45.00	0.00	7.00	-3.03	0.00	2.35	0.70	0.17	0.25	120
Main engine room	18.00	0.00	2.00	-30.03	0.00	-2.65	0.70	0.17	0.25	120
Battery room	18.00	0.00	2.00	-30.03	0.00	-2.65	0.70	0.17	0.25	120
H2 fuel tanks room	24.00	0.00	2.00	-24.03	0.00	-2.65	0.70	0.17	0.25	120

Figure 17-1 Remote location for seakeeping criteria check

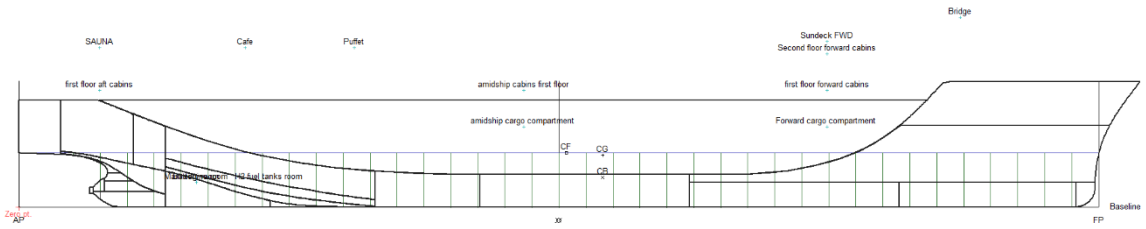

Figure 17-2 Visual illustration of the considered remote locations

Maxsurf Motions can calculate the absolute and relative (to wave surface) vertical motion, velocity and acceleration and MSI at the specified remote locations.

The last three columns in the figure above are used to specify the coefficients to be used when calculating motion induced interruptions (MII) at the remote location. Standard sliding and tipping coefficients are given in the Maxsurf manual, see figure below, which is cited from “Standard material requirements for RAN ships and submarines” reference. For sake of simplification, the personnel recommended values are selected for all the considered locations.

MII coefficients for different events

Incident	Coefficient
Personnel	
Fore-and-aft tipping	0.17
Side-to-side tipping	0.25
Sliding on dry deck	0.70
Equipment	
Sliding of chair on linoleum floor	0.19
Sliding of helicopters, typical minimum	0.20
Sliding of helicopters, typical maximum	0.80

Figure 17-3 MII coefficients for different events

17.5 Sea states for seakeeping criteria checking

Three sea states represent the severe, normal and most probable sea state conditions were considered in the following analysis. The severe sea state refers to the worst motions that the ship may experience, the normal one is assumed has zero up crossing period of wavelength nearly equal ship length and average wave height 2.75m, while the most probable sea state is the one that our ship is normally encounters in everyday operation.

Name	Type	Char. height [m]	Modal period [s]	Average period [s]	Zero crossing period [s]
Severe	ITTC(2 Param. Pierson Moskowitz\Bretschn	6.500	10.993 s	8.494 s	7.858 s
Normal	ITTC(2 Param. Pierson Moskowitz\Bretschn	2.750	7.997 s	6.179 s	5.716 s
most probable	ITTC(2 Param. Pierson Moskowitz\Bretschn	0.750	3.999 s	3.090 s	2.859 s

17.6 Results

The following spectral density functions and results are obtained using Maxsurf, strip theory. First we compared the results in the most probable sea states with the limits of ISO, it can be clearly observed from the figure below all the acceleration SPD are quite below the ISO limits when the ship advance with maximum forward speed 12 knot and in beam seas (where the highest vertical acceleration can be observed)

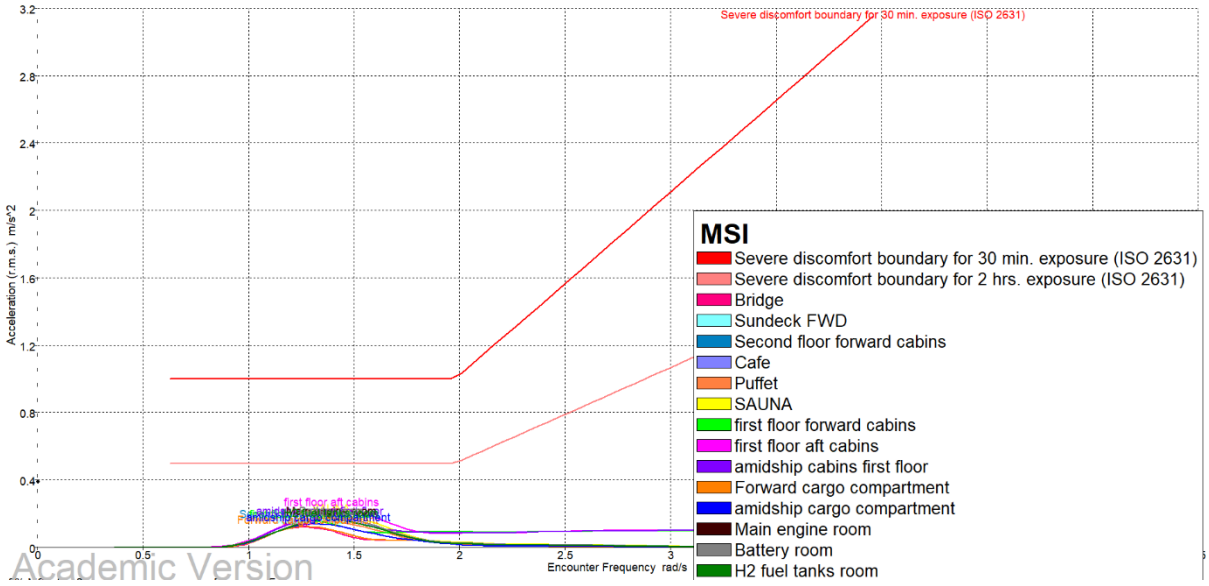

Figure 17-4 Most probable sea sate and ISO limits (maximum forward speed 12 knot and beam seas)

Similarly for the subjective magnitude, we can observe that most of the acceleration quite below the 2% MSI curve (moderate condition).

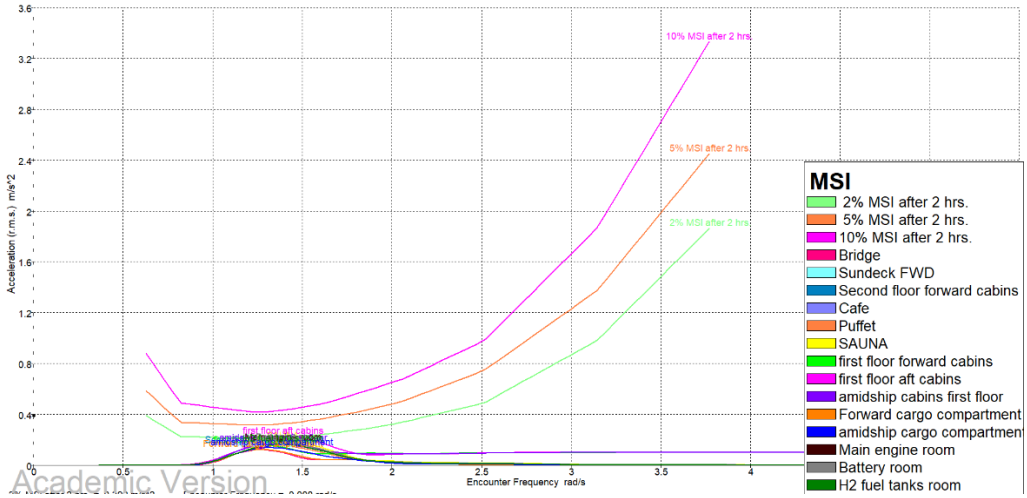

Figure 17-5 Most probable sea sate MSI comparison (maximum forward speed 12 knot and beam seas)

In normal sea state condition and for comfortability of the passengers we expect to encounter the waves in 180 degree (head seas) with forward speeds don't exceed 5 knots, hence we will remain in the MSI moderate zone for locations below the first floor and many locations near amidship. Some places will experience serious MSI condition, especially those at the ship ends

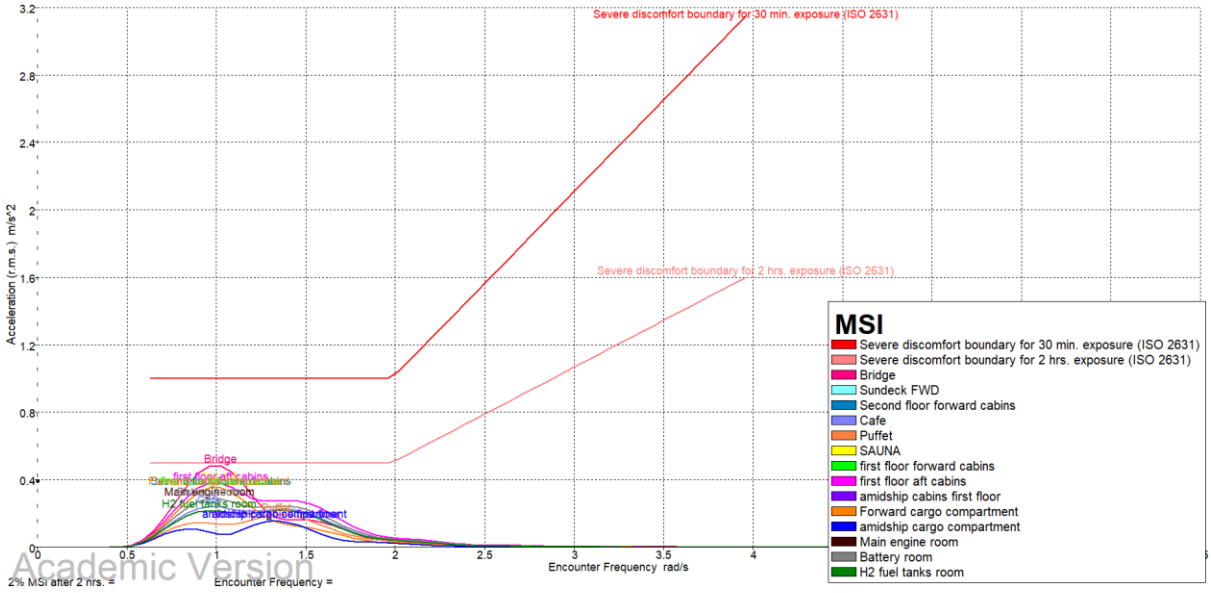

Figure 17-6 Normal sea sate ISO comparison (forward speed 5 knot and head seas)

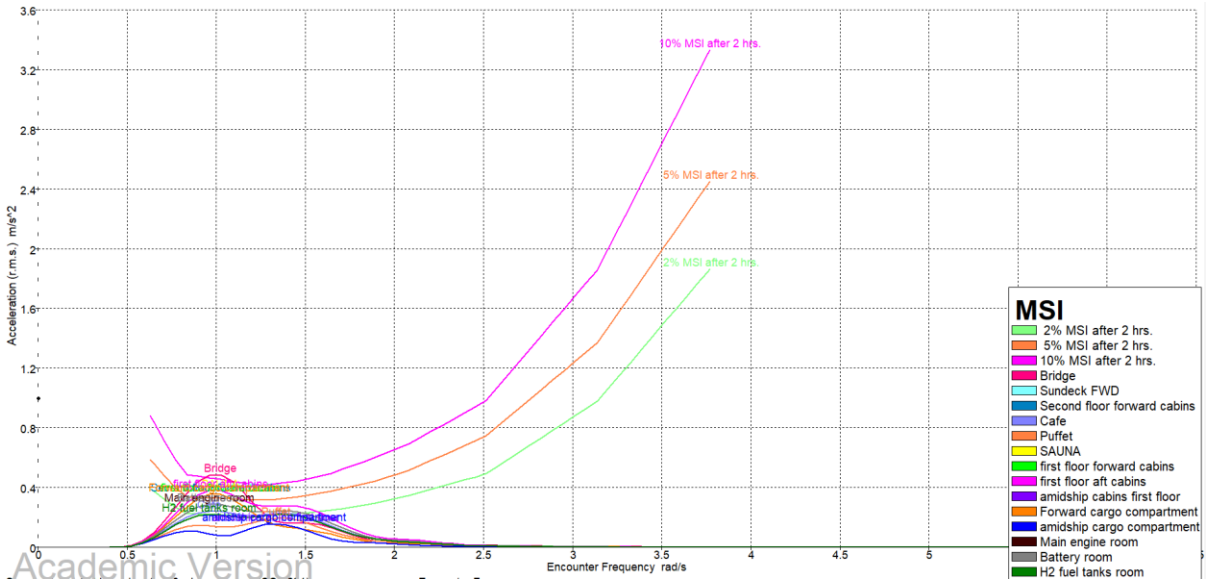

Figure 17-7 Normal sea sate MSI comparison (forward speed 5 knot and head seas)

It is noteworthy that increasing the speed up to 12 knot in this normal sea states will have very bad and serious influence on the crew at the bridge and also on the passengers on board, especially in the cabins at the forward and aft parts of the vessel, see figure below. However, all the accelerations still below the ISO limit of 30-min exposure and many are higher than 2 hour exposure

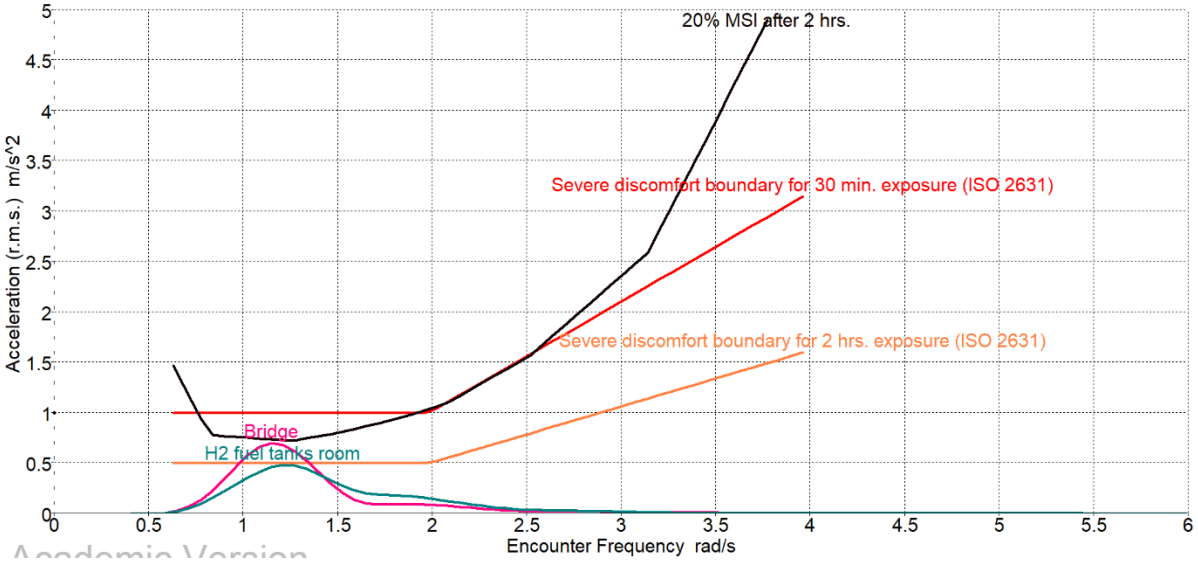

Figure 17-8 Normal sea sate MSI and ISO comparison (forward speed 12 knot and head seas)

On the other hand, in severe sea states we will have to reduce the speed to small values, here 5.5 knots forward speed, to keep the acceleration below the limits of ISO for 30-min exposure. The pilots and crew on the bridge will experience quite serious seasickness as the MSI there exceeds 20 %. However, we don't expect to encounter this severe sea states, may be 2 or 3 times only throughout the whole ship life.

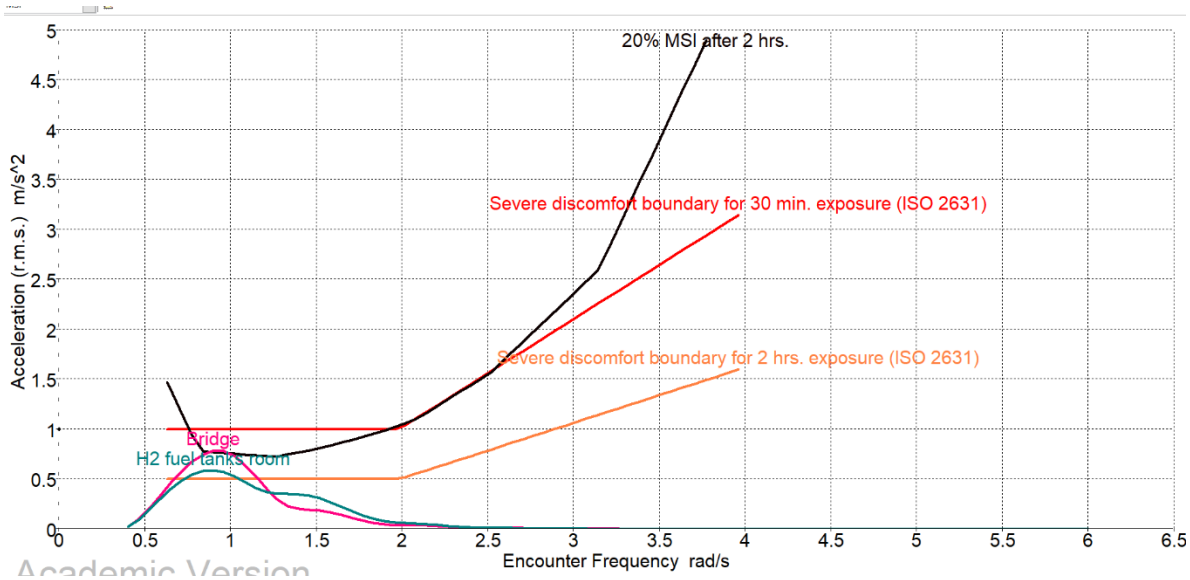

Figure 17-9 severe sea sate MSI and ISO comparison (forward speed 5 knot and head seas)

From the figures above we can conclude that the most comfortable location for passenger cabins is in the first floor near amidship, where they will not experience any seasickness during the journey, even in severe sea states. For the same reason we have selected this place for setting the hydrogen tanks to reduce the acceleration as possible and to achieve higher safety for these dangerous tanks.

18 Added resistance

Ship will experience added resistance in a seaway due to the waves. This energy dissipation can be divided into three different components mainly: drifting force, diffraction effects and viscous effects. Drifting force is related to the radiated waves, which are generated by the ship motions. The biggest contributors to this are the vertical motions heave and pitch. Diffraction effects are related to the reflection of incident waves from the ship hull and to the interaction between incident waves and radiating waves. And finally, the viscous effects are related to the viscous damping. The viscous effects are insignificant compared to hydrodynamic damping and therefore it can be neglected. This is a common simplification done since it also allows the application of potential theory. Out of the two remaining components, radiated waves is dominating when the ship motions are large. Diffraction effects are significant with short waves. (Perez Arribas 2007). Overall, it is important to consider the added resistance in a seaway because the total resistance can increase significantly. Commonly this increase can be within a range of 15-30%.

18.1 NAPA computations

The added resistance in irregular waves was estimated with NAPA. The NAPA computations are based on the strip theory using this so-called radiated energy method. This means that the added resistance is assumed to be related to the product of the sectional damping and the vertical velocity squared integrated over the ship length (see equation below). More detailed description can be found on literature (e.g. Perez Arribas or course notes).

$$R_{aw} = \frac{-k \cdot \cos(\beta)}{2 \cdot \omega_e} \int_0^L b' \left| V_{z_b} \right|^2 \cdot \partial x_b$$

The strip theory method is used for the regime where the ship motions are dominating. On top of this, NAPA uses reflection coefficient method to apply corrections to the strip theory results. This is because the strip theory results are quite poor with the short wavelengths, where the diffraction effects are dominating. Once the responses are calculated for the regular waves, the response for irregular waves can be achieved by super-positioning the regular wave responses.

For the computations Pierson-Moskowitz spectrum was used, heading angle was set to 180 degrees and speed to design speed of 12 knots. The added resistance was evaluated for two different significant wave heights; 1m and 1.5m. These wave heights are something we can expect in normal day to day operations in Gulf of Finland. The results are shown in Figure *18-1*.

Tz sec	RRAW kN
1.00	3.60
2.00	10.43
3.00	10.74
4.00	10.10
5.00	11.64
6.00	11.93
7.00	10.11
8.00	7.72
9.00	5.66
10.00	4.11
11.00	2.99
12.00	2.21
13.00	1.65
14.00	1.25
15.00	0.96
16.00	0.75
17.00	0.60
18.00	0.48
19.00	0.39
20.00	0.31

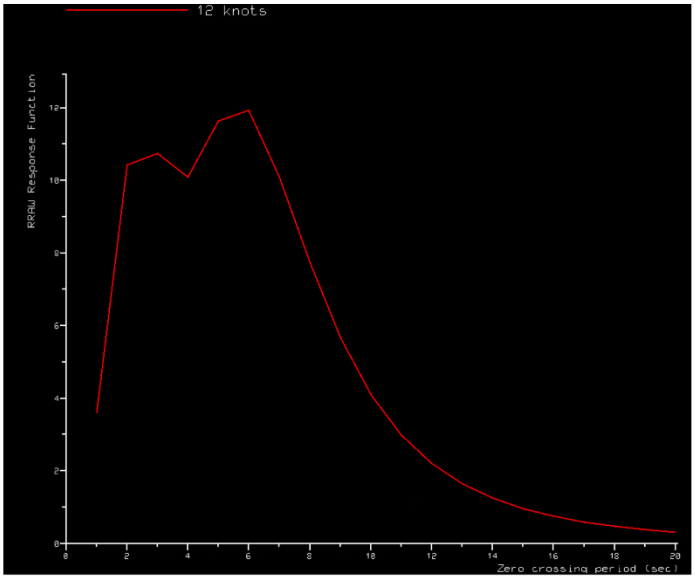

Tz sec	RRAW kN
1.00	8.09
2.00	23.47
3.00	24.17
4.00	22.72
5.00	26.19
6.00	26.84
7.00	22.74
8.00	17.38
9.00	12.74
10.00	9.24
11.00	6.73
12.00	4.96
13.00	3.71
14.00	2.82
15.00	2.17
16.00	1.69
17.00	1.34
18.00	1.07
19.00	0.87
20.00	0.71

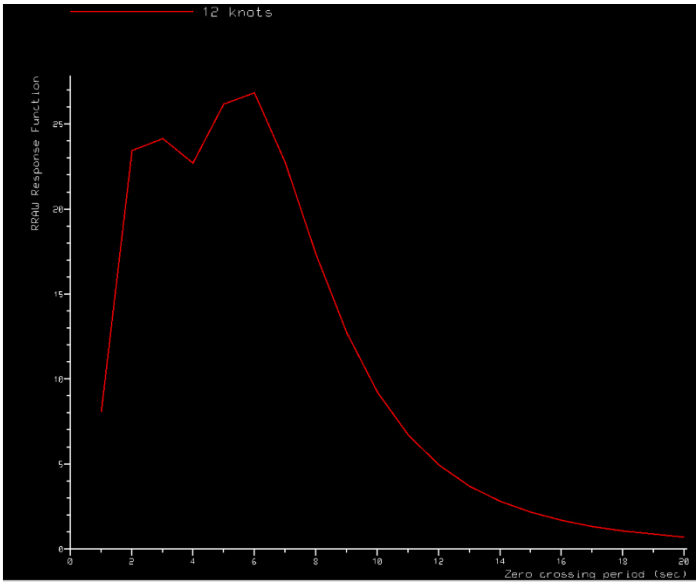

Figure 18-1 Added resistance in significant wave heights of 1m and 1.5m respectively

We can observe added resistance of 12 kN and 27 kN in significant wave heights of 1m and 1.5m, respectively. If we compare these results to the total resistance in calm water going 12 knots (see figure below), we can see roughly an increase of up to 10% and 24% in total resistance. It is safety to say that this increase of resistance is significant and has a major impact on the fuel consumption. We can also observe a rapid growth in the added resistance with increasing significant wave height.

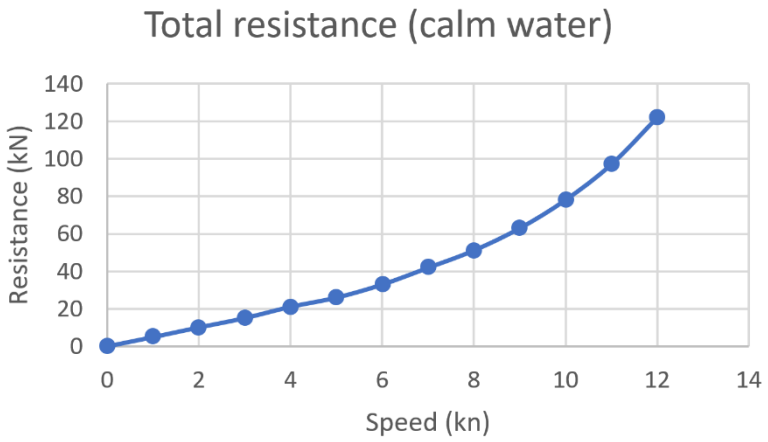

Figure 18-2 Total calm water resistance obtained using Holtrop method. Computations done in NAPA.

18.2 Accuracy of the results

Regarding the accuracy of these results, we can expect a margin of error between 20-30%. This can be considered quite a lot but acceptable in this context. This is because the added resistance is treated as a 2nd order problem. This makes it really sensitive to motion prediction. Essentially this means that the error related to the motion prediction gets amplified. We can already expect a margin of error around 10-15% in the motion prediction due to the used methods and simplifications. The viscous effects are neglected, and linear methods are used to approximate the hydrodynamic damping, which is more often nonlinear. This evidently leads to an error of

20-30%. This being said, Perez Arribas (2007) states that "*an accurate prediction of vertical motions is more important than developing more sophisticated added resistance theories*".

19 Manoeuvering

Maneuvering simulations were performed to assess the motion characteristics of Saimaa Hybrid in different situations. Following four maneuvering simulations were selected:

- Man overboard
- Turning circle (deep & shallow water)
- Emergency stopping
- Zig-zag

The simulations were based on list of recommended maneuvering tests by IMO. Also, the operational profile of the ship was considered in the selection when selecting the simulation parameters. Simulations were performed with NAPA. The used loading conditions were fully loaded and arrival condition although the zig-zag simulation was performed only for fully loaded condition due to challenges with NAPA script. All the simulations used windspeed condition of 7 m/s. The accuracy of the results can vary as some of the simulations were dependent from the power setting of the ship. Overall, the simulations seemed to achieve reasonable results.

19.1 Man overboard simulation

The man overboard simulation was performed with full speed of 12 knots. The time of elapse for simulation was 6 min 58 sec for fully loaded condition and 6 min 51 sec for arrival condition. The simulation route is plotted on *Figure 19-1* and the results seem reasonable although lower time of elapse could have been achieved by iterating the power settings of the vessel in the tests.

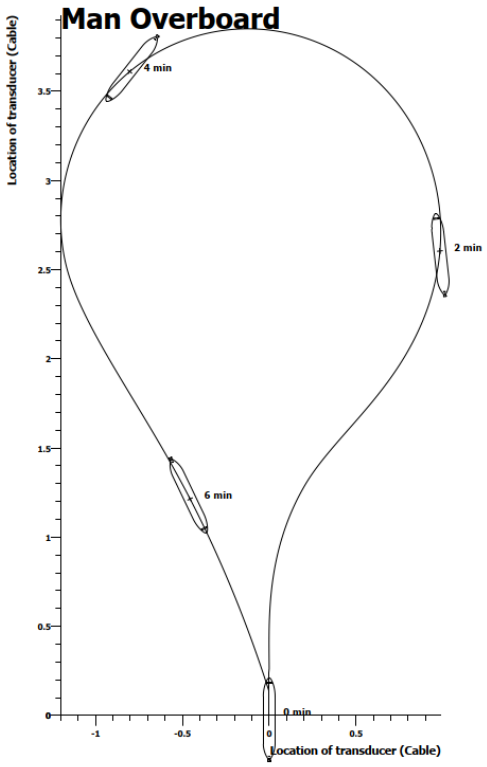

Figure 19-1 Man overboard simulation

19.2 Turning circle simulation

The turning circle simulation was performed with deep water and shallow water parameters for both loading conditions. The estimated time of elapse for turning circle with fully loading condition is 5.5 min in deep water and 5.4 min in shallow water. For arrival condition, the times are both 5.2 min. According to the difference between loading conditions, the results seem reasonable also in this simulation. The difference between turning circle in deep and shallow deviates from the general pattern where time of elapse should be greater in shallow water. According to Vantorre et al. (2017), the small L/B ratio or T/B ratio can result to opposite effect. Saimaa Hybrid has relatively small L/B ratio. Plotting of the results can be seen on *Figure 19-2* and *Figure 19-3*.

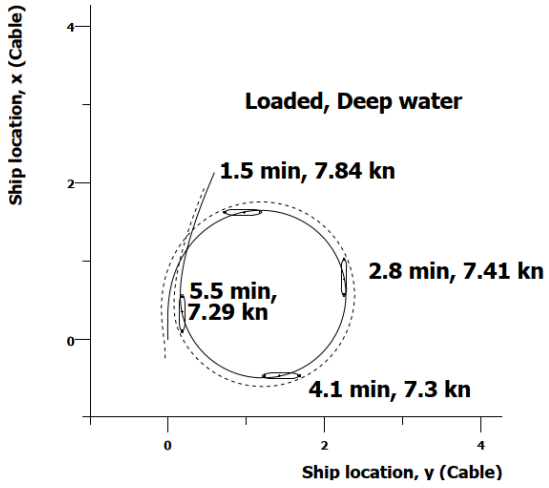

Figure 19-2 Turning circle (deep water and fully loaded)

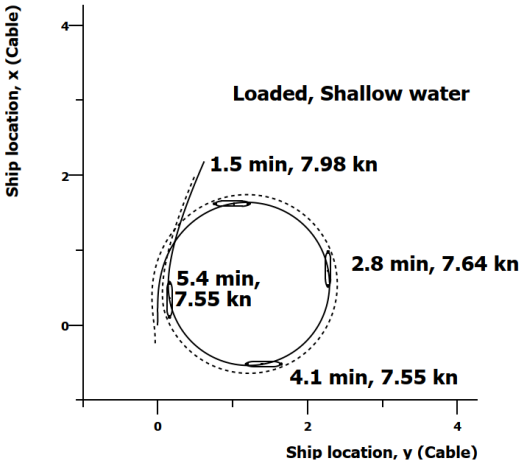

Figure 19-3 Turning circle (shallow water and fully loaded)

19.3 Emergency stopping simulation

The emergency stopping simulation was performed for two different speeds. The maximum speed of 12 knots and operation speed at the canal (4.5 knots) were used. The stopping characteristics for canal operation were especially important as the canal has 8 locks and other potential spots where there could be a need for stopping the vessel. The stopping time for fully loaded condition was 2 min 38 sec for 12 knots and 1 min 23 sec for 4.5 knots. The stopping time for arrival condition was 2 min 44 sec for 12 knots and 1 min 25 sec for 4.5 knots. The plotting of the results with fully loaded condition can be seen in *Figure 19-4* and *Figure 19-5* with comparison to the turning circle test.

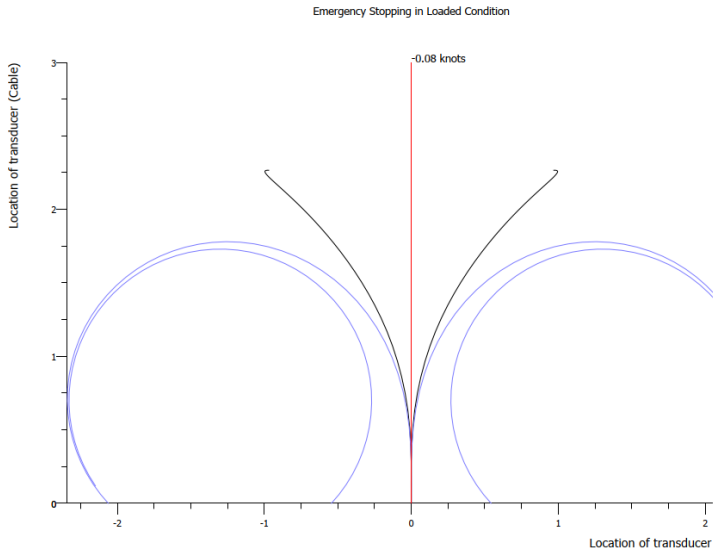

Figure 19-4 Emergency stopping (12 knots and fully loaded)

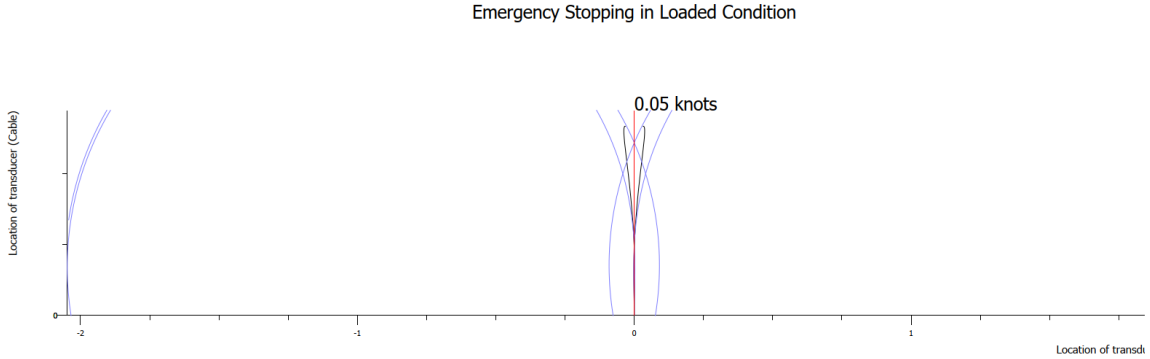

Figure 19-5 Emergency stopping (4.5 knots and fully loaded)

19.4 Zig-Zag -manoeuvre simulation

The simulation of the zig-zag manoeuvre was performed for fully loaded condition. The estimated time of elapse for the manoeuvre was 3 min 23 sec and the plotted result can be seen in *Figure 19-6*.

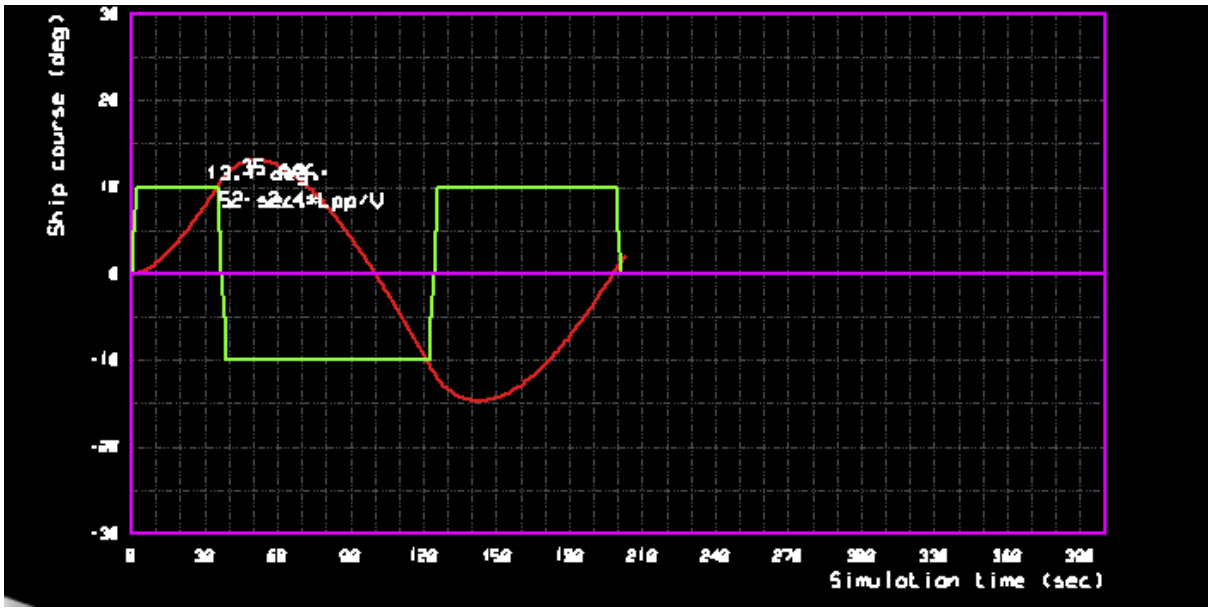

Figure 19-6 Zig-Zag -maneuvre simulation

19.5 Manoeuvring in literature and Saimaa hybrid

Chapter 6 of the Bertram textbook was selected due to the relevance and topics covered regarding manoeuvring. This chapter gives good context to what is meant by manoeuvring with a brief introduction and relevant terms, then the simulation of many types of manoeuvres with known coefficients are presented and discussed, as well as experimental approaches of model and full-scale tests, and the special attention if focuses on rudders with design, concepts, types, interactions, and conclusions are presented.

For Saimaa Hybrid, the selected maneuvres (man overboard, turning circle, emergency stopping, and zig-zag) are relevant to the operating mission of the vessel. Since this is a passenger vessel which operates in shallow waters, it is particularly important to know the capabilities of the ship for safety of all passengers and the seaways that will be travelled. Depending on the conditions of the sea and also seaway geography it may not be possible to

perform a man overboard maneuver in a canal and there must be a developed portfolio of how to respond to unexpected events and emergencies. This book chapter confirms the understanding of the design team that each of these maneuvers can be performed within a reasonable amount of time given the operating mission of the ship, but also should be performed at lower speeds to round out the understanding of how the ship performs when moving slowly in places where it is speed limited. This likely would be categorized during a sea trial, or confirmed as such, but is good practice to have an understanding of the effect of speed.

The figure below shows common rudder profiles, with Saimaa Hybrid being closely related to NACA 64_3018 on the far left. The book profiles the difference between these rudders and gives numerical methods to determine what effect the shape of the rudder has based on different hydrodynamic phenomena. It would behove the design team to investigate another shape of rudder to determine whether better maneuverability could result from a change in rudder shape.

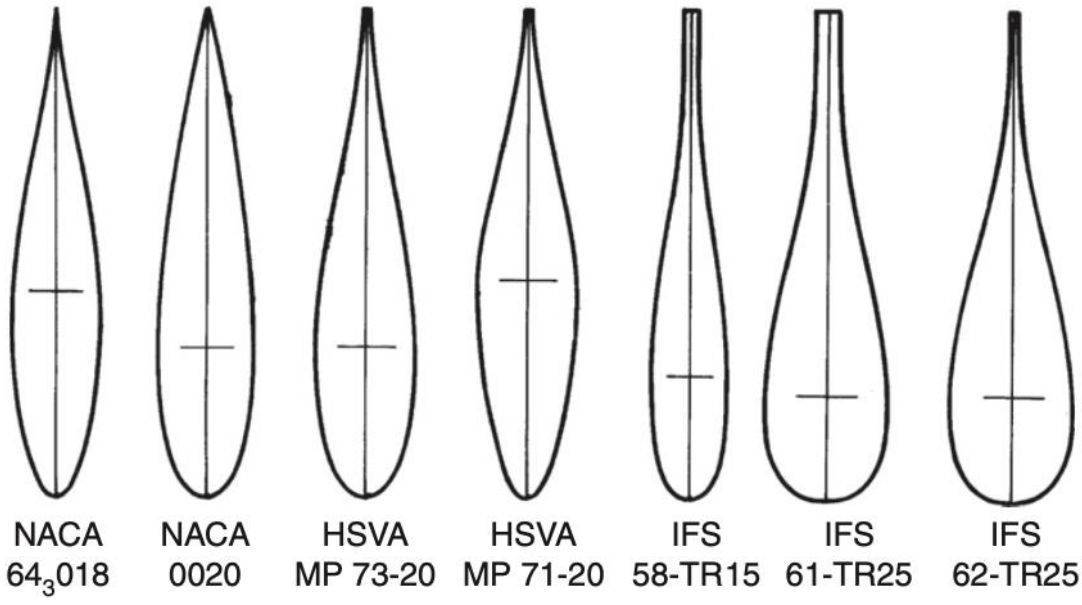

Figure 19-7 rudder profiles

In summary, this book chapter gives a good outline for performing a well-rounded maneuvering analysis and further study into each of the topics is recommended prior to launching Saimaa Hybrid. In the category of pax ships, there have been maneuvering errors made in the past by the captains and detailing the capability of the project ship is the most important aspect of these analyses. As with the other book chapters, they are quite rich with information and each section is only an introduction to what produces volumes of additional topics and research which all need to be considered to some extent as to whether they are relevant to the project ship or not.

20 Improvements and unknown areas of Saimaa Hybrid

The topics presented in this report and complimentary reports with Ship Design Portfolio and Ship Structures and Construction are not finalized and as such there are many areas of improvement that could be discussed. In this section, the biggest unknowns or areas of need for improvement are presented and discussed but might not encompass every area that needs to be refined.

20.1 Conceptual unknown topics for Saimaa Hybrid

There are many unknowns with the design concept presented in this report; the design team is learning what areas are important using the tools available and learning rapidly, but still unknowns persist. With regards to the topics presented in ship dynamics course, the actual response during any given input load or wave condition cannot be fully known until sea trials can confirm proper response.

Additional study could be performed on non-uniform loading of the vessel, and with varied inputs to build out a matrix of responses that the vessel would exhibit. This approach would be quite time consuming because there are many possible loading scenarios. The reason why it would be important is that possible incidents could be prevented if they are considered. For example, the maneuvering capability of the ship is not constant regardless of loading conditions, so there could be more study performed to seek out the worst-case loading which makes the ship have slow responses and find ways to prevent them from occurring.

Another area which is difficult to predict is the berthing process and whether tug assistance is required for berthing in Saimaa region or in the Gulf of Finland for a given sea state. This is a topic that needs to be covered for normal operation, and there might be improvements that could be made in the next iteration of the ship design cycle. If the ship is used as intended for the lifetime of the vessel, it will need to berth quite often and having a firm understanding of this is required.

The feasibility of using LNG, batteries, and fuel cells for the zero-emission operation of the project ship is another topic that could use additional study into exactly how much risk is associated with each energy source with respect to the operation of the ship. The studies that have been performed in PNA and this course do not encompass all the nuances of each technology and in order to sell this ship as a futuristic vessel, much more detail and studying is needed to prove that it will work as advertised. As this is a developing field, some expertise is probably needed to present the figures with authority, but it is absent from the results presented aside from some tank sloshing study that has been presented.

20.2 Areas for improvement

As with all iterative design projects, there are many areas for improvement that are constantly evolving and after reflecting on the topics presented in the ship dynamics course there are two areas that the Saimaa Hybrid could improve upon, namely manoeuvring and directional control, and dynamic stability.

For manoeuvring and directional control, there are several limitations to the ship as designed and not many can be altered greatly without changing the operating mission. The ferry must be large and bulky to accommodate the required cargo but operate like a slender ship with high efficiency and be able to utilize modern technology which has inherent risks. The amount of time it takes to perform a man overboard manoeuvre should be decreased and additionally

studied to see if rudder optimization could improve this metric, the shallow water resistance and appendage added resistance needs to be fully detailed to make sure that the bow thruster is placed optimally to prevent unnecessary power loss, and further wave resistance calculations should be performed to see if any hull modifications are justified and reduce the MSI of Saimaa Hybrid. These areas for improvement are not critically impaired currently, but compared to other aspects that have better performance, would be areas that could make the ship better with relatively less efforts.

And finally, for dynamic stability there could be improvements made to the hull form for roll angle and slamming optimization. The current design is a traditional shape for a ro-pax ferry and there is significant inertia to keep the hull a certain shape, but for the development of a futuristic ferry that will be in operation for many years it would be a good topic area to study and determine if even a single-digit percent increase in performance is possible.

20.3 Summary

In summary, the conceptual unknowns and areas for improvement have been presented and briefly discussed. These have been shown without knowing what other advanced topics will be discussed in further ship design courses and many of them would naturally be improved as a result of the next time around the ship design spiral. The focus of this section is the vision of how to improve the ferry ship so that it overcomes the shortcomings of traditional ferries and yet satisfies the requirements set forth by the design criteria. It is not a simple task and many aspects must be considered to accomplish this goal.

References

ASME 2011 30th International Conference on Ocean, Offshore and Arctic Engineering.

2020a. "Bureau Veritas Hydrostar." https://marine-offshore.bureauveritas.com/hydrostar-software-powerful-hydrodynamic.

2020b. "Sesam Det Norske Veritas Germanischer Lloyd." https://www.dnvgl.com/software/products/sesam-products.html.

ANSYS, AQWA. 2013. "AQWA theory manual." *ed. Canonsburg, PA 15317, USA*.

Bentley Systems, Incorporated. 2018. User Manual, MAXSURF Motions, MOSES Motions, SACS Motions.

Bertram, Volker. 2012. "Chapter 3 - Resistance and Propulsion." Practical Ship Hydrodynamics (Second Edition), Pages 73-141. Accessed from: https://www.sciencedirect.com/science/article/pii/B978008097150610003X

Bertram, Volker. 2012. "Chapter 4 - Ship Seakeeping." Practical Ship Hydrodynamics (Second Edition), Pages 143-204. Accessed from: https://www.sciencedirect.com/science/article/pii/B9780080971506100041

Bertram, Volker. 2012. "Chapter 6 - Ship Maneuvering" Practical Ship Hydrodynamics (Second Edition), Pages 241-298. Accessed from: https://www.sciencedirect.com/science/article/pii/B9780080971506100065

Bitner-Gregersen, Elzbieta M, and Sverre Haver. 1991. "Joint environmental model for reliability calculations." The First International Offshore and Polar Engineering Conference.

Collu, M., and M. Borg. "Design of floating offshore wind turbines." *Offshore wind farms*. Woodhead Publishing, 2016. 359-385.

DHI. MIKE 21 wave modelling

DHI. 2020. "metocean-on-demand." accessed 9/10. https://www.metocean-on-demand.com/#/main.

DNVGL-CG-0130. January 2018. "Wave loads." *CLASS GUIDELINE*.

Guedes Soares, C. 1995. "Effect of wave directionality on long-term wave-induced loas effects in ships." *Journal of ship research* 39 (2):150-159.

Hasselmann, Klaus, TP Barnett, E Bouws, H Carlson, DE Cartwright, K Enke, JA Ewing, H Gienapp, DE Hasselmann, and P Kruseman. 1973. "Measurements of wind-wave growth and swell decay during the Joint North Sea Wave Project (JONSWAP)." *Ergänzungsheft 8-12*.

Hirdaris, S.E., White, N.J., Angoshtari, N, Johnson, M.C., Lee, Y., Bakkers, N., Strategic Research Group, Lloyd's Register Marine Business, London, UK. 2010. "Wave loads and flexible fluid-structure interactions: current developments and future directions."

Kahma, Kimmo, Heidi Pettersson, and Laura %J MERI–Report Series of the Finnish Institute of Marine Research Tuomi. 2003. "Scatter diagram wave statistics from the northern Baltic Sea." 49:15-32.

Lee, Yongwon, Zhenhong Wang, Nigel White, and Spyros E Hirdaris. 2011. "Time domain analysis of springing and whipping responses acting on a large container ship." ASME 2011 30th International Conference on Ocean, Offshore and Arctic Engineering.

Lewis, E.V., 1988. Principles of naval architecture second revision. *Jersey: Sname*, *2*.

Li, M, E Boulougouris, I Lazakis, and G Theotokatos. 2016. "Analysis of the wave-induced vertical bending moment and comparison with the class imposed design loads for

4250 TEU container ship." International Conference of Maritime Safety and Operations 2016.
LR. 2020. "Lloyd's Register FD Waveload ". http://www.webstore.lr.org/products/2858-waveload-fd-12-months-subscription-licence.aspx.
Perez Arribas, F. 2007. "Some methods to obtain the added resistance of a ship advancing in waves". Ocean Engineering. 2007. Vol 34. pp. 946-955.

Prince-Wright, R. 1995. Maximum likelihood models of joint environmental data for TLP design. American Society of Mechanical Engineers, New York, NY (United States).
Vantorre, Marc & Eloot, Katrien & Delefortrie, Guillaume & Lataire, Evert. Maneuvering in Shallow and Confined Water. 2017. Encyclopedia of Maritime and Offshore Engineering.
Veritas, Det Norske. 2009. "Hull structural design ships with length 100 metres and above." *Rules For Classification of SHIPS, Newbuildings*.
Wallnöfer, Timo. 2015. "From Hydrodynamic Loading to Global Strength Assessment of Offshore Vessels." *ANSYS Conference & 33rd CADFEM Users' Meeting 2015*.

Wärtsilä. 2020. "Encyclopedia of Marine Technology"

Appendices

Appendix 1, Wave sketch

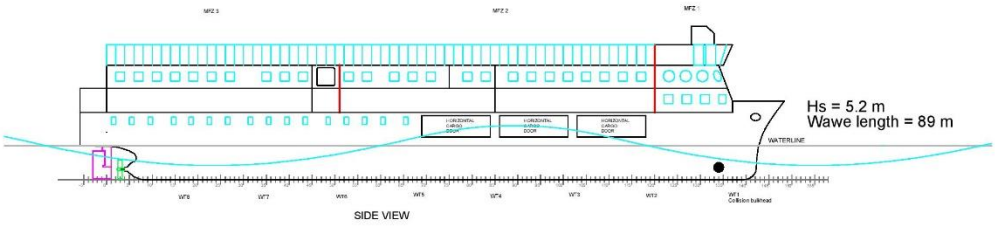

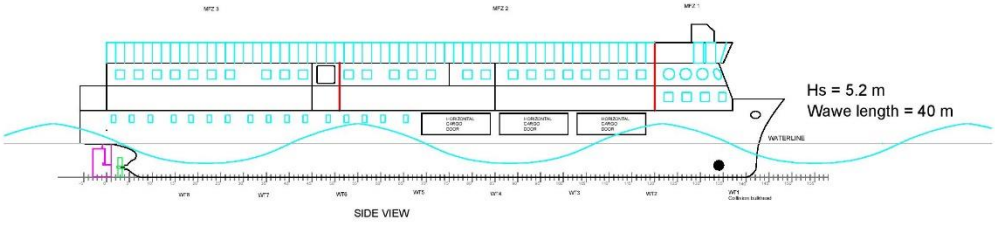

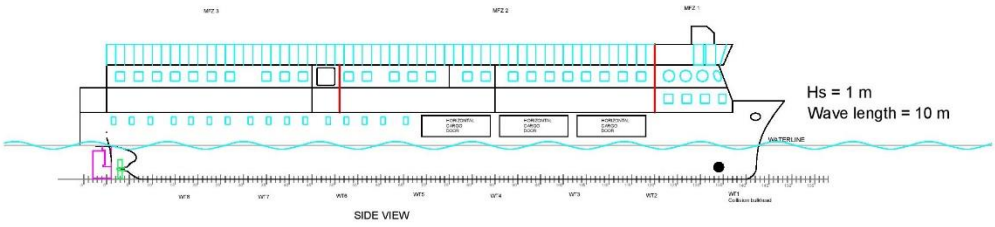

Appendix 2, General Arrangement